Supporting Information for

The Alkyne Moiety as a Latent Electrophile in Irreversible Covalent Small Molecule Inhibitors of Cathepsin K

Elma Mons,[†,‡] Ineke D. C. Jansen,[§] Jure Loboda,[⊥,∥] Bjorn R. van Doodewaerd,[†] Jill Hermans,[†] Martijn Verdoes,[∇] Constant A. A. van Boeckel,[O] Peter A. van Veelen,[#] Boris Turk,[⊥,¶] Dusan Turk,[⊥,¤] and Huib Ovaa*[,†,‡]

† Department of Cell and Chemical Biology, Oncode Institute, Leiden University Medical Center, Leiden, The Netherlands

‡ Division of Cell Biology, Netherlands Cancer Institute, Amsterdam, The Netherlands

§ Department of Periodontology, Academic Center For Dentistry Amsterdam (ACTA), Amsterdam, The Netherlands

⊥ Department of Biochemistry and Molecular and Structural Biology, Jožef Stefan Institute, Ljubljana, Slovenia

∥ Jožef Stefan International Postgraduate School, Ljubljana, Slovenia

∇ Department of Tumor Immunology, Institute for Molecular Life Sciences Radboud UMC, Nijmegen, The Netherlands

O Leiden Institute of Chemistry, Leiden University, Leiden, The Netherlands

Centre for Proteomics and Metabolomics, Leiden University Medical Center, Leiden, The Netherlands

¶ Faculty of Chemistry and Chemical Technology, University of Ljubljana, Ljubljana, Slovenia

¤ Centre of Excellence for Integrated Approaches in Chemistry and Biology of Proteins , Ljubljana , Slovenia

E-mail: h.ovaa@lumc.nl

Table of contents

Figure S1. Reversible covalent binding of ODN to hCatK

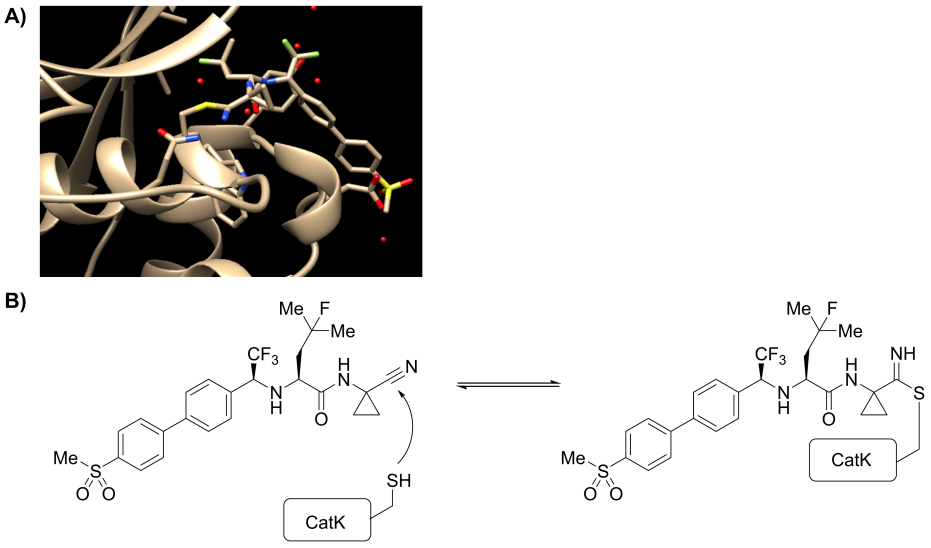

A) Crystal structure of Odanacatib covalently bound to catalytic cysteine residue (Cys139 in proCatK, Cys25 in mature CatK) in hCatK through the nitrile warhead. PDB; 5TDI. **B**) Schematic representation of nucleophilic attack of Cys25 to electrophilic nitrile warhead in ODN.

Figure S2. (Indiscriminate) Thiol Reactivity

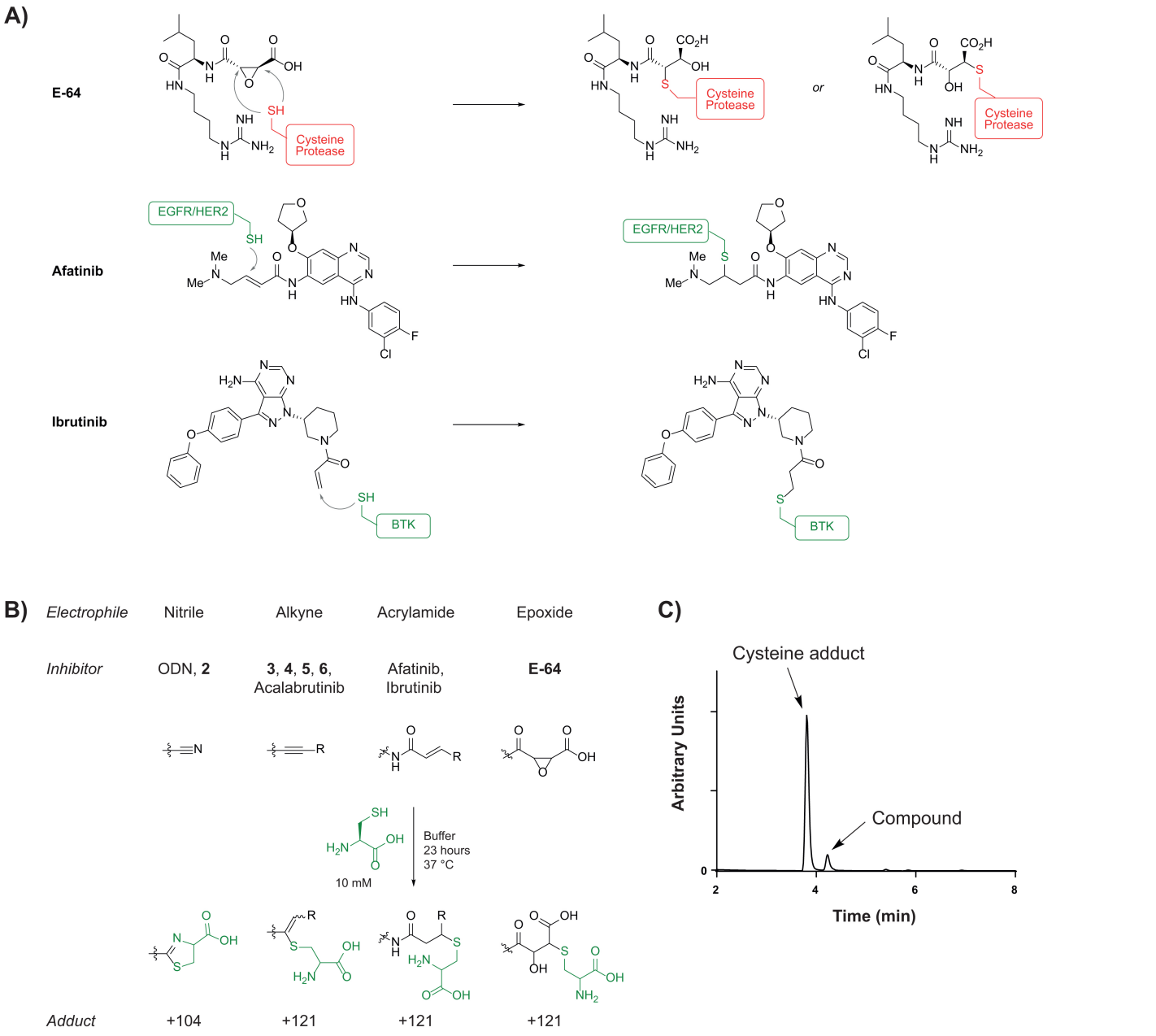

A) Chemical structure of unbound and covalently bound E-64, Afatinib and Ibrutinib. Structure for E-64 covalently bound to CatK: PDB 1ATK.

B) Irreversible cysteine adduct that can be formed with different (ir)reversible covalent warheads when treated with cysteine in phosphate buffer.[1]

C) Representative example of LC-MS UV trace of the reaction mixture.

Figure S3. Labeling of hCatK with quenched fluorescent probe BMV109

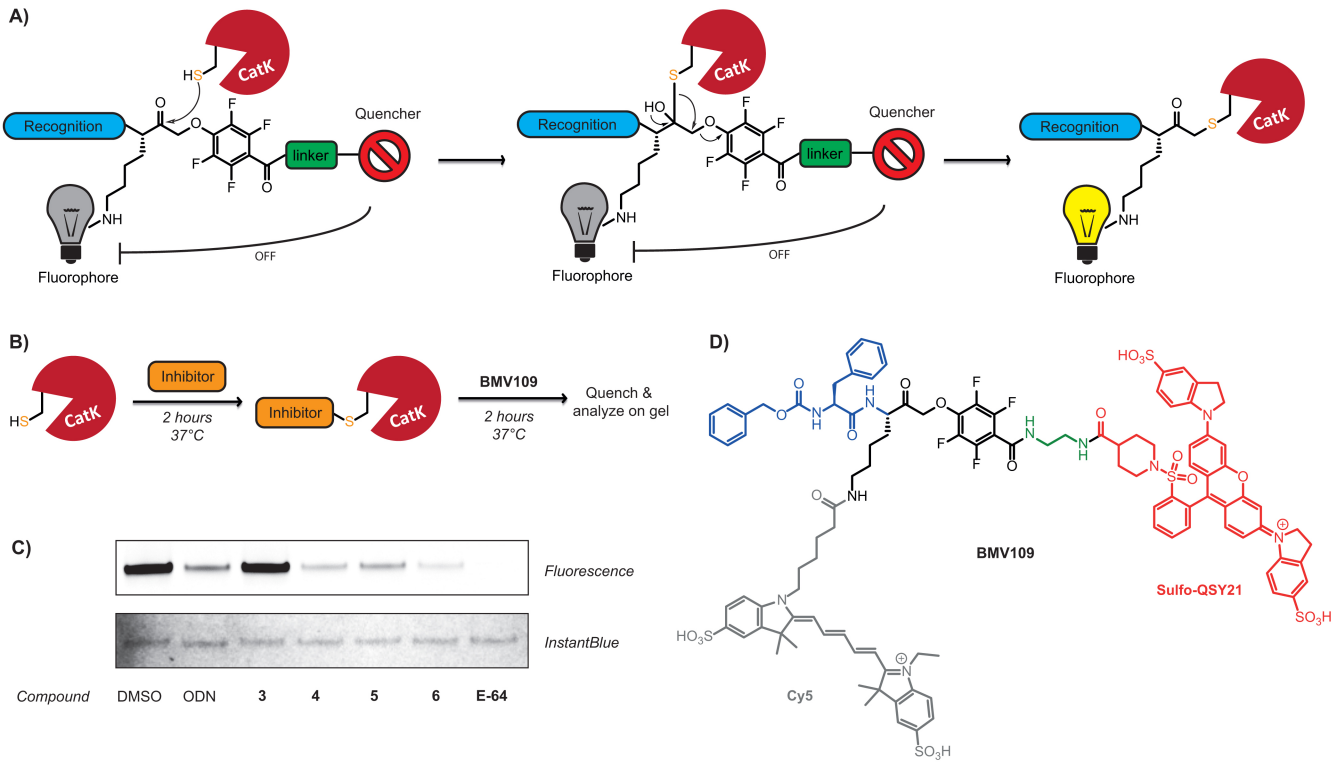

A) Schematic representation of quenched activity-based probes (qABPs). The catalytic cysteine residue reacts form an irreversible bond with the electrophile, while the quencher is removed as a leaving group, thus no longer quenching the fluorophore.[2] **B**) Schematic overview of competitive probe labelling procedure. CatK is incubated with inhibitor to allow full active site occupation, after which the quenched probe BMV109 is added. Inactive CatK cannot attack the quenched probe, resulting in the absence of a fluorescent band. **C**) Samples were run in 12% Bis-tris gel with MES running buffer. Top; fluorescent gel scan for Cy5. DMSO was taken along as a positive control (full CatK activity) and E-64 as a negative control (full irreversible CatK inhibition). All inhibitors except for alkyne **3** inhibit probe labeling at 100 μM. Bottom; InstantBlue™ Ultrafast Protein Stain of the gel as a loading control. **D**) Chemical structure of BMV109.[3]

Figure S4. Bottom-up proteomic analysis of trypsin-digested CatK and CatK-inhibitor **4** complex

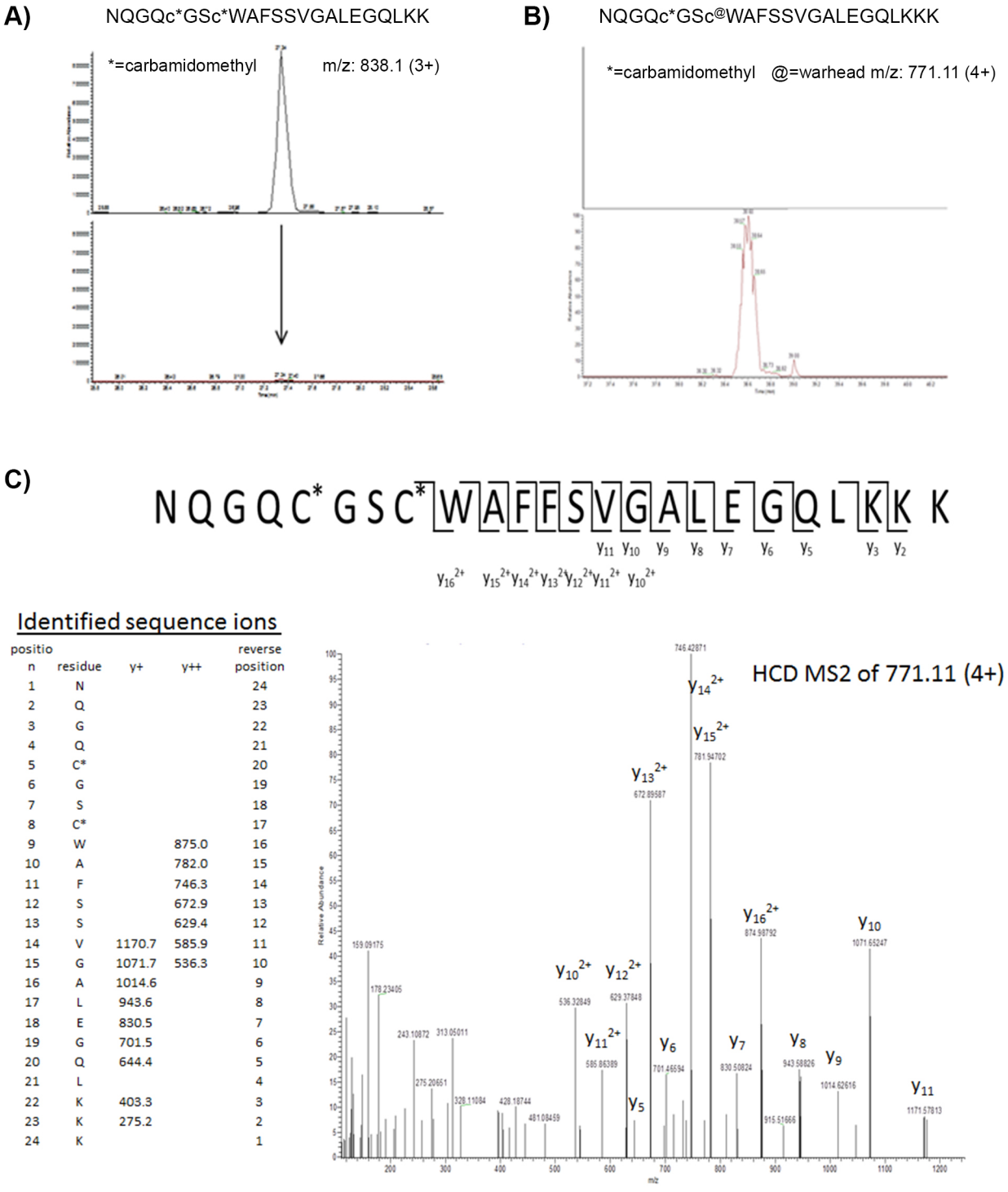

position	residue	y+	y++	reverse position
1	N			24
2	Q			23
3	G			22
4	Q			21
5	C*			20
6	G			19
7	S			18
8	C*			17
9	W		875.0	16
10	A		782.0	15
11	F		746.3	14
12	S		672.9	13
13	S		629.4	12
14	V	1170.7	585.9	11
15	G	1071.7	536.3	10
16	A	1014.6		9
17	L	943.6		8
18	E	830.5		7
19	G	701.5		6
20	Q	644.4		5
21	L			4
22	K	403.3		3
23	K	275.2		2
24	K			1

A) Mass chromatogram of peptide NQGQc*GSc*WAFSSVGALEGQLKK before (top panel) and after reaction (bottom panel) with the warhead (inhibitor **4**). As can be seen the double carbamidomethylated (*) peptide disappears nearly completely. **B**) The appearance of peptide NQGQc*GSc@WAFSSVGALEGQLKKK with a single carbamylation and a single warhead (@) can be seen in the bottom panel. **C**) Tandem mass spectrum of peptide NQGQc*GSc@WAFSSVGALEGQLKKK (*=carbamidomethyl; @=warhead), confirming the sequence of the peptide with the warhead. Identified fragment ions are indicated in the table and annotated in the spectrum.

Figure S5. X-ray structure of CatK-inhibitor **7** complex

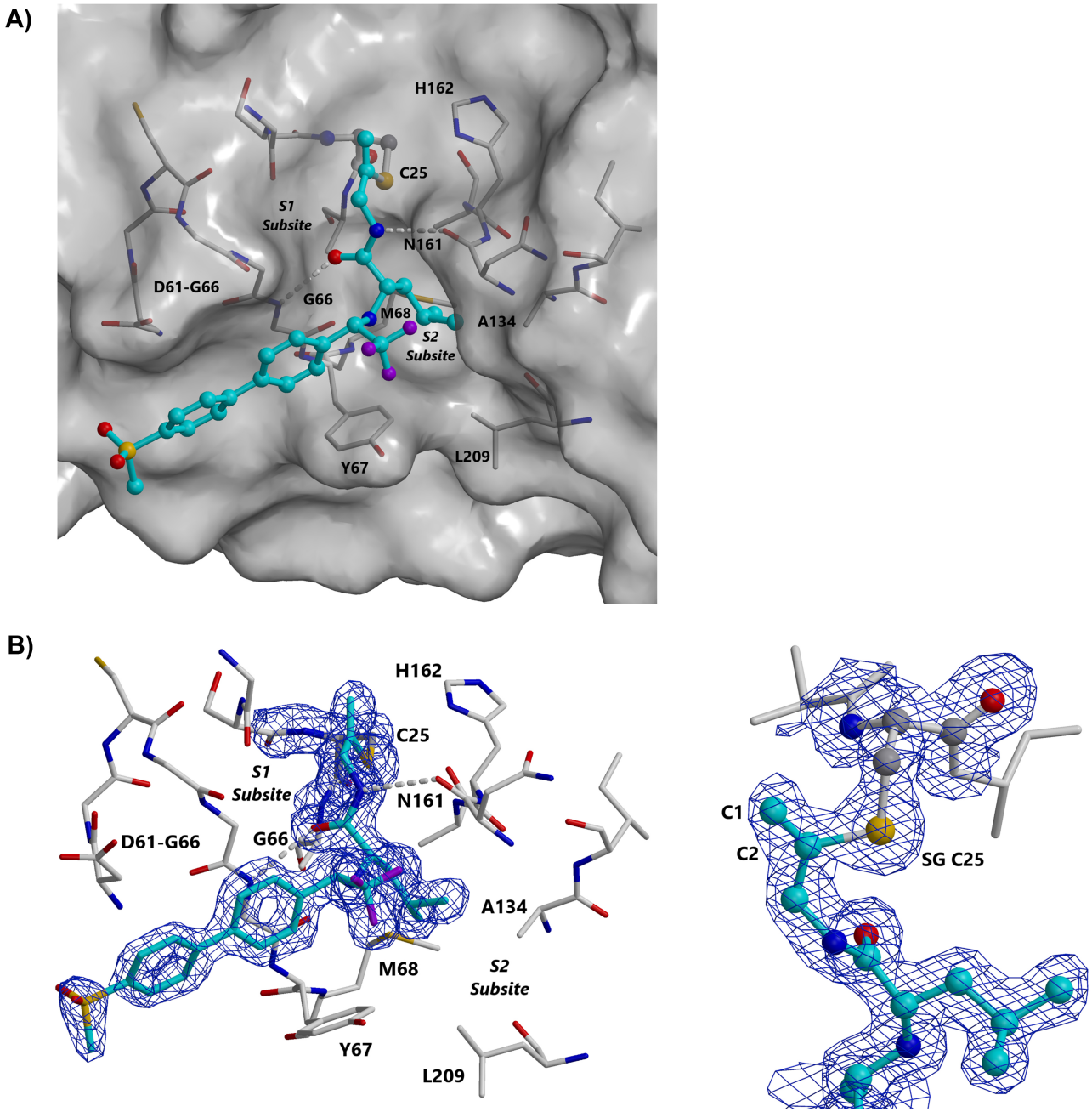

Crystal structure of alkyne **7** bound covalent to catalytic Cys25 in CatK. Nitrogen, oxygen, fluorine, and sulphur atoms are shown in blue, red, violet, and yellow, respectively, whereas carbon atoms of inhibitor **7** and CatK are shown in cyan and grey, respectively. **A)** Binding of inhibitor **7** to CatK. Inhibitor is shown with ball-and-stick model, relevant residues in CatK are shown with stick model. Covalent bonds of inhibitor **7** are shown as cyan sticks, whereas those of CatK are shown as white sticks. CatK is wrapped in white transparent surface. **B**) Free kick weighted electron density map[4] around inhibitor **7** and Cys25. Blue represents maximum-likelihood free-kick (ML FK) map contoured at 1.3 σ. Relevant CatK residues are shown with stick model. Inhibitor is shown in stick model (left) or ball-and-stick model (right).

Figure S6. Quantification of bone resorption area

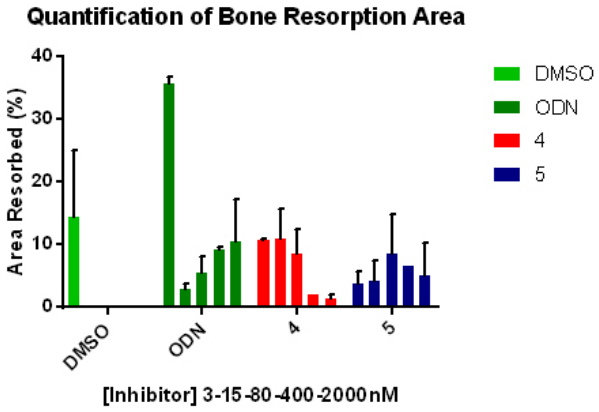

Bone resorption quantified as percentage of the total area on each bone slice. This measurement does not distinguish between pits and trenches, so depth of the resorption pit is not taken into account.

Figure S7. Counting mature OCs on plastic

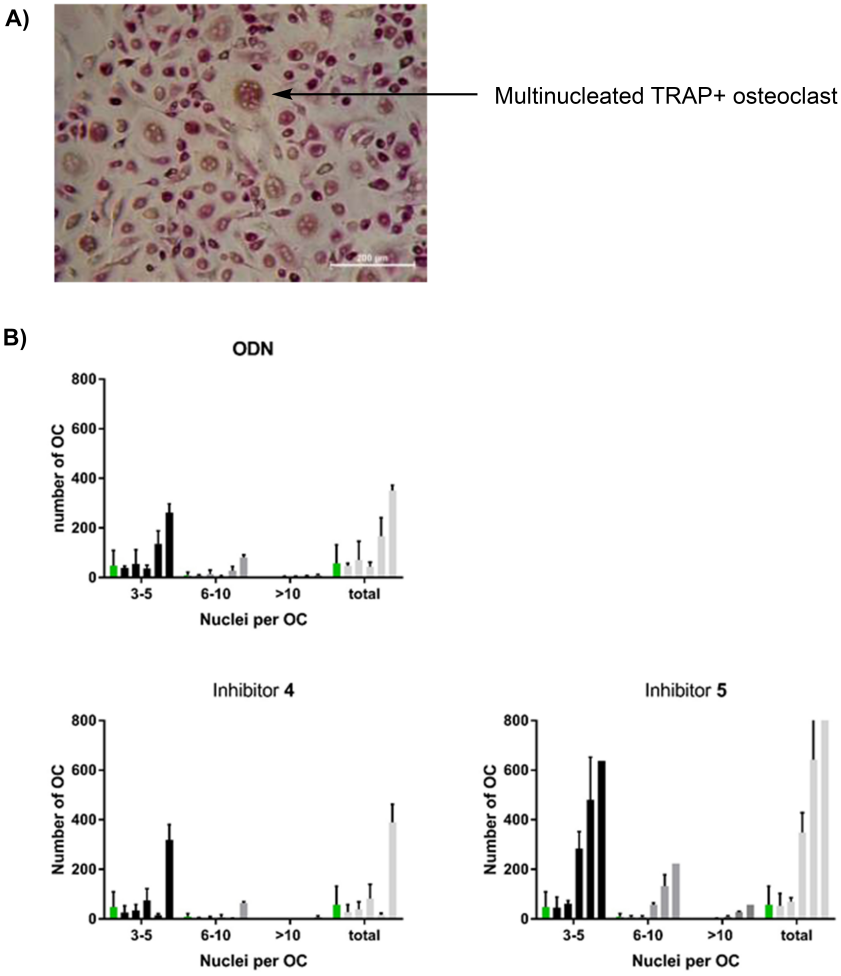

A) Example multinucleated osteoclast. **B**) Osteoclast formation on plastic with different inhibitors. For each condition DMSO (green), 3-15-80-400-2000 nM. All inhibitors show an increase in number of mature OCs at high concentrations of inhibitor.

Scheme S1. Synthesis of precursor **1** from affordable building blocks

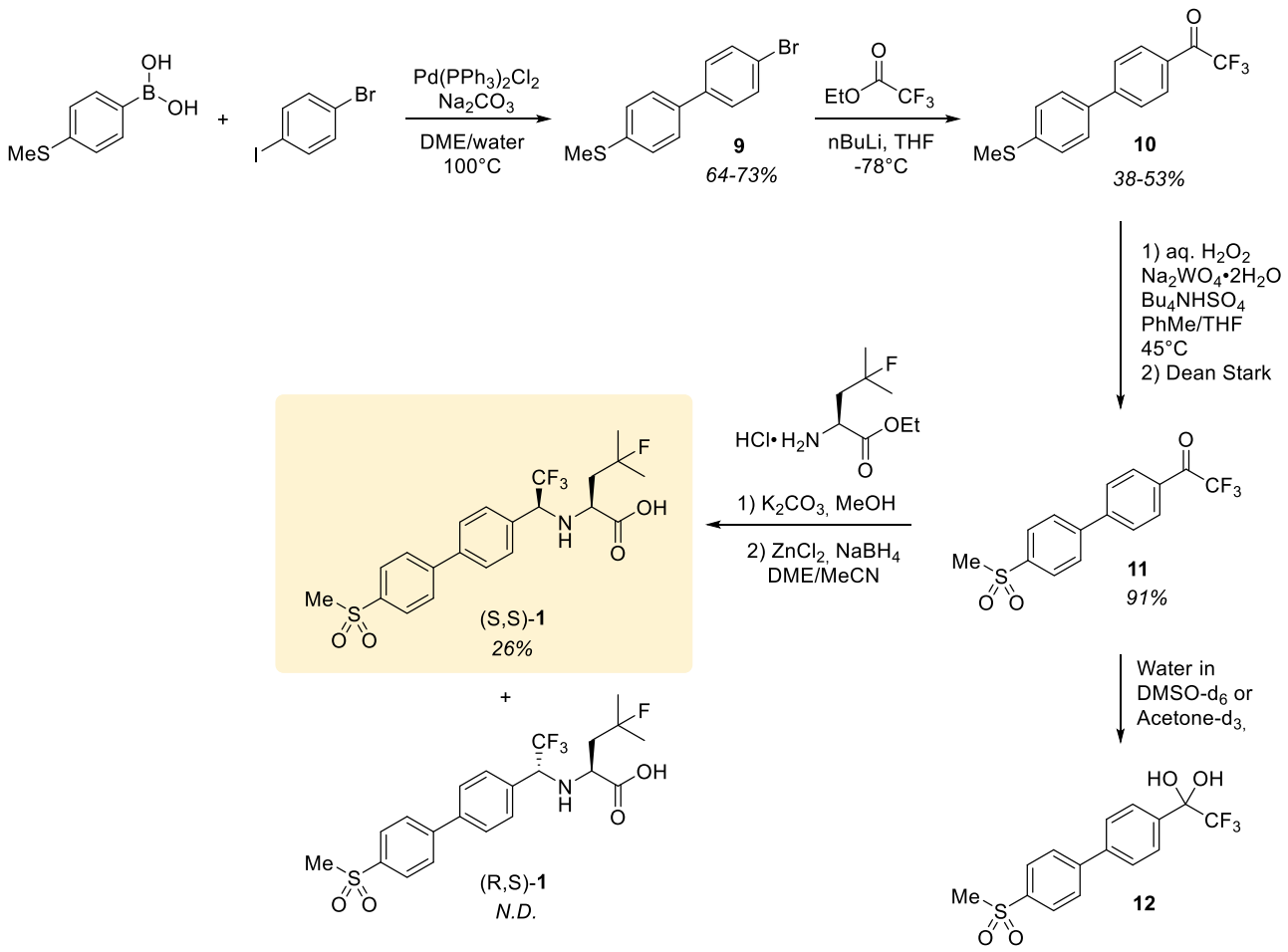

Synthesis of precursor **1** was started with a Suzuki coupling between commercially available boronic acid and 1-bromo-4-iodobenzene. Obtained product **9** was lithiated in the presence of ethyl trifluoroacetate to give sulphide **10**. Subsequent oxidation resulted in ketone **11**, which is prone to hydrolysis forming hydrate **12**. ^{13}C NMR analysis in $CDCl_3$ revealed ketone **11** was the only compound present, but when this sample was analyzed in DMSO-d_6 full hydrolysis to diol **12** was observed. Ketone **11** was submitted to a diastereoselective reductive amination. The imine intermediate was formed with 4-fluoro-L-Leucine, after which it was reduced with $NaBH_4/ZnCl_2$. Aqueous acidic work-up and purification by flash chromatography resulted in a mixture of diastereoisomers, which could be separated on reversed phase preparative HPLC. Diastereoisomers (S,S)-**1** and (R,S)-**1** were assigned based on comparison of ^1H NMR to the published spectra of (S,S)-**1**.[5] Ester hydrolysis of both diastereoisomers was also observed.[5]

Scheme S2. Synthesis of inhibitor **7** for crystallography

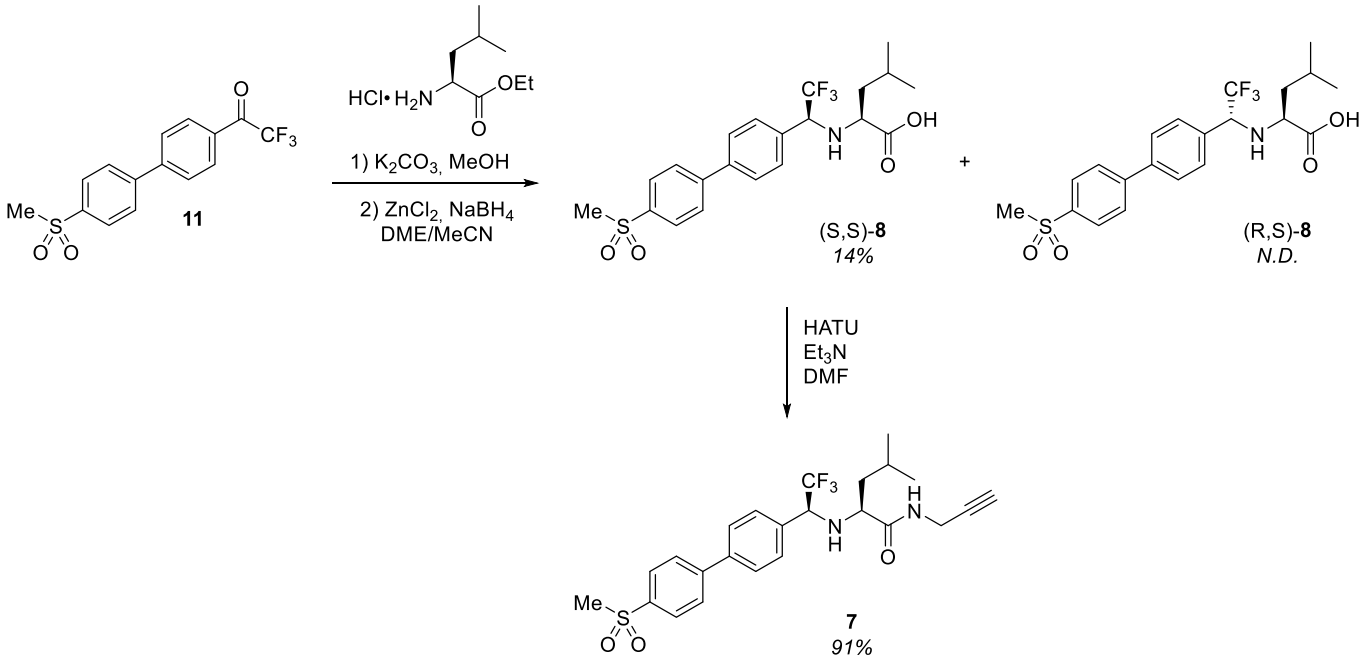

Ketone **11** was submitted to a diastereoselective reductive amination. The imine intermediate was formed with L-Leucine, after which it was reduced with $NaBH_4/ZnCl_2$. Aqueous acidic work-up resulted in a mixture of diastereoisomers, which could be separated on reversed phase preparative HPLC with (S,S)-**8** as the major isomer.[5] Peptide coupling with propargylamine resulted in inhibitor **7**. Stereocenters were assigned based on the X-ray diffraction data of the CatK-inhibitor **7** complex (Figure S5).

Materials and Methods

General Information on Activity Assays

Human recombinant Cathepsin K/L/V/S/B for *in vitro* inhibition assays were prepared as published previously.[6-8] Purified human Cathepsin was diluted in freshly prepared reaction buffer consisting of 50 mM MES pH 5.5, 25 mM EDTA and 2.5 mM DTT. 0.05% Tween20 (v/v) was added to the reaction buffer of Cathepsin K. Papain (Sigma Aldrich, P3125) was diluted in freshly prepared reaction buffer consisting of 50 mM Tris pH 7.6, 100 mM NaCl, 1 mM DTT, 1 mg/mL CHAPS and 0.5 mg/mL BGG. Activity assays were conducted in Corning 3820 Low Volume 384 Well Assay Plate in a final assay volume of 20 µL. Compounds were transferred using an ECHO 550 Liquid Handler (Labcyte Inc.) acoustic dispenser. Plates were shaken at 600 rpm for 1 minute and centrifuged at 1000 rpm for 1 minute prior to incubation. Protease activity was quantified using synthetic fluorogenic peptide substrates Z-FR-AMC (Bachem, I-1160) for Cathepsin K, L, V and Papain, Z-RR-AMC (Sigma Aldrich, C5429) for Cathepsin B or Z-FVR-AMC for Cathepsin S. Fluorescence intensity (λ_{ex} = 350 nm, λ_{em} = 440 nm) was measured every 2 minutes in arbitrary units (A.U.) on a CLARIOstar (BMG Labtech) microplate reader and values were converted to product formation using a calibration graph for AMC. All measurements were performed in triplicate. Data were plotted and analyzed using GraphPad Prism 7. Graphical data represents the mean ± standard deviation for a single representative experiment.

Indiscriminate thiol reactivity assay with cysteine. Inhibitors were dissolved in DMSO and diluted 100x in aqueous buffer containing cysteine, to a final concentration of 100 µM inhibitor and 10 mM cysteine. The reaction mixture was incubated at 37 °C for 23 h, after which the reaction was quenched with 0.1% formic acid in water. The samples were analyzed on the Waters Alliance 2795 Separation Module system equipped with Waters 2996 Photodiode Array Detector (190-750 nm), Waters Xbridge C18 column (2.1x30 mm, 3.5 µm) and LCT ESI- Orthogonal Acceleration Time of Flight Mass Spectrometer. Samples were run with a 13 min gradient using 2 mobile phases: A = 1% CH_3CN, 0.1% formic acid in water and B = 1% water and 0.1% formic acid in CH_3CN. Data processing was performed using Waters MassLynx Mass Spectrometry Software 4.1. Adduct formation was quantified from peak integration of the UV trace from the peaks corresponding to the remaining compound and the formed adduct, and normalized to 100%.

Indiscriminate thiol reactivity assay with GSH. Inhibitors were dissolved in DMSO and diluted 100x in PBS and 5 mM GSH (Chem-Impex Int., 00159), to a final concentration of 100 µM inhibitor and 5 mM GSH. The reaction mixture was incubated at 37 °C for 23 h, after which it the sample was analyzed as described above.

***In vitro* inhibition assay.** Inhibitors (200 nL, 100x final concentration in DMSO) were dispensed using an ECHO acoustic dispenser and diluted with reaction buffer (10 µL). Purified human Cathepsin (5 µL, 4x final concentration, list of final concentrations can be found on page SI-25) was added and the reaction mixture was incubated for 30 min at room temperature. Fluorogenic substrate (5 µL, 4x final concentration) was added and hydrolysis was measured

every 2 minutes for 90 minutes. Dose-response curves were calculated from the initial velocity v_i (slope 0-20 min, steady state kinetics), and fitted to obtain IC_{50}-values using non-linear least squares curve fitting (GraphPad Prism 8, inhibitor vs. response – variable slop (four parameters)) with fixed values for the top (DMSO) and bottom (E-64 (Apollo Scientific, BIMI2157) for Cathepsins, Iodoacetamide (Sigma Aldrich, I6125) for papain).

Reversibility; jump dilution assay. Inhibitors and 120 nM Cathepsin K (EnzoLifeSciences, BML-SE553-0010) were incubated for 30 minutes at room temperature and quickly diluted 300x in reaction buffer containing Z-FR-AMC (4 μM). Positive and negative controls are DMSO and E-64 (19 nM). As a control inhibitors at different concentrations were taken along; inhibitor and Cathepsin K (0.5 nM) were incubated and substrate (20 μM) was added without significant dilution. The total volume/well and final concentration of Cathepsin K and Z-FR-AMC were kept constant between the controls and jump dilution samples. Inhibitor concentrations were selected to correspond to full inhibition prior to dilution, and full activity after dilution, if inhibition is reversible and a new equilibrium is reached.

Kinetic evaluation of covalent inhibitors. Inhibitors (200 nL, 100x final concentration in DMSO) were dispensed using an ECHO acoustic dispenser and diluted with reaction buffer (10 μL). Fluorogenic substrate Z-FR-AMC (16 μM, 5 μL, 4x final concentration) was added and the reaction was started by addition of Cathepsin K (100 pM, 5 μL, 4x final concentration). Fluorescence intensity was measured every 2 minutes for 60 minutes and the curve was fitted to obtain kinetic parameters. (detailed information in appendix on page SI-66)

Labeling of hCatK with quenched activity-based probe BMV109. Cathepsin K (50 nM) was incubated with inhibitors (100 μM) for 2 hours at 37 °C to allow full active site occupancy. Then quenched fluorescent probe BMV109[3] (500 nM) was added, and the reaction mixture was incubated at 37 °C for an additional 2 hours. The reaction was quenched by addition of loading buffer (3x SDS-PAGE loading buffer, NuPAGE, Invitrogen) containing β-mercaptoethanol as a reducing agent and boiling the samples for 10 minutes at 94ºC. Samples were loaded on 12% Bis-Tris gels (Invitrogen) and resolved by SDS-PAGE gel electrophoresis with MES (NuPAGE MES SDS running buffer 20x, Novex by Life Technologies) as running buffer. Labeled enzyme was visualized by in-gel fluorescence using Typhoon FLA 9500 imaging system (GE Healthcare Life Sciences) (λ_{ex} = 635 nm, λ_{em} = 665 nm). Subsequently, gels were stained with InstantBlue™ Ultrafast Protein Stain (Expedeon Protein Solutions) and scanned using an Amersham Imager 600.

LC-MS for intact CatK and CatK-inhibitor complexes. Cathepsin K (~1.5 μM) in reaction buffer (20 μL) was incubated with inhibitor (100 μM) at 37 ºC for 6 hours prior to analysis. 1 μL injections of the sample were made onto a Waters XEVO-G2 XS QTOF UPLC-MS system with a Waters Acquity CM detector. Chromatographic separation was carried out on a Waters ACQUITY UPLC® Protein BEH C4 Column (300 Å, 1.7 μm, 2.1 x 50 mm) over a 12 minute gradient elution of 2% to 100% acetonitrile in water (0.1% formic acid) at a flow rate of 0.500 mL/min. For the first 4 minutes the flow was diverted to the waste to avoid contamination of the MS with high concentrations of buffer

components. After 4 minutes, the gradient was started and the elution flow was ionized with an ESI ionization source in positive ion mode. The data was analyzed using Waters MassLynx Mass Spectrometry Software V4.1. The total mass of the complex was obtained by deconvolution of electrospray ionization mass spectrum envelope (average isotopes) with the MaxEnt1 function.

Proteomic analysis of CatK-inhibitor 4 complex. CatK and preformed CatK-inhibitor **4** complex (as described above) were submitted for MS analysis. Samples were run on a 4-12% polyacrylamide gradient gel (NuPAGE Bis-Tris Precast Gel, Life Technologies), and stained with Coomassie. The CatK band was cut out, and the proteins subjected to reduction with DTT, alkylation with iodoacetamide and in-gel trypsin digestion using Proteineer DP digestion robot (Bruker). Tryptic peptides were extracted from the gel slices, lyophilized, dissolved in 95/3/0.1 v/v/v water/acetonitrile/formic acid and subsequently analyzed by on-line C18 nanoHPLC MS/MS with a system consisting of an Easy nLC 1200 gradient HPLC system (Thermo, Bremen, Germany), and a LUMOS mass spectrometer (Thermo). Digests were injected onto a homemade precolumn (100 μm × 15 mm; Reprosil-Pur C18-AQ 3 μm, Dr. Maisch, Ammerbuch, Germany) and eluted via a homemade analytical nano-HPLC column (15 cm × 75 μm; Reprosil-Pur C18-AQ 3 um). The gradient was run from 0% to 50% solvent B (20/80/0.1 water/acetonitrile/formic acid (FA) v/v/v) in 20 min. The nano-HPLC column was drawn to a tip of ∼5 μm and acted as the electrospray needle of the MS source. The LUMOS mass spectrometer was operated in data-dependent MS/MS (top-10 mode) with collision energy at 32 V and recording of the MS2 spectrum in the orbitrap. In the master scan (MS1) the resolution was 120,000, the scan range 400-1500, at an AGC target of 400,000 @maximum fill time of 50 ms. Dynamic exclusion after n=1 with exclusion duration of 10 s. Charge states 2-5 were included. For MS2 precursors were isolated with the quadrupole with an isolation width of 1.2 Da. HCD collision energy was set to 32 V. First mass was set to 110 Da. The MS2 scan resolution was 30,000 with an AGC target of 50,000 @maximum fill time of 60 ms. EThcD was performed at at an AGC value of 50,000, at a max fill time of 240 ms, and performed with an additional activation of 15V. Fragment ion spectra were recorded at 120,000 resolution. In a post-analysis process, raw data were first converted to peak lists using Proteome Discoverer version 2.2 (Thermo Electron), and then submitted to the Homo sapiens database (71591 entries), using Mascot v. 2.2.04 (www.matrixscience.com) for protein identification. Mascot searches were with 10 ppm and 0.02 Da deviation for precursor and fragment mass, respectively, and trypsin as enzyme. Up to four missed cleavages were allowed, and methionine oxidation, and carbamidomethyl on cysteine, and the warhead on cysteine and lysine were set as a variable modification.

Expression, purification and activation of CatK for crystallography. *p*PIC9 vector (Invitrogen) carrying cDNA of human procathepsin K (Deutsche Ressourcenzentrum für Genomforschung) was introduced into *P. Pastoris* strain GS115 (Invitrogen) by electroporation. The highest expressing transformant was selected by screening according to Invitrogen *Pichia* Expression kit (Invitrogen, K1710-01). Large scale expression took place in 10 5-liter Erlenmeyer flasks of 400 mL of BMMY with the addition of 40 μL antifoam 204 (Sigma, A8311) per flask, feeding interval 1% MeOH per day and 22 °C for 4 days. The supernatant was then collected, concentrated to 300 mL and diluted at 1:1

ratio with 20 mM HEPES pH 7.1. Then 25 mL of SP-sepharose FF (GE Healthcare, 17-079-01) was added to the sample and left shaking overnight at 6 °C. Procathepsin K was eluted from the exchanger with elution buffer (10 mM HEPES pH 7.1, 400 mM NaCl), concentrated to 0.5 mg/mL and stored at -80 °C. Activation of proCatK was initiated by adding DTT (5 mM final conc.) to purified procathepsin K and the sample was diluted at 1:1 ratio with the activation buffer (100 mM NaOAc pH 4) containing 40 μg/mL pepsin (Sigma, P6887) and incubated for 45 min at 37 °C. Pepsin was inactivated by raising pH of the sample to approximately 5.5 with 1 M Tris (pH 8.5). The sample was then purified on MONO S 5/50 column (GE Healthcare, 17-5168-01) on Äkta Express system (GE Healthcare). Mature Cathepsin K was captured with elution buffer (50 mM NaOAc, pH 5.5) at approximately 1 M NaCl and its proteolytic activity was blocked by incubating with approximately 10-fold molar excess of MMTS (Sigma, 208795) for 20 min at 6 ℃. The sample was desalted using HiTrap 5 mL column (GE Healthcare) to the final buffer (50 mM NaOAc, pH 5.5, 50 mM NaCl) and stored at -80 °C. Active enzyme concentration was determined by titration with E-64 (Sigma, E3132) based on previously described procedures.[9-11]

Complex formation and crystallization of CatK-inhibitor 7 complex. DTT (final conc. 10 mM) and 160 μL of inhibitor **7** (10 mM stock in DMSO, final inhibitor conc. 200 μM, final conc. DMSO 2%) were added to 8 mL of Cathepsin K (approx. 20 μM) and incubated at 37 °C for 8 h. To ensure complete inhibition, the sample was spiked with DTT (final 3 mM) after 8 hours and left incubating for additional 2 hours. The complex was then centrifuged and supernatant was collected and concentrated with Amicon Ultra devices (cut-off 10 kDa) to 15 mg/mL and stored at -80°C. Crystals suitable for data collection grew from 20% PEG-3350, 0.2 M $CaCl_2$ at 20 °C with sitting drop method. For the optimization, the complex was diluted to 10 mg/mL and drop sizes of both precipitant and complex were varied. Best diffracting crystal grew from the drop consisting of 0.5 μL of complex and 1 μL of precipitant. The crystal was soaked in 35% PEG-3350, 0.2 M $CaCl_2$ for 10 seconds for cryoprotection.

Data collection, structure determination and refinement for X-ray diffraction. Diffraction data was collected at XRD2 beamline at Elettra synchrotron, Trieste[12] under cryogenic conditions. Data were first processed with XDS software[13] and the unmerged HKL file was used as an input for Pointless, Aimless and Ctruncate (CCP4 suite)[14-16] to obtain the merged MTZ file. The Cathepsin K part of the 2FTD[17] model from Protein Data Bank was used for molecular replacement with Molrep (CCP4 suite)[18]. The refinement was done with MAIN software[19] with ML FK target function.[4] Inhibitor **7** was introduced in the model during refinement and fitted in the difference ML FK map. The geometric restraints for inhibitor **7** were generated by PURY.[20] The established complex was then further refined. Pictures were generated in PyMOL v2.2.0 or MAIN using RASTER 3D rendering software.[21]

Isolation of CD14+ cells from PBMCs. Osteoclast precursors (CD14+-cells) were isolated from human peripheral blood mononuclear cells (PBMCs). Briefly, human buffy coats were obtained from Sanquin Blood Supply (Amsterdam, the Netherlands), diluted with PBS containing 1% citrate (1:1) and spun down (800 g for 30 min, without brake) in lymphoprep (Elitech, Puteaux, France) gradient solution. The resulting interphase containing peripheral blood

mononuclear cells (PBMCs) was collected and washed with 1% citrate in PBS before it was passed through a cell strainer (40 µm Greiner Bio-One Monroe, NC) to ensure the recovery of a pure mononuclear cell population. The cells were counted (Muse cell counter, Merck, Darmstadt, Germany), and cell pellet was resuspended in 80 µL buffer (PBS containing 0.5% BSA and 2 mM EDTA) for 10^7 cells. 20 µL of CD14- magnetic beads was added to this cell suspension MACS microbeads Miltenyi Biotech, Bergisch Gladbach,Germany). According to the manufacturer's instructions the cells and CD14-beads were mixed and incubated for 15 minutes at 4 °C. The column was placed in the magnetic field, rinsed and subsequently the cell suspension was applied onto the column. Unlabeled cells pass through. Then the column was removed from the magnet and CD+ cells were flushed out and collected.

Osteoclast cultures. These cells were plated in 96 well plates (Cellstar, Greiner Bio-One) on plastic and on bovine cortical bone slices (650 µm thick) at a density of $1.3 \cdot 10^6$ cells/well. Cells were cultured for 21 days in α-MEM (Gibco, Paisley, UK) supplemented with 5% fetal calf serum (HyClone, Logan, UT), 100 U/mL penicillin, 100 µg/mL streptomycin and 250 ng/mL amphotericin B (Antibiotic Antimycotic solution, Sigma, St. Louis, MO), for 3 days with 25 ng/mL human recombinant M-CSF (R&D systems, Minneapolis, MN). After 3 days the concentration of M-CSF was reduced to 10 ng/mL and combined with 2 ng/mL recombinant RANKL (R&D systems) till the end of the culture period. From day 7 on various concentrations of Cathepsin K inhibitors were added to the cultures. An equal amount of vehicle (DMSO) was added to the control cultures without inhibitors. During culture the cells were maintained at 37 °C and 5% CO_2 and culture media were refreshed every 3-4 days. After 21 days of culture, wells were washed with PBS and either fixed in 4% PBS buffered formaldehyde, stored at 4 ºC, and used for tartrate-resistant acid phosphatase (TRAcP) staining, or the cells were lysed with phosphate buffer (100 mM, pH 6.0) containing 0.1% triton-X100. This cell extract was stored at -20 °C and used for cathepsin K activity osteoclast lysates (see below). The bone slices were stored in MilliQ water at 4 ºC for bone resorption visualization.

TRAcP staining and cell counting. The cells were stained for TRAcP by using the Acid Phosphatase, Leukocyte (TRAcP) Kit from Sigma (Sigma-Aldrich, St. Louis, MO). The procedure was according to the manufacturer's instructions. Nuclei were visualized with 4'6-diamino-2-phenylindole dihydrochloride (DAPI). Multinucleated TRAcP+ cells with three or more nuclei were considered osteoclasts and were counted on bone in standardized fields and on plastic per well using combination of light and fluorescence microscopy (Leica DFC320; Leica Microsystems, Wetzlar, Germany).

Staining of resorption pits on bone slices. Resorption was measured on slices of bovine cortical bone of 650 µm thick and fit into a 96-well plate. CD14+ monocytes were cultured on these bone slices for 21 days with M-CSF and RANKL and without or with inhibitors in various concentrations, as described above. After this period, the cells present on the bovine cortical bone slices were removed with 0.25 M NH_4OH. The slices were washed in distilled water, incubated in a saturated alum ($KAl(SO_4)_2 \cdot 12H_2O$) solution, washed in distilled water, and stained with Coomassie Brilliant Blue. Resorption pits were visualized by light microscopy (Leica DFC320). The resorbed area micrographs were made with

x10 magnification. Total resorbed area was quantified using Image Pro Plus (Media Cybernetics, Rockville, MD) and calculated as a percentage of the total area.

Cathepsin K activity in osteoclast lysates. Osteoclast lysates were treated with quenched fluorescent probe BMV109 (1 μM),[3] and the reaction mixture was incubated at 37 °C for 2 hours. The reaction was quenched by addition of loading buffer (3x SDS-PAGE loading buffer, NuPAGE, Invitrogen) containing β-mercaptoethanol as a reducing agent and boiling the samples for 10 minutes at 94 ºC. Samples were loaded on 12% Bis-Tris gels (Invitrogen) and resolved by SDS-PAGE gel electrophoresis with MES (NuPAGE MES SDS running buffer 20x, Novex by Life Technologies) as running buffer. Labeled enzyme was visualized by in-gel fluorescence using Typhoon FLA 9500 imaging system (GE Healthcare Life Sciences) (λ_{ex} = 635 nm, λ_{em} = 665 nm). Subsequently, gels were stained with InstantBlue™ Ultrafast Protein Stain (Expedeon Protein Solutions) and scanned on an Amersham Imager 600.

Cathepsin K expression in osteoclast lysates. Gels were transferred to nitrocellulose membrane using a Trans-Blot Turbo Transfer System (Biorad) and subjected to standard Western Blotting protocols. Antibodies: rabbit anti-CatK (1:500, Abcam19027), mouse anti-β-Actin (1:10000, Sigma Aldrich, A5441), swine anti-rabbit HRP (1:5000, Dako P0217) and Goat anti-mouse 800 (1:5000, LiCOR 926-32210). Blots with HRP secondary antibody were incubated with SuperSignal™ West Dura Extended Duration Substrate (Thermo Scientific, 34076) according to manufacturer protocols and scanned on an Amersham Imager 600. Blots with fluorescent secondary antibodies were scanned on a LiCOR Odyssey system v3.0.

Supporting Data

Indiscriminate Thiol Reactivity with Cysteine and GSH

Cysteine and GSH were added freshly to the buffer. Samples were prepared by addition of 1 μL inhibitor (10 mM in DMSO) to 99 μL buffer containing 10 mM cysteine or 5 mM GSH. Directly after addition, a sample of 50 μL was quenched with 50 μL 0.1% FA in water (t = 0). The remaining 50 μL was incubated at 37 ºC under gentle agitation, and quenched with 50 μL 0.1% FA in water after 23 hours (t = 23). For all ODN derivatives 1% DMSO was present in the quenching liquid to prevent precipitation upon quenching. The samples were submitted to LC-MS analysis as soon as possible after quenching, after at most five hours. UV trace area was calculated by defining the start and end of the peaks in MassLynx software using the 'Edit - integrated peaks' functionality. The intensity of UV signal was determined at a fixed wavelength, corresponding to maximum absorption by the compound and adduct: 265 nm (ODN derivatives), 192 nm (E-64), 260 nm (Afatinib/Ibrutinib) or 292 nm (Acalabrutinib). Adduct formation is reported as 'not detected' if the mass for the cysteine adduct was not observed, if the mass of cysteine adduct was observed in trace amounts, it is reported as <1%. Adduct formation with cysteine is an irreversible reaction for all compounds. Adduct formation with GSH is reversible for nitriles ODN and inhibitor **2**, but irreversible for all the other tested compounds.

Please be aware that the non-conserved cysteine residues that are targeted by kinase inhibitors are less nucleophilic than the active site cysteine residues in proteases, which is why most kinase inhibitors contain electrophiles that have indiscriminate thiol reactivity in these assays.

In some samples hydrolysis of inhibitor and/or adduct was observed. The intensity of these signals was added to the intensity of the inhibitor/adduct. It should be noted that hydrolysis of the inhibitor at the electrophilic moiety renders the inhibitor inactive towards thiols. For inhibitor **6** loss of Br (resulting in a m/z of 499, corresponding to inhibitor **4**) is observed; the rate of degradation is faster than the rate of adduct formation at pH7.5-8.0. Percentage adduct is calculated as a percentage of adduct relative to the remaining reactive inhibitor **6**.

PBS buffer = 10 mM phosphate buffer pH7.45, 140 mM NaCl, 2.7 mM KCl (Gibco PBS tablets).
MES buffer = 50 mM MES pH 5.5, 25 mM EDTA.

Table S1. Cysteine Reactivity in PBS pH7.45.

	Unbound			Cysteine adduct			
Compound	*m/z*	*Rt (min)*	*UV trace* [a]	*m/z*	*Rt (min)*	*UV trace* [a]	*Adduct (%)* [b]
ODN	526	7.17	12405	630 648	6.89 5.94	2012 498	17
2	500	7.04	9981	622 + 741 604 + 622	5.82 6.69	31739 67789	91
3	525	7.37	7680	646	N.D.	N.D.	0
4	499	7.22	33340	620	5.95	N.D.	0
5	513 531	7.45 7.20	3372 655	634	6.08	19	<1
6	577 +579 499	7.62 7.24	2777 14285	698 +700	6.12	3333	55 16*
E-64	358	3.48	13865	479	2.29	29459	68
Afatinib	486	4.24	672	607	3.83	40287	98
Ibrutinib	441	6.52	221	562	5.48	38525	99
Acalabrutinib	466 484	4.37 3.98	830 11577	587 587	3.65 3.83	3045 44337	98 79*

Table S2. Cysteine Reactivity in PBS pH8.0.

	Unbound			Cysteine adduct			
Compound	*m/z*	*Rt (min)*	*UV trace* [a]	*m/z*	*Rt (min)*	*UV trace* [a]	*Adduct (%)* [b]
ODN	526	7.17	4254	630	6.89	3991	48
2	500	7.05	2788	622 + 741 604 + 622	5.82 6.69	25216 88531	98
3	525	7.37	4808	646	N.D.	N.D.	N.D.
4	499	7.23	56360	620	5.95	120	<1
5	513 531	7.45 7.20	4292 736	634	6.08	N.D.	N.D.
6	577 +579 499	7.60 7.24	2521 20884	698 +700	6.12	4949	66 17*
E-64	358	3.35	10768	479	2.30	41119	79
Afatinib	486	4.20	1515	607	3.80	26503	95
Ibrutinib	441	6.53	221	562	5.47	31391	96
Acalabrutinib	466 484	4.35 3.97	1259 16347	587 587	3.64 3.82	2384 32415	97 66*

Reactivity with thiols determined by LC-MS. Black = expected/calculated m/z. Blue = hydrolysis of expected mass (+18). Red = degradation or unknown transformation. Adduct calculated as percentage of total adduct to remaining inhibitor. N.D.; not detected. [a] Integrated area under the curve using MassLynx software. [b] Adduct formation calculated from UV trace, after incubation of 100 µM inhibitor with 10 mM cysteine or 5 mM GSH in buffer at 37 °C for 23 hours. * Percentage adduct relative to inhibitor + hydrolysis/degradation of inhibitor.

Table S3. Cysteine Reactivity in MES pH5.5

	Unbound			Cysteine adduct			
Compound	*m/z*	*Rt (min)*	*UV trace* [a]	*m/z*	*Rt (min)*	*UV trace* [a]	*Adduct (%)* [b]
ODN	526	7.16	7517	630	6.92	72	<1
2	500	7.04	40007	622 + 741 604 + 622	5.80 6.67	1709 226	5
3	525	7.34	7895	646	5.85	47	<1
4	499	7.21	39781	620	5.92	107	<1
5	513 531	7.45 7.20	3559 743	634	6.08	16	<1
6	577 +579 499	7.59 7.21	7190 868	698 +700	6.14	65	<1
E-64	358	3.33	28853	479	1.67	184	<1
Afatinib	486	4.22	1806	607	3.81	19851	92
Ibrutinib	441	6.53	40920	562	5.46	4154	9
Acalabrutinib	466	4.36	32294	587 587	3.64 3.82	499 6949	19

Table S4. GSH Reactivity in PBS pH7.45.

	Unbound			GSH adduct			
Compound	*m/z*	*Rt (min)*	*UV trace* [a]	*m/z*	*Rt (min)*	*UV trace* [a]	*Adduct (%)* [b]
ODN	526	7.14	6870	833		N.D.	N.D.
2	500	7.03	43682	807	5.68	155	<1
3	525	7.34	1424	832		N.D.	N.D.
4	499	7.21	52505	806	5.86	24	<1
5	513 531	7.46 7.21	3145 721	820	5.84	56	2
6	577 +579 499	7.59 7.22	3564 21239	884 + 886 822	6.04 5.83	2561 559	47 11*
E-64	358	3.34	16266	665	2.59 2.80	28375	64
Afatinib	486	4.32	2209	793	3.88	35744	94
Ibrutinib	441	6.49	2725	748 764	5.41 5.21	28737 426	91
Acalabrutinib	466 484	4.29 4.91	3494 597	773	3.93	60735	95 94*

Reactivity with thiols determined by LC-MS. Black = expected/calculated m/z. Blue = hydrolysis of expected mass (+18). Red = degradation or unknown transformation. Adduct calculated as percentage of total adduct to remaining inhibitor. N.D.; not detected. [a] Integrated area under the curve using MassLynx software. [b] Adduct formation calculated from UV trace, after incubation of 100 µM inhibitor with 10 mM cysteine or 5 mM GSH in buffer at 37 °C for 23 hours. * Percentage adduct relative to inhibitor + hydrolysis/degradation of inhibitor.

Figure S8. Thiol Reactivity of **ODN**, nitrile **2** and alkyne **3**.

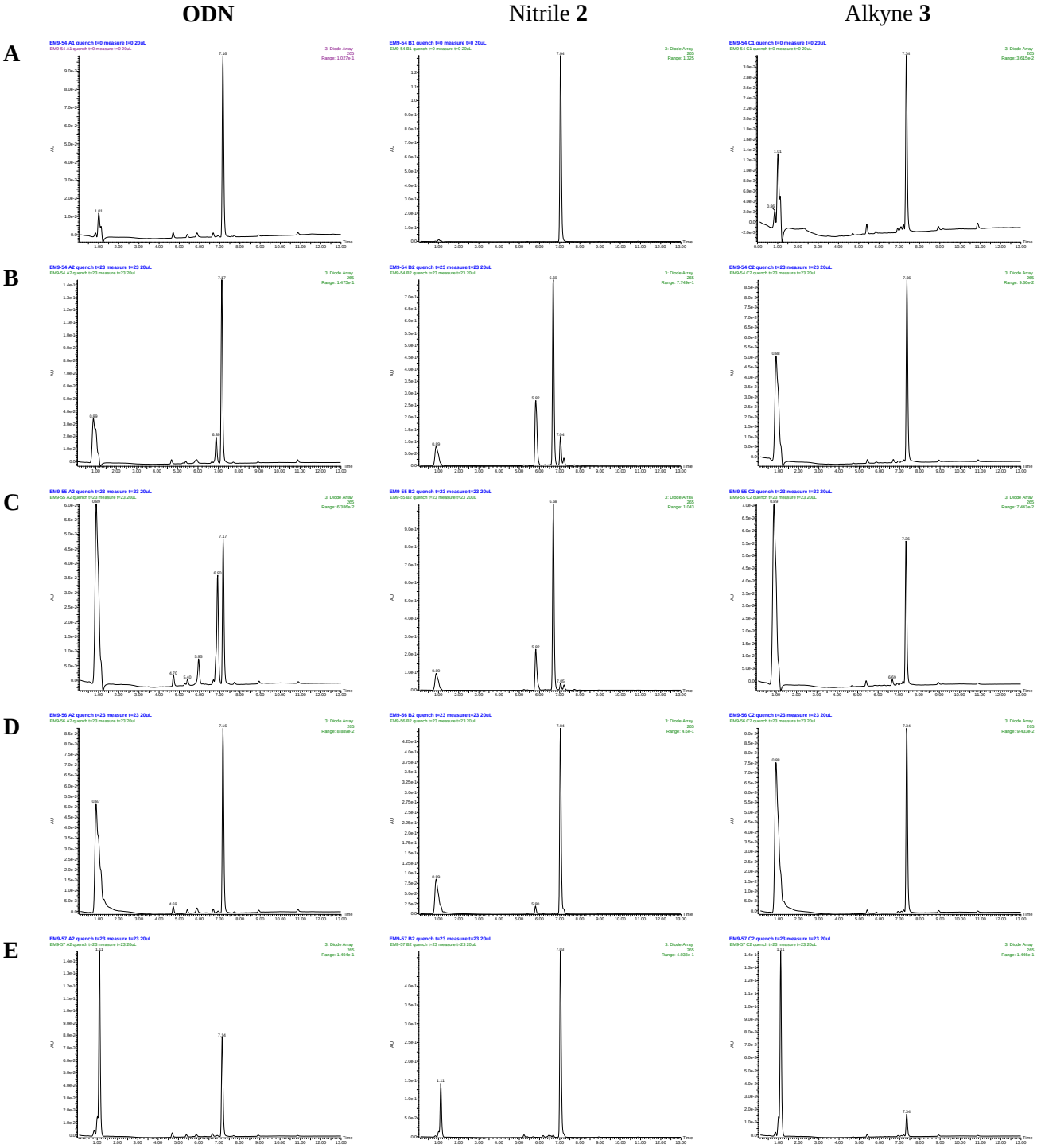

LC-MS UV traces (265 nm) of inhibitor in buffer A) Inhibitor in PBS pH 7.45. B) PBS pH 7.45 + 10 mM cysteine. C) PBS pH 8.0 + 10 mM cysteine. D) MES pH 5.5 + 10 mM cysteine. E) PBS pH 7.45 + 5 mM GSH.

Figure S9. Thiol Reactivity of alkyne **4**, alkyne **5** and alkyne **6**

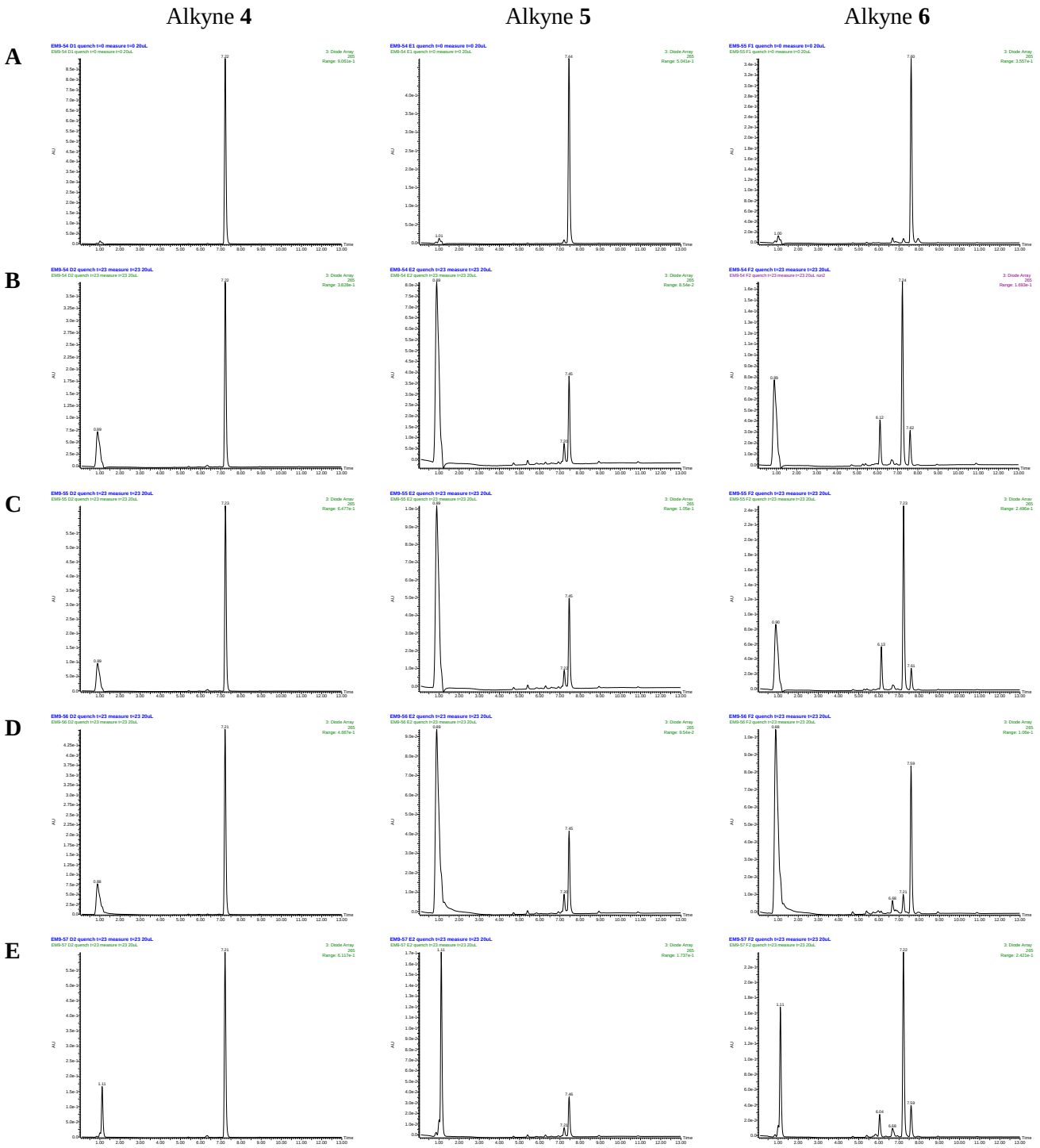

LC-MS UV traces (265 nm) of inhibitor in buffer A) Inhibitor in PBS pH 7.45. B) PBS pH 7.45 + 10 mM cysteine. C) PBS pH 8.0 + 10 mM cysteine. D) MES pH 5.5 + 10 mM cysteine. E) PBS pH 7.45 + 5 mM GSH.

Figure S10. Thiol Reactivity of E-64, Afatinib and Ibrutinib

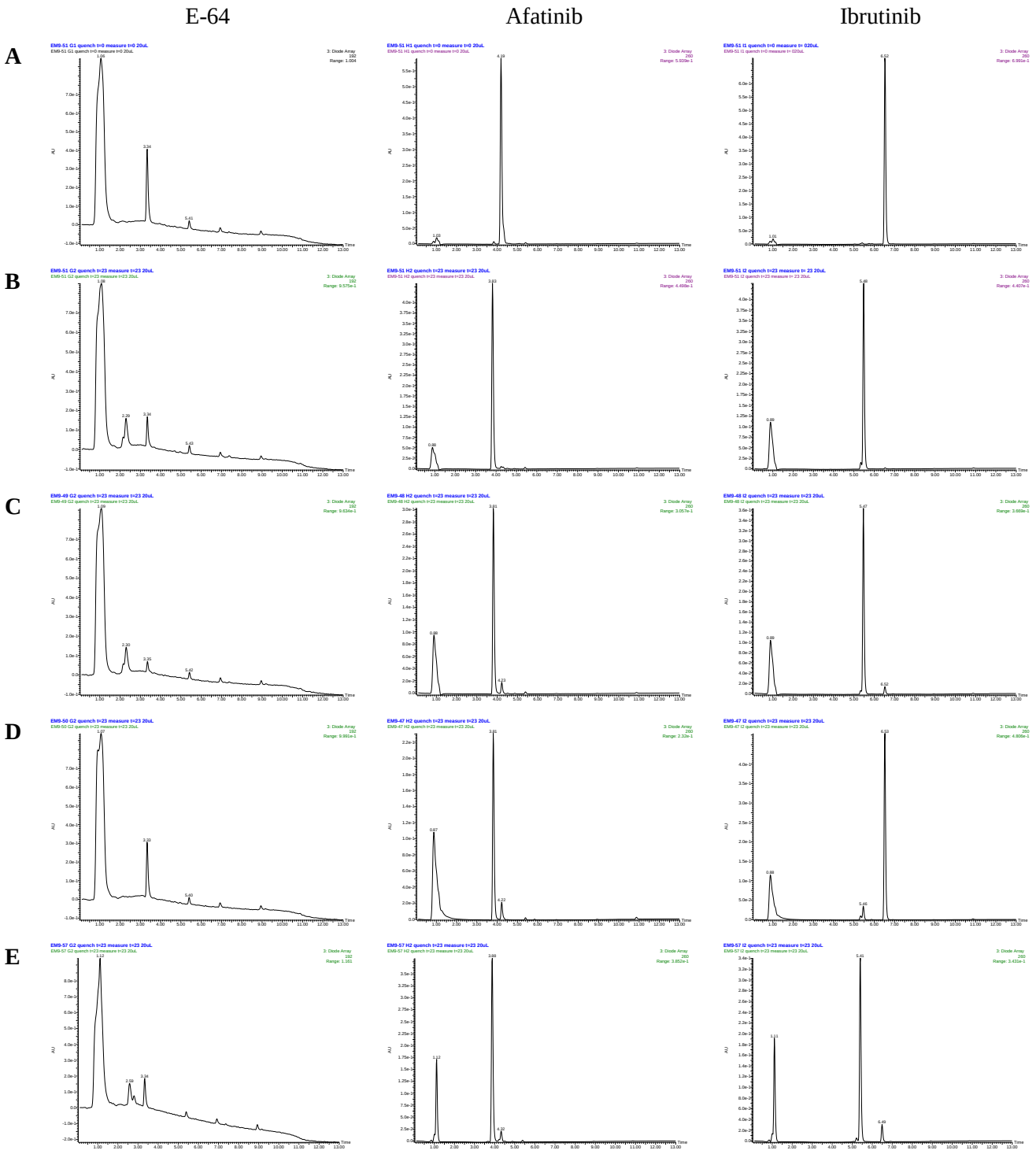

LC-MS UV traces (192 nm for E-64, 260 nm for Afatinib and Ibrutinib) of inhibitor in buffer A) Inhibitor in PBS pH 7.45. B) PBS pH 7.45 + 10 mM cysteine. C) PBS pH 8.0 + 10 mM cysteine. D) MES pH 5.5 + 10 mM cysteine. E) PBS pH 7.45 + 5 mM GSH.

Figure S11. Thiol Reactivity of Acalabrutinib

Acalabrutinib

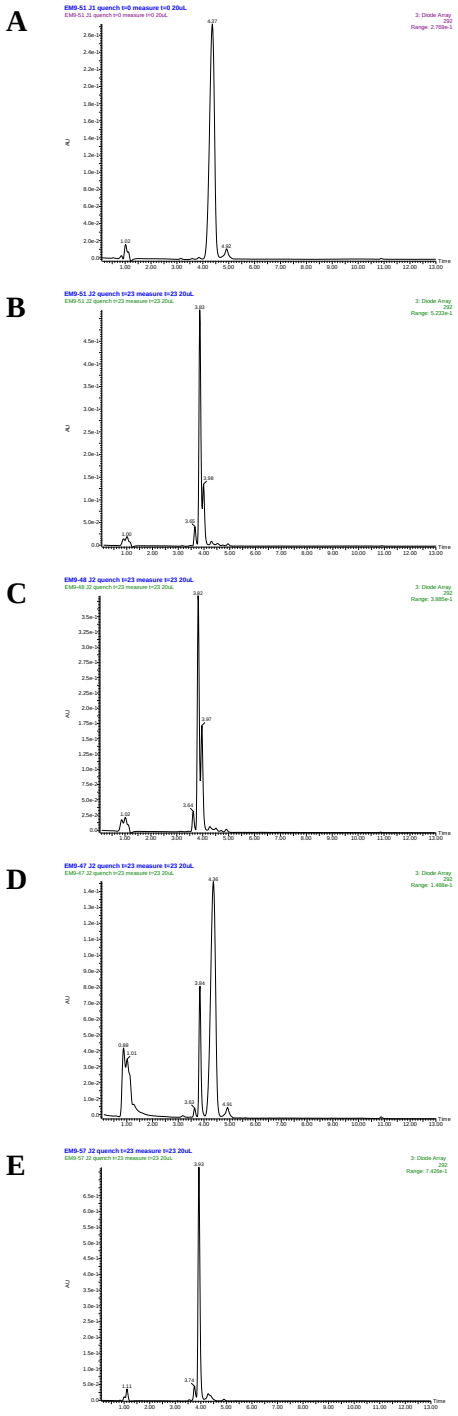

LC-MS UV traces (292 nm) of inhibitor in buffer A) Inhibitor in PBS pH 7.45. B) PBS pH 7.45 + 10 mM cysteine. C) PBS pH 8.0 + 10 mM cysteine. D) MES pH 5.5 + 10 mM cysteine. E) PBS pH 7.45 + 5 mM GSH.

***In vitro* inhibition assay**

Protease and substrate concentrations were optimized to allow for low inhibitor concentrations while keeping a linear increase in product formation for at least 20 minutes. Concentrations reported below are final concentrations (after addition of substrate). All substrate concentrations were at or below K_m-value if practical. Inhibitor concentrations range from 10 mM until 1-10x[protease].

Protease		*Fluorogenic substrate*		K_m
CatK	150 pM	Z-FR-AMC	40 μM	48.5 μM[22]
CatL	5 pM	Z-FR-AMC	4 μM	2.2 μM[9]
CatS	1 nM	Z-FVR-AMC	8 μM	8 μM[9]
CatV	25 pM	Z-FR-AMC	4 μM	4.8 μM[23]
CatB	1 nM	Z-RR-AMC	25 μM	173 μM[24]
Papain	3 nM	Z-FR-AMC	10 μM	0.42 mM[25]

Figure S12. Dose-Response Curves (DRC) for cysteine protease inhibition.

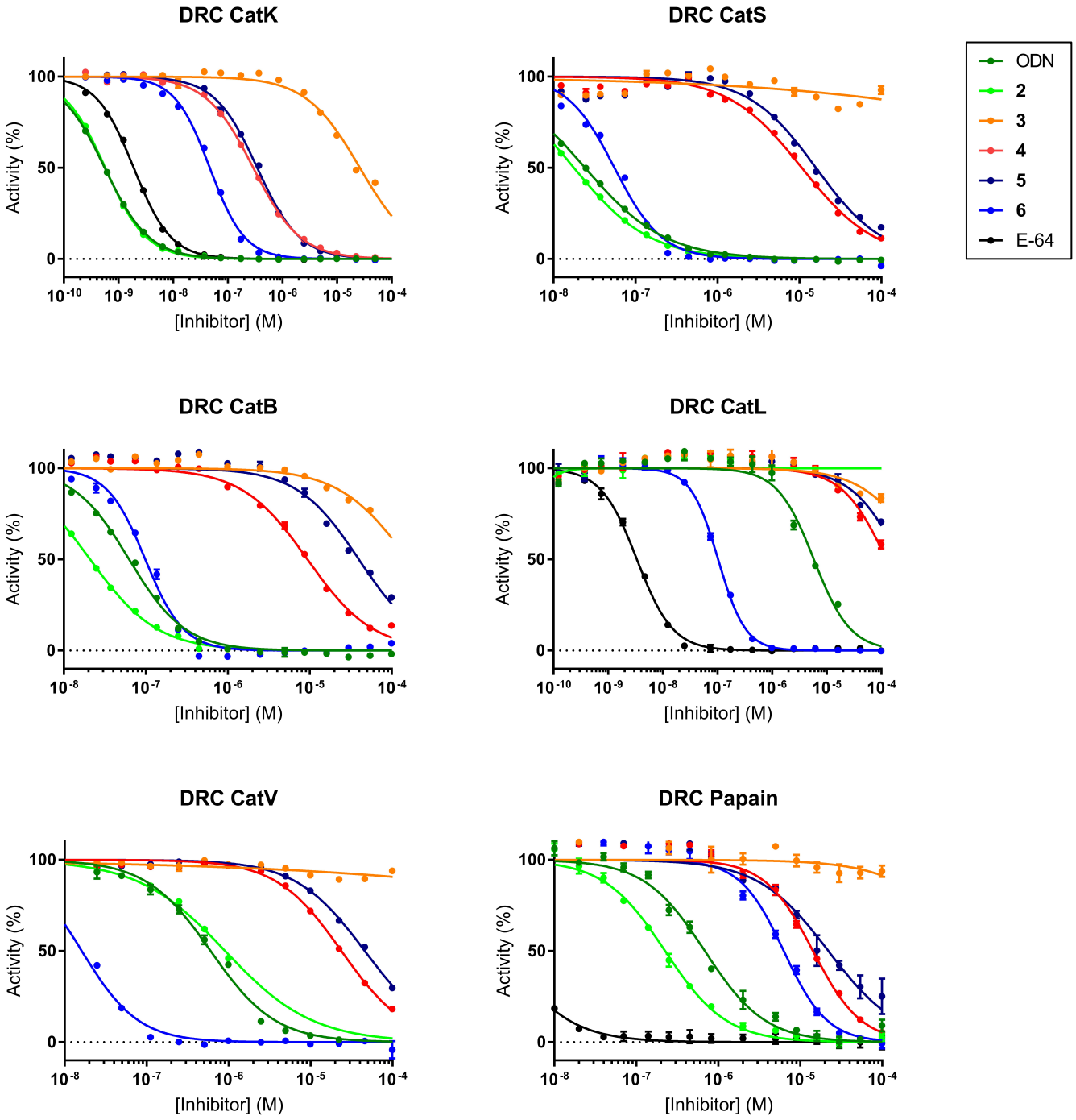

Dose-Response Curves (DRC) of concentration-dependent inhibition of cysteine protease hydrolysis activity by ODN and inhibitors **2**-**6**. Graphical data represents the mean ± standard deviation for a single representative experiment.

Reversibility of Inhibition; Jump dilution assay data

Detailed procedure jump dilution samples. Cathepsin K (120nM) in buffer containing 10 mM DTT was activated at 37 °C for 10 minutes. Compound (100 nL) was transferred to a 384-well plate and DMSO (1 μL) was added, followed by Cathepsin K (120 nM, 8.9 μL). The material was mixed (600 rpm, 26 °C) for 1 minute and the plate was spun down (1000 rpm) for 1 minute. The mixtures were incubated at 37 °C for 40 minutes, followed by incubation at 26 °C for 20 minutes. Then 1 μL was transferred to 99 μL Z-FR-AMC (4 μM), and 30 μL was further diluted in 60 μL Z-FR-AMC (4 μM) to yield a final Cathepsin K concentration of 0.35 nM. A sample of 25 μL was transferred to 384-well plate, which was shaken (600 rpm, 26 °C, 1 min) and spun down (1000 rpm, 1 min).

Detailed procedure control samples. Cathepsin K (0.5 nM) in buffer containing 10mM DTT was activated at 37 °C for 10 minutes. Compound (2.5-250 nL) was transferred to a 384-well plate with DMSO backfill to 250 nL, and DMSO (2.25 μL) was added, followed by Cathepsin K (0.5 nM, 17.5 μL). The material was mixed (600 rpm, 26 °C) for 1 minute and the plate was spun down (1000 rpm) for 1 minute. The mixtures were incubated at 37 °C for 40 minutes, followed by incubation at 26 °C for 20 minutes. Then 5 μL Z-FR-AMC (20 μM) was added to yield a final Cathepsin K concentration of 0.35 nM. The plate shaken (600 rpm, 26 °C, 1 min) and spun down (1000 rpm, 1 min).

Figure S13. Jump dilution assay

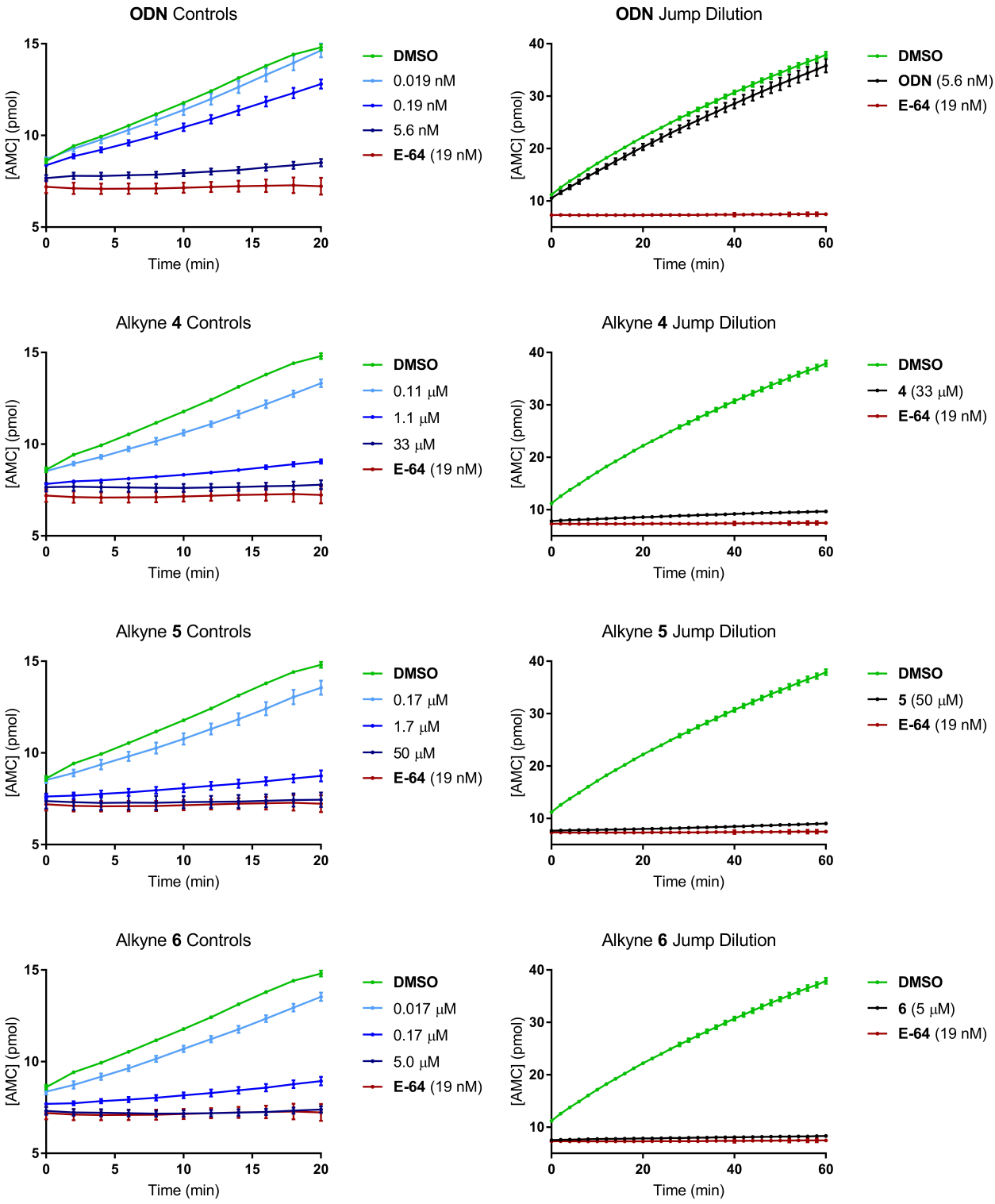

Left; Progress curves of substrate hydrolysis in the presence of inhibitor at different concentrations. Right; Progress curves of substrate hydrolysis after 300x dilution for DMSO, E-64 and inhibitor. Shown inhibitor concentrations correspond to concentration after addition of Z-FR-AMC substrate (controls) or prior to dilution (jump dilution samples).

Kinetic evaluation of covalent inhibitors

Equations and theoretical background on measurements can be found in the appendix on page SI-66. Fluorescence was measured in arbitrary units (A.U.) and converted to AMC formation in pmol. Values represent the increase in product formation relative to t=0 (baseline removal) to allow fitting to equation 1 (irreversible inhibitors) or equation 2 (reversible inhibitors). Assay conditions were optimized to obtain a robust signal with a linear increase in product formation for 60 minutes, but a strictly linear rate of product formation for the DMSO control could not be obtained. Therefore, the observed rate (k_{obs}) for DMSO was used as the minimum when calculating the inactivation rate (k_{inact}) or covalent bond formation/dissociation rates (k_5 and k_6). Standard deviations (SD) for k_{inact}/K_I were calculated by fitting the values to $SD_x/x = \sqrt{((SD_a/a)^2+(SD_b/b)^2)}$.

Figure S14. Kinetic Evaluation of Covalent Inhibitors

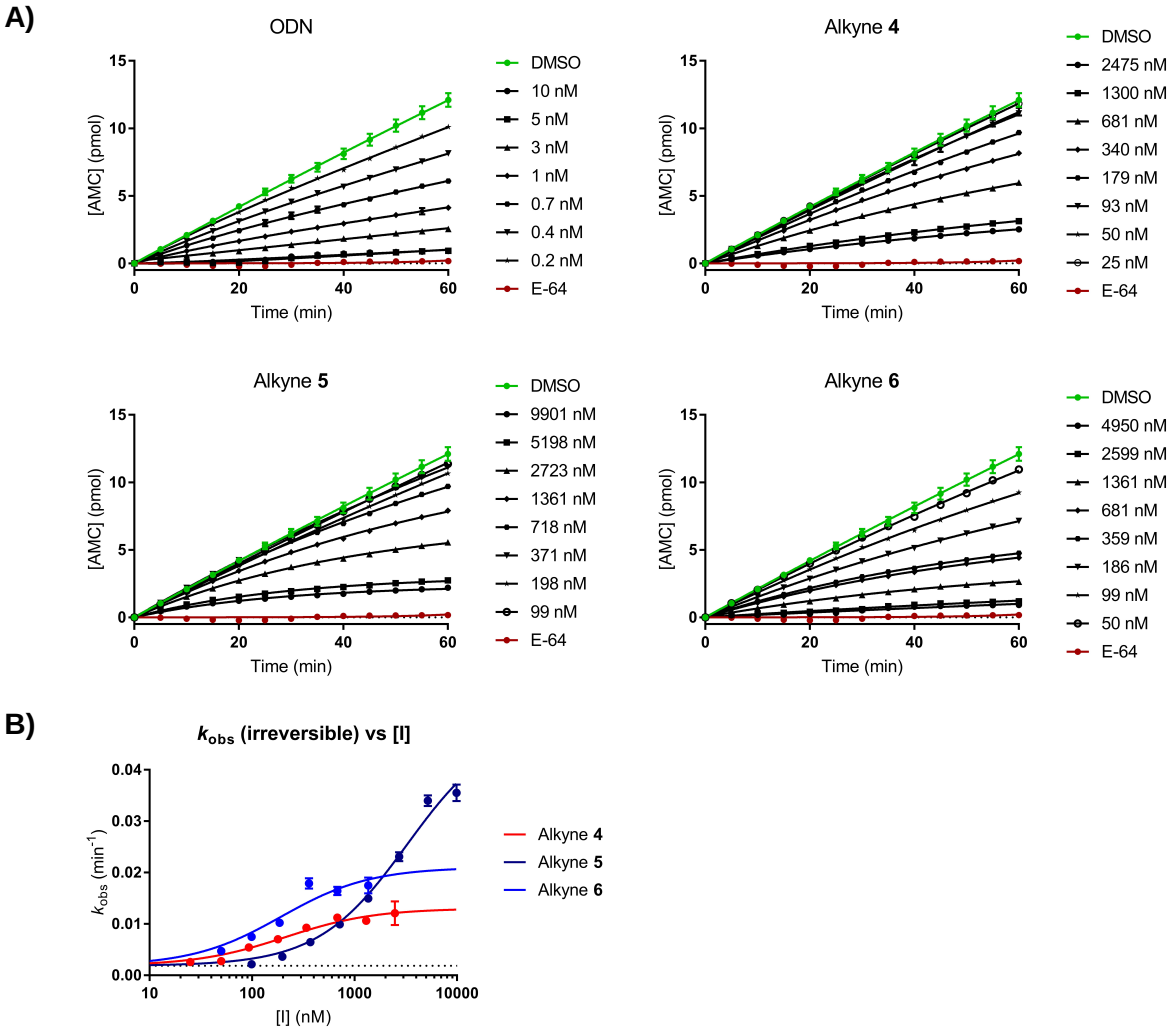

A) Progress curves of substrate hydrolysis in the presence of inhibitor at different concentrations (nM). Values were fitted to equation 2 (**ODN**) or equation 1 (alkyne **4**-**6**) to obtain k_{obs} at different inhibitor concentrations. B) Plot of k_{obs} vs. inhibition concentration. Values were fitted to equation 3 to obtain kinetic constants k_{inact} and K_I.

LC-MS for intact CatK and CatK-inhibitor complexes

Covalent bond formation was not observed for inhibitor **3**.

Figure S15. LC-MS of intact CatK-inhibitor complexes

Sample	*UPLC chromatogram*	*Electrospray ionization mass spectrum*	*Deconvoluted electrospray ionization mass spectrum (average isotopes)*
CatK	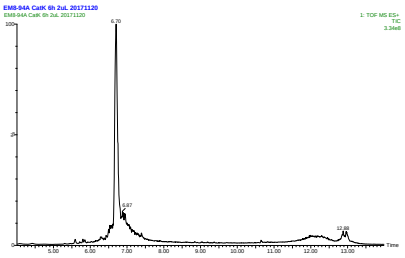	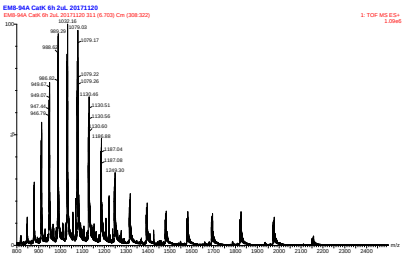	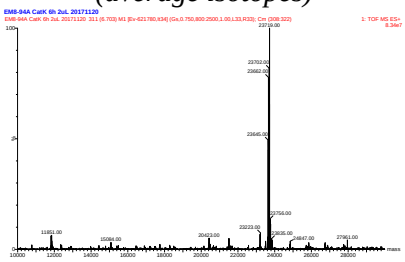 Measured 23719
CatK•**ODN**	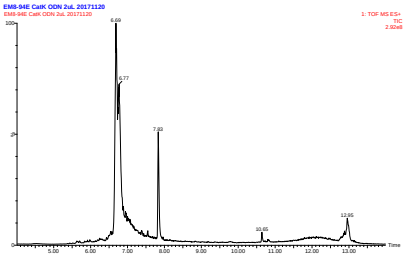	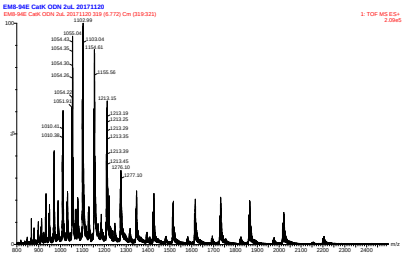	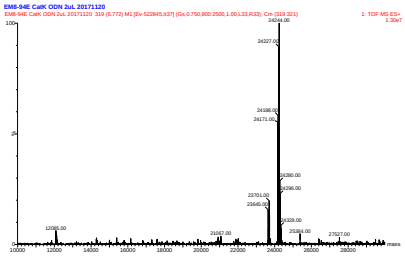 Calc. 24244 Measured 24244
CatK•**4**	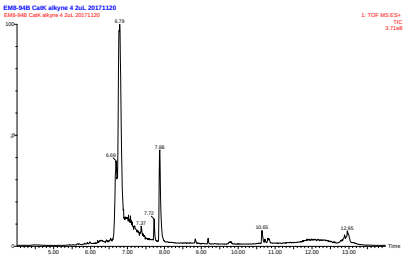	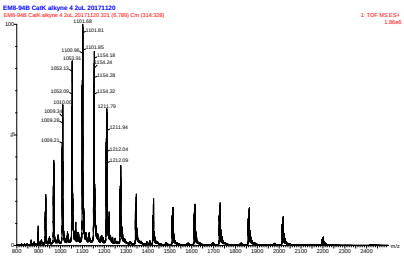	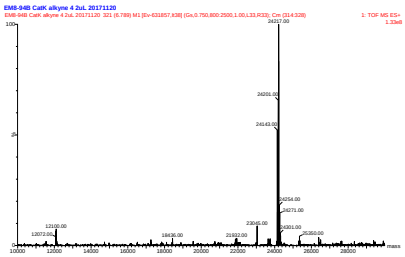 Calc. 24217 Measured 24217
CatK•**5**	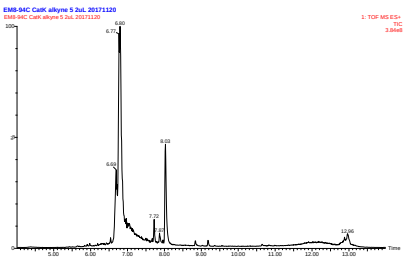	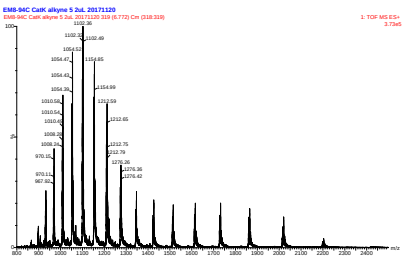	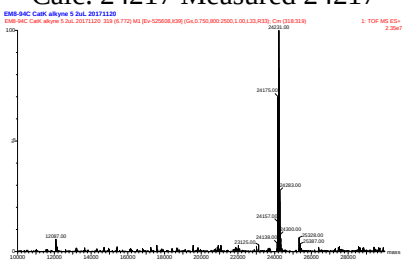 Calc. 24231 Measured 24231
CatK•**6**	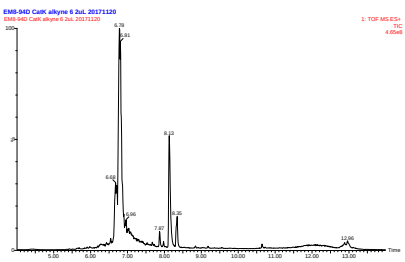	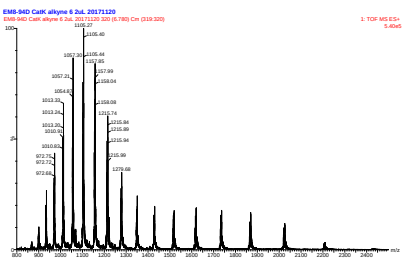	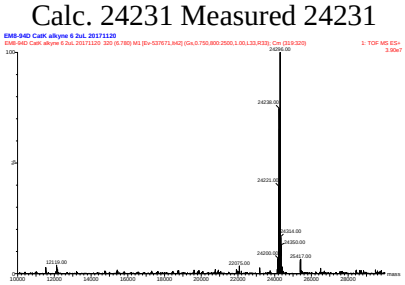 Calc. 24296 Measured 24296

Crystal structure of inhibitor 7 bound to CatK

Cathepsin K (CatK) crystallized in hexagonal space group P6122 with two molecules in the asymmetric unit. Both CatK molecules are well resolved along the whole chain from A1 to M215 as also indicated by the absence of Ramachandran plot outliers. The two molecules superimpose to each other with root-mean-square deviations (RMSD) of 0.33 Å over 215 CA atoms. Their positions are related by an approximately two-fold axis (177° and a screw of 0.93 Å). Inhibitors **7** bind to both molecules in the same way. In addition the crystal structure contains a calcium ion that stabilizes the packing of the two molecules forming the asymmetric unit, two chloride ions and 654 solvent molecules. The two active sites are positions at the 2-fold non-crystallographic symmetry axes, with Y67 rings positioned between the two inhibitor **7** molecules.

Inhibitor **7** binds in the non-primed site of the active site of CatK (Figure S5A). Positions of all its non-hydrogen atoms were unambiguously resolved by the electron density maps (Figure S5B). Only the weaker density of the terminal SO_2-methyl group indicated possible rotational disorder along the C27 and S30 bond. The comparable atomic B-factors (mean 14.9 $Å^2$) of inhibitor 7 to those of CatK residues in its vicinity indicated that inhibitor bound to close to 100% of CatK molecules in the crystal. The alkyne moiety of inhibitor **7** binds in the S1 subsite of CatK. The electron density map in the Figure S5B shows that C2 atom of inhibitor **7** is covalently attached to the SG atom of the reactive site Cys25, whereas the angles and planarity of the electron density map at the C1 atom indicate that the alkyne moiety has undergone transition from the sp hybridization represented by linear structure to the sp2 hybridization of vinyl fragment observed in the structure. The amide links vinyl moiety to the leucine-like fragment. The amide stabilizes the binding by hydrogen bonds formed on both sides - with the carbonyl of N161 on the right and peptidyl nitrogen of G66 on the left. The hydrophobic part of the leucine fragment is bound into the S2 subsite of CatK in a substrate like manner. It packs against hydrophobic surfaces of Y67, M68, A134, A163, and L209. The amino protons form another hydrogen bond with the G66 carbonyl. The C13 is a chiral atom to which the trifluoromethyl group, that points into the solvent on the right, and the biphenyl group, that binds along the aromatic surface of two peptide bonds of G65-G66 and N60-D61, are attached. The phenyl rings are slightly (17°) out of plane. The terminal SO_2 methyl groups is facing solvent and packs against the Y67 side chain from the other CatK molecule in the asymmetric unit.

Table S5. Data collection and refinement statistics

Unit cell	a = 75.351, b = 75.351, c =340.184, α = β = 90.0˚, γ = 120.0˚
Space group	P61 2 2 (number 178)
molecules per au	2
wavelength (Å)	0.97912
Resolution range (Å)	47.09 - 1.7
No. of unique reflections	64186
Completeness (last shell) (%)	99.9 (99.3)
Multiplicity (last shell)	33.1 (24)
R meas (last shell) (%)	0.177 (0.978)
I/σ	16.3 (2.2)

PDB ID	6QBS
Resolution range (Å)	47.09 - 1.7
No. of reflections in working set	64031
No. of reflections in test set	64031
R-kick value	21.0
RMSD Bond lengths (Å)	0.02
RMSD Bond angles (°)	2.0
No. of atoms in au	4018
Protein atoms	3298
Water molecules	654
Cl^-	2
Ca^{2+}	1
Mean *B* value (Å^2)	19.3
Ramachandran plot statistics	
Favored	412
Allowed	14
Outliers	0

Staining cells for TRAP & Cell counting

Mature, resorbing osteoclasts are multinucleated and are TRAcP positive. Tartrate-resistant acid phosphatase (TRAcP) is a commonly used histochemical marker of osteoclasts, and secretion of TRAcP is correlated with resorptive behavior.[26] TRAcP is upregulated upon selective CatK inhibition (either genetic or pharmaceutical).[27] We could observe an increase in the number of mature osteoclasts upon treatment with high concentrations of inhibitor.

Figure S16. TRAcP Staining of OCs treated with DMSO or E-64

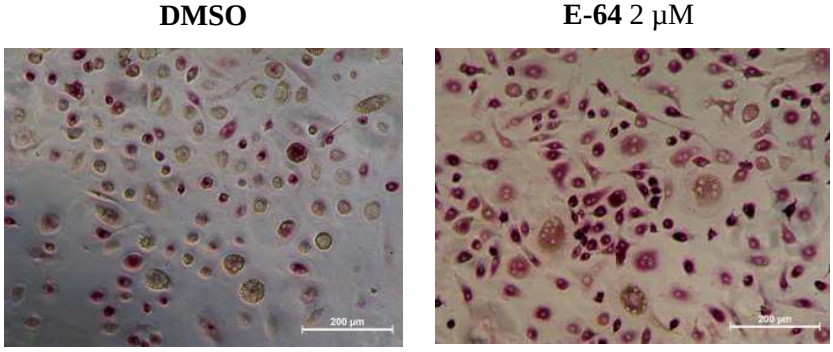

Figure S17. TRAcP Staining of OCs on plastic treated with ODN, alkyne **4** and alkyne **5**

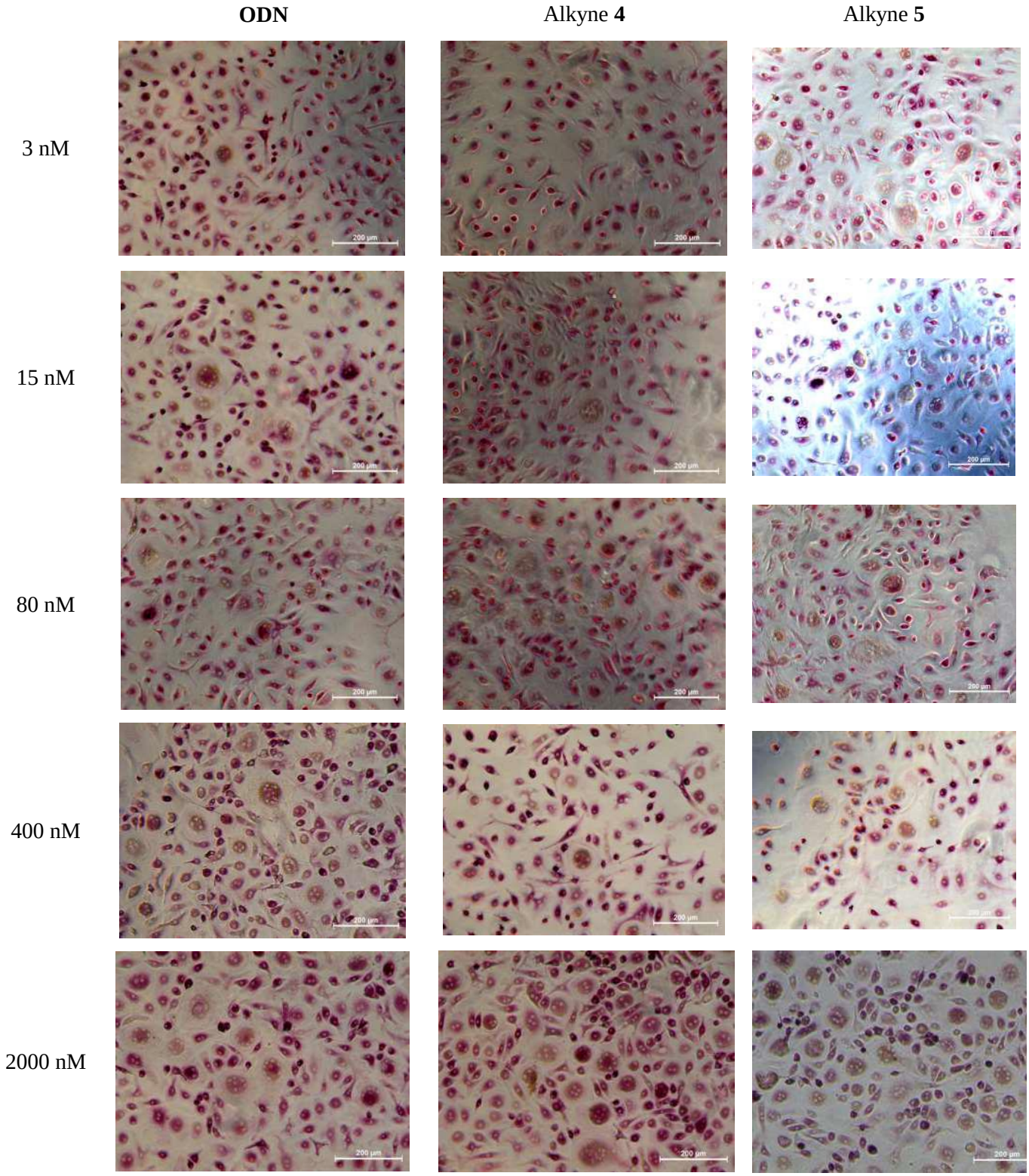

Staining of resorption pits on bone slices

Bone resorption by osteoclasts is not homogeneously distributed over bone slices, and it can be hard to select representative areas on the bone for bone resorption quantification. Therefore, we included an overview to compare the total bone resorption on a bone slices, as judged by visual assessment. A larger number of resorption areas correlates with more active, resorbing osteoclasts. Trenches are characteristic of fully functional osteoclasts, pits are more commonly seen in osteoclasts with impaired CatK activity. However, trenches and pits can be observed in both cases, possibly because mature osteoclasts are formed between day 3 and day 7 in absence of inhibitor, allowing osteoclasts that matured before day 7 to resorption. Additionally, we determined the total bone resorption area (Figure S6). Please note that this only considers the area of resorption, not the depth of the resorption pits (trenches are deeper than trenches, so more bone is resorbed in the same area).

Table S6. Average bone resorption

Inhibitor	*Conc. (nM)*	*Number of resorption areas*	*Trench*	*Pit*
E-64	2000	++	+	-
ODN	3	++	+	-
	16	-	+/-	+
	80	+	+/-	+
	400	++	-	+
	2000	+	+	+
4	3	+	+	-
	16	+	+	-
	80	+/-	+	+
	400	+/-	-	+
	2000	-	+/-	+
5	3	+/-	+	+
	16	+/-	+	+
	80	+/-	+	-
	400	+/-	+	-
	2000	-	+	+

Figure S18. Staining of bone resorption area for OCs treated with DMSO or E-64

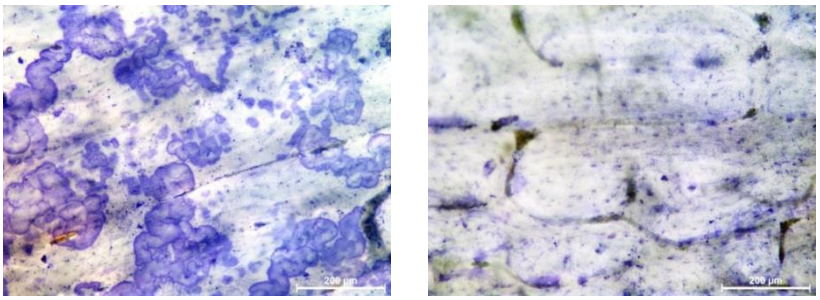

DMSO **E-64** (2 µM)

Figure S19. Staining of bone resorption area for ODN, alkyne **4** and alkyne **5**

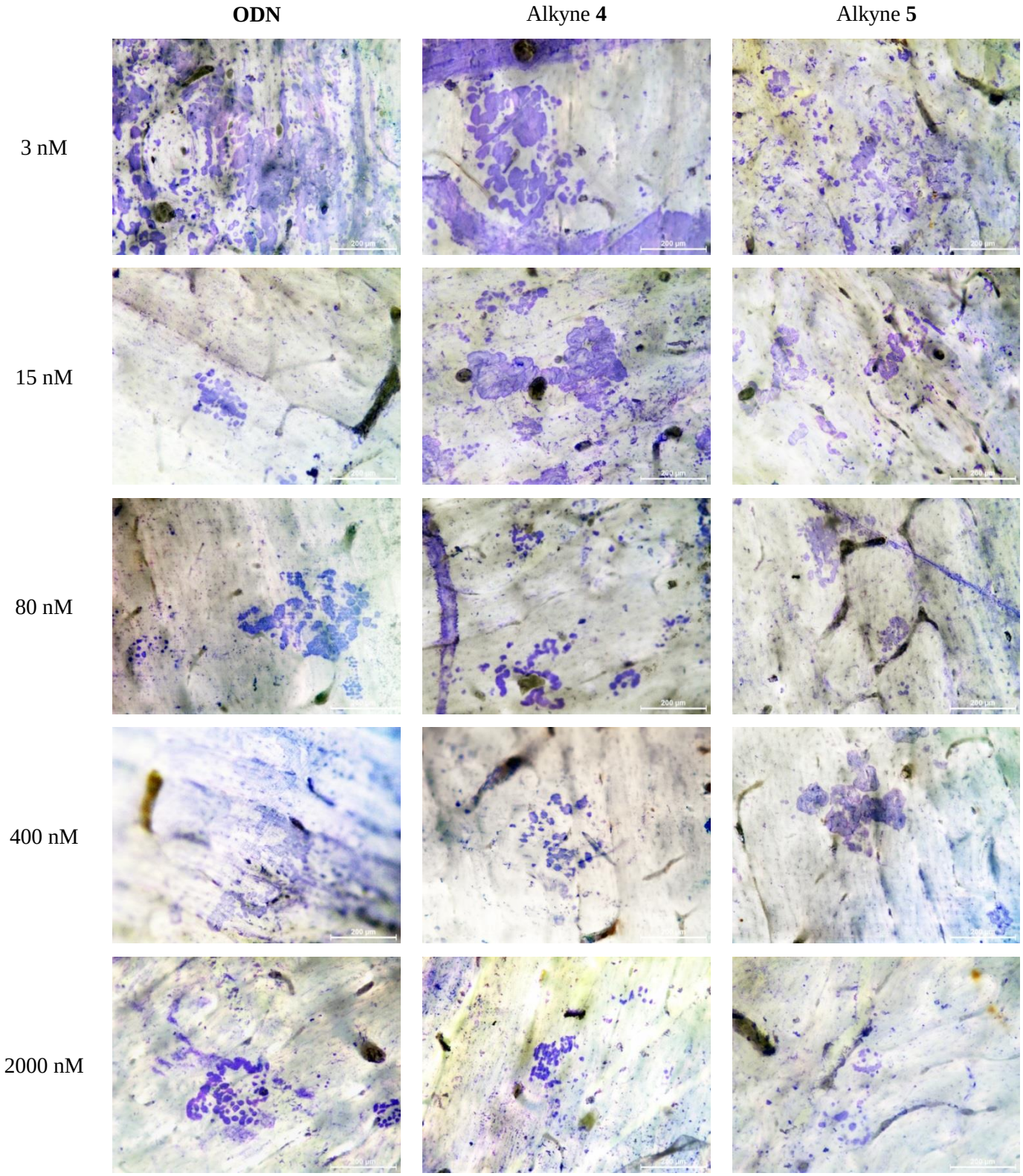

Cathepsin K activity in osteoclast lysates

Lysates were stored at -20 ºC, thawed and incubated with quenched activity-based probe BMV109. In the first lane was loaded 5 nM human Recombinant CatK (Enzo Lifesciences, BML-SE553-0010) that also was incubated with BMV109 for 2 hours. Fluorescence Scan revealed that only small amounts of mature CatK are present in DMSO-treated OCs, possibly because mature CatK is self-degrading. Surprisingly, all concentrations of ODN show an increase of CatK activity, while OCs treated with alkyne **4** and **5** do not show any CatK activity. Staining of the gels shows that differences in CatK activity are not the result of loading differences. As stated in the paper, we believe the observed CatK activity in ODN-treated OC lysates is an artifact caused by competition between the reversibly binding ODN and excess of the irreversibly binding activity-based probe BMV109. We did not observe this effect for alkynes **4** and **5** because these inhibitors form an irreversible bond with CatK and can thus not be removed by addition of excess probe BMV109.

Figure S20. Full gel scans for OC lysates treated with 1 µM BMV109 for 2 hours.

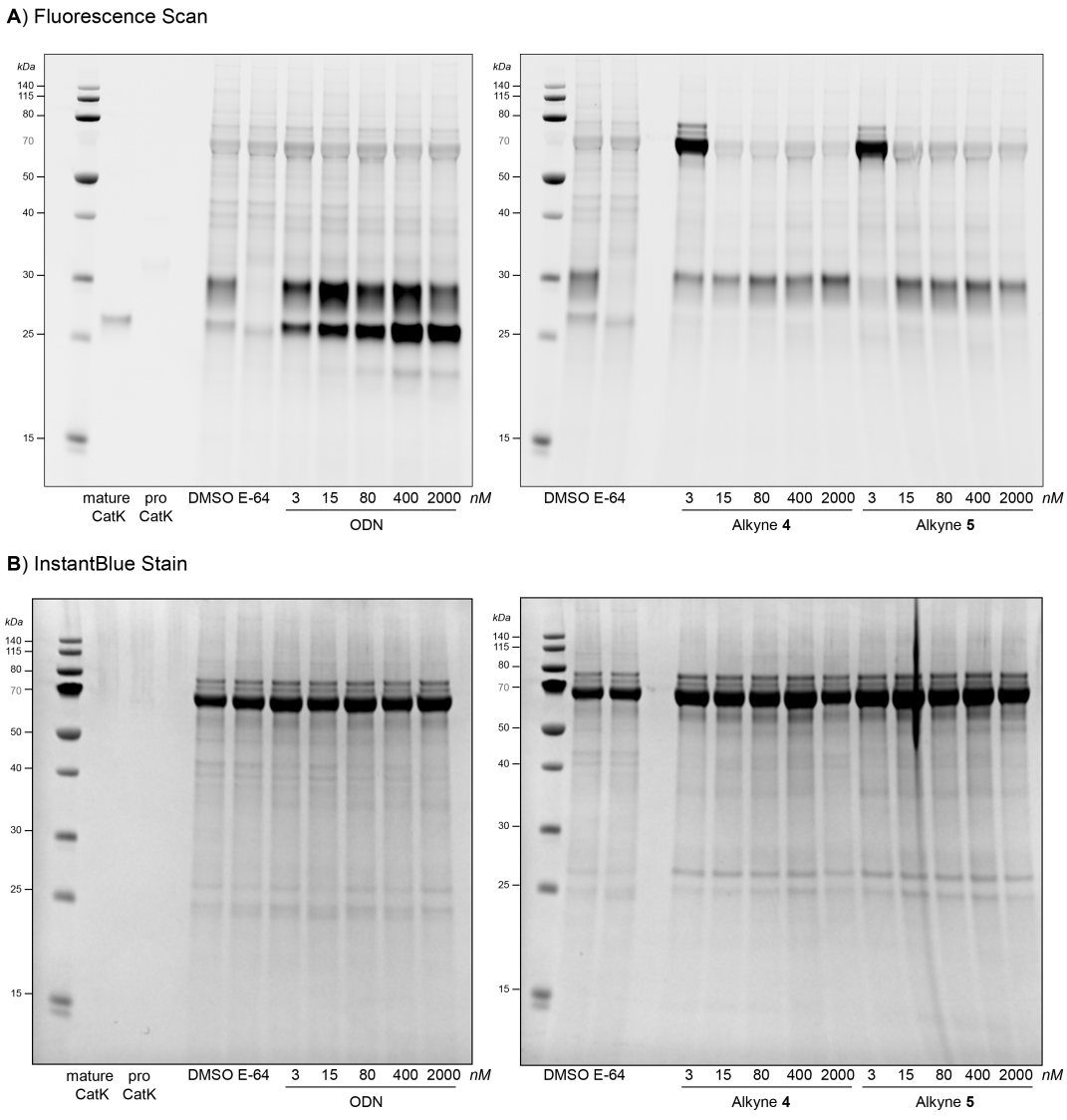

Cathepsin K expression in osteoclast lysates

Lysates were stored at -20 ºC, thawed and 10 μL was loaded on gel. Human recombinant mature CatK (230 ng) and human recombinant pro-CatK (300 ng) were loaded on gel as references. The CatK concentration in OC lysate was very low and could best be visualized using an HRP secondary antibody. The different CatK species could be clearly identified in the controls. OC lysates treated with ODN showed an increase in mature CatK inside the cells, which confirmed that the increase in CatK activity observed with activity-based probe BMV109 was the result of mature CatK activity. For OC lysates treated with high concentrations of inhibitor **4** and **5** we also observed an increase of mature CatK inside the cells, but its activity was inhibited (shown in Figure S20).

Figure S21. Full blots for OC lysates.

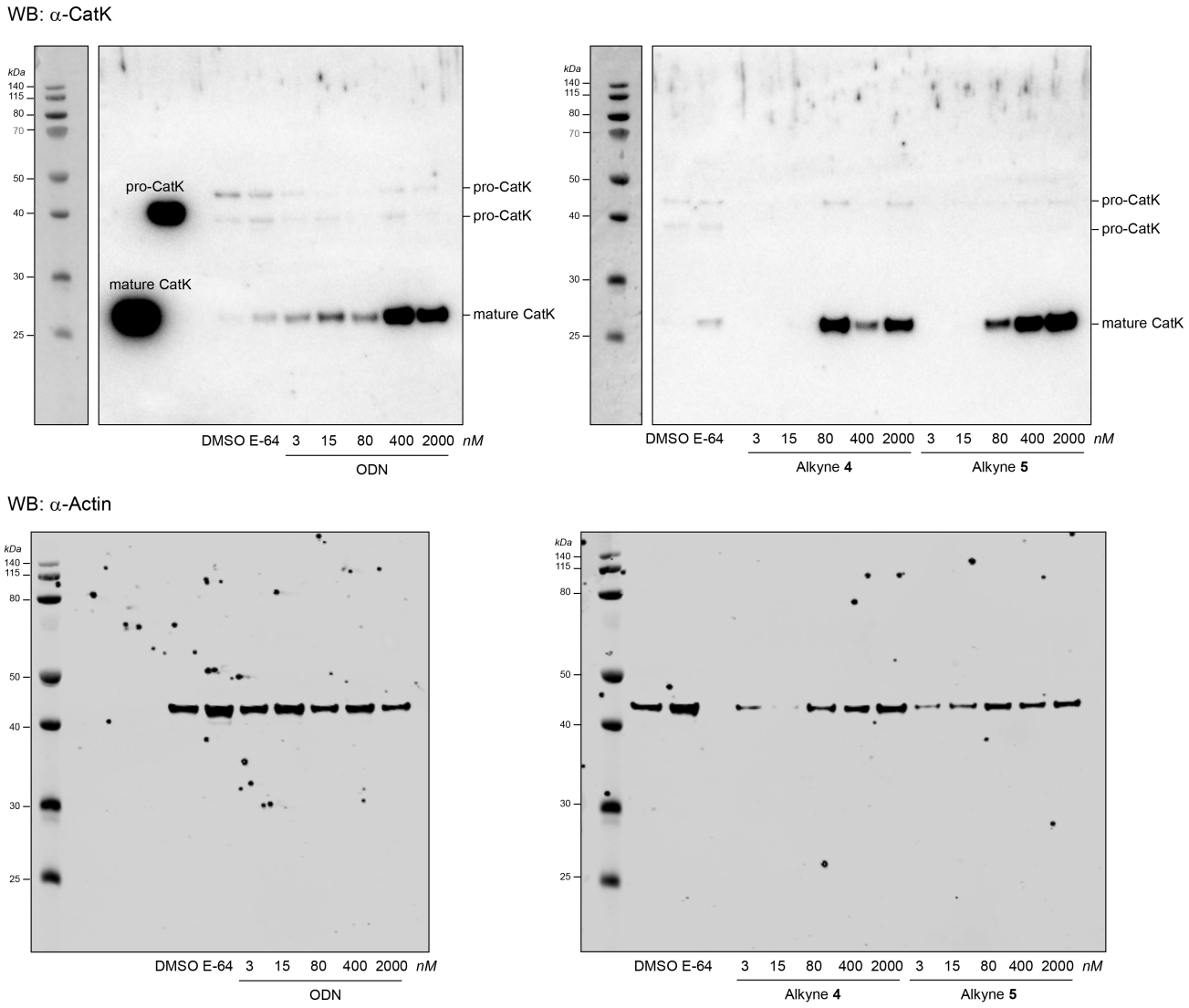

Top: anti-CatK. Bottom: anti-Actin.

Chemical Synthesis

General Information

All commercially available reagents and solvents were used as purchased. Nuclear magnetic resonance (NMR) spectra were recorded on a Bruker Avance 300 (300 MHz for ^{1}H, 75.00 MHz for ^{13}C) using the residual solvent as internal standard (^{1}H: δ 7.26 ppm for $CDCl_3$ and 2.50 ppm for DMSO. $^{13}C\{^{2}H\}$: δ 77.16 ppm for $CDCl_3$ and 39.52 ppm for DMSO). Chemical shifts (δ) are given in ppm and coupling constants (*J*) are quoted in hertz (Hz). Resonances are described as s (singlet), d (doublet), t (triplet), q (quartet), b (broad) and m (multiplet) or combinations thereof. Compounds were analyzed using 2D NMR techniques HSQC and HMBC, and coupling constants (*J*) are reported accordingly. ^{13}C APT spectra were obtained to assign C-F coupling constants (*J*) when relevant. Analytical LC-MS analysis was performed on a Waters Alliance 2795 Separation Module system equipped with Waters 2996 Photodiode Array Detector (190-750 nm), Waters Xbridge C_{18} column (2.1x100 mm, 3,5 µm) and LCT ESI- Orthogonal Acceleration Time of Flight Mass Spectrometer. Samples were run with a 13 min gradient using 2 mobile phases: A = 1% CH_3CN, 0.1% formic acid in water and B = 1% water and 0.1% formic acid in CH_3CN. Data processing was performed using Waters MassLynx Mass Spectrometry Software 4.1. Electrospray Ionization (ESI) high-resolution mass spectrometry was carried out using a Waters XEVO-G2 XS QTOF UPLC-MS system with a Waters Acquity CM detector in positive ion mode in combination with a Waters Acquity UPLC system equipped with a ACQUITY UPLC® Protein BEH C4 Column (300 Å, 1.7 µm, 2.1 x 50 mm) using water/acetonitrile mixtures containing 0.1% formic acid. Thin Layer Chromatography (TLC) was performed using TLC plates from Merck (SiO_2, Kieselgel 60 F254 neutral, on aluminum with fluorescence indicator) and compounds were visualized by UV detection (254 nm) unless mentioned otherwise. Flash column chromatography (FCC) purifications were performed using Grace Davisil Silica Gel (particle size 40–63 µm, pore diameter 60 Å) and the indicated eluent. Reversed phase preparative HPLC/MS was carried out on a Waters AutoPurification system equipped with a Waters 2998 photodiode array detector, Waters 3100 mass detector and a Waters 2767 sample manager using preparative Waters X-bridge C_{18} 5 µm (30 mm x 150 mm or 19 mm x 150 mm) column in combination with water acetonitrile mixtures containing 0.1% TFA. Fractions containing the product were automatically collected based on observed mass and UV-signal after which they were lyophilized to obtain the pure products. Reported yields are not optimized.

Synthesis of Precursors 1 and 8

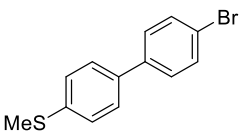

(4'-bromo-[1,1'-biphenyl]-4-yl)(methyl)sulfane **9**

(4-(methylthio)phenyl)boronic acid (3.81 gr, 22.67 mmol), 1-bromo-4-iodobenzene (5.83 gr, 20.61 mmol) and sodium carbonate (6.55 gr, 61.8 mmol) were dissolved in a mixture of DME/water (180 mL, 4:1 v/v). The mixture was degassed with argon for 5 minutes, then Bis(triphenylphosphine)palladium(II) dichloride (579 mg, 0.824 mmol) was added and the mixture was heated to

100 °C. After stirring for 5 hours, the reaction mixture was allowed to cool to room temperature. The reaction was quenched with water and extracted with EtOAc (2x). The combined organic layers were washed with brine (2x), dried (Na_2SO_4) and concentrated under vacuum to give a reddish solid as residue (18.5 gr). The crude material was coated on silica and purified by FCC (5% diisopropyl ether in heptane) to give product **9** as a white solid (4.04 gr, 13.6 mmol, 66%). Spectral data was in agreement with published data.[28]

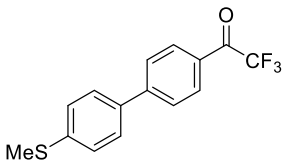

2,2,2-trifluoro-1-(4'-(methylthio)-[1,1'-biphenyl]-4-yl)ethanone **10**

According to published procedure,[28] the reaction of (4'-bromo-[1,1'-biphenyl]-4-yl)(methyl)sulfane **9** (4.04 gr, 14.47 mmol) with ethyl trifluoroacetate (3.44 mL, 28.9 mmol) and n-BuLi (8.68 mL, 2.5M in hexanes, 21.71 mmol) afforded product **10** as a light-yellow solid (2.27 gr, 7.66 mmol, 53%). Spectral data was in agreement with published data.[28]

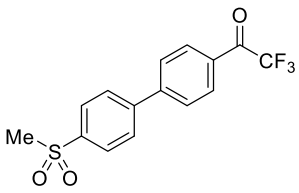

2,2,2-trifluoro-1-(4'-(methylsulfonyl)-[1,1'-biphenyl]-4-yl)ethanone **11**

According to published procedure,[28] the reaction between 2,2,2-trifluoro-1-(4'-(methylthio)-[1,1'-biphenyl]-4-yl)ethanone **10** (2.27 g, 7.66 mmol), tetrabutylammonium hydrogen sulfate (130mg, 0.383 mmol), sodium tungstate dehydrate (126 mg, 0.383 mmol) and hydrogen peroxide (2.3 mL, 30% aqueous, 22.98 mmol) afforded ketone **11** as a white solid (2.42gr). The material was then dehydrated in a Dean-Start set up by drying the water/toluene azeotrope over molecular sieves. The toluene solution (250 mL) was refluxed overnight. The solution was then cooled to room temperature and concentrated under vacuum to afford ketone **11** as a white crystalline solid (2.30 g, 7.01 mmol, 91%) which was used in the next step. Spectral data was in agreement with published data.[28] ^{1}H NMR (300 MHz, $CDCl_3$) δ = 8.19 (ddt, *J* = 8.0, 2.3, 1.1 Hz, 2H), 8.11 – 8.03 (m, 2H), 7.89 – 7.74 (m, 4H), 3.11 (s, 3H). ^{13}C NMR (75 MHz, $CDCl_3$) δ = 180.11 (q, *J* = 35.4 Hz), 146.02, 144.65, 140.76, 131.02 (q, *J* = 2.0 Hz), 129.80, 128.48, 128.36, 128.20, 116.73 (q, *J* = 291.2 Hz), 44.67.

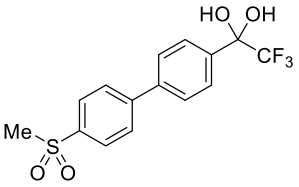

2,2,2-trifluoro-1-(4'-(methylsulfonyl)-[1,1'-biphenyl]-4-yl)ethane-1,1-diol **12**

Analysis of ketone **11** in Acetone-d_6 or DMSO-d_6 containing trace amounts of water resulted in the (partial) formation of hydrate **12**, which was confirmed by the shift of the CF_3 signal from 180.11 ppm to 123.53 ppm in ^{13}C NMR (APT). ^{1}H NMR (300 MHz, DMSO-d_6) δ 8.05 – 7.93 (m, 4H), 7.85 – 7.70 (m, 4H), 7.67 (s, 2H), 3.27 (s, 3H). ^{13}C NMR (75 MHz, DMSO-d_6) δ 144.54, 139.85, 139.01 (d, *J* = 4.6 Hz), 128.25, 127.73, 127.71, 126.65, 123.53 (q, *J* = 289.0 Hz), 92.47 (q, *J* = 31.2 Hz), 43.59.

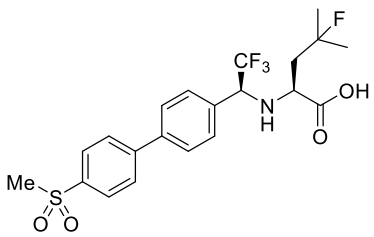

(S)-4-fluoro-4-methyl-2-(((S)-2,2,2-trifluoro-1-(4'-(methylsulfonyl)-[1,1'-biphenyl]-4-yl)ethyl)amino)pentanoic acid **1**

According to published procedure,[29] the reaction of ketone **11** (1.23 gr, 3.75 mmol) with (S)-ethyl 2-amino-4-fluoro-4-methylpentanoate hydrochloride (1.00 gr, 4.68 mmol), potassium carbonate (2.07 gr, 15 mmol), and subsequent reduction with zinc chloride (1.02 gr, 7.49 mmol) and sodium borohydride (567 mg, 15 mmol) afforded a mixture of desired (S,S)-**1** and (R,S)-**1**, which were separated by preparative reverse phase HPLC to yield precursor (S,S)-**1** as a white solid (460 mg, 1.0 mmol, 27%). Spectral data of (S,S)-**1** was in agreement with published data.[30] LCMS (ESI^+); Rt = 7.32 min. m/z = 462.11 $[M+H]^+$. ^1H NMR (300 MHz, $CDCl_3$) δ = 8.08 – 7.96 (m, 2H), 7.83 – 7.73 (m, 2H), 7.68 – 7.59 (m, 2H), 7.51 (d, J = 8.1 Hz, 2H), 4.31 (q, J = 7.1 Hz, 1H), 3.68 (dd, J = 8.1, 4.1 Hz, 1H), 3.10 (s, 3H), 2.19 (ddd, J = 24.8, 15.1, 4.2 Hz, 1H), 1.99 (ddd, J = 17.7, 15.0, 8.1 Hz, 1H), 1.48 (d, J = 21.8 Hz, 3H), 1.46 (d, J = 21.7 Hz, 3H). ^{13}C NMR (75 MHz, $CDCl_3$) δ = 175.93, 145.75, 140.55, 139.74, 133.89, 129.44, 128.19, 128.16, 125.26 (q, *J* = 281.8 Hz), 95.77 (d, *J* = 165.0 Hz), 62.91 (q, *J* = 29.5 Hz), 56.61, 44.74, 43.58 (d, *J* = 21.5 Hz), 27.53 (d, *J* = 24.3 Hz), 26.84 (d, *J* = 24.4 Hz).

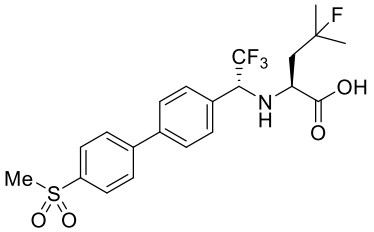

(S)-4-fluoro-4-methyl-2-(((R)-2,2,2-trifluoro-1-(4'-(methylsulfonyl)-[1,1'-biphenyl]-4-yl)ethyl)amino)pentanoic acid **1**

(R,S)-**1** was obtained as the minor isomer in above described synthesis. LCMS (ESI^+); Rt = 7.04 min. m/z = 462.11 $[M+H]^+$. ^1H NMR (300 MHz, $CDCl_3$) δ = 8.08 – 7.99 (m, 2H), 7.82 – 7.73 (m, 2H), 7.67 (d, *J* = 8.2 Hz, 2H), 7.52 (d, *J* = 7.9 Hz, 2H), 4.12 (q, *J* = 7.1 Hz, 1H), 3.47 – 3.37 (m, 1H), 3.11 (s, 3H), 2.15 – 1.91 (m, 2H), 1.39 (d, *J* = 22.1 Hz, 3H), 1.15 (d, *J* = 21.6 Hz, 3H). ^{13}C NMR (75 MHz, $CDCl_3$) δ = 174.52, 145.64, 140.73, 139.82, 133.00, 129.73, 128.21, 128.06, 124.72 (q, *J* = 280.7 Hz), 96.47 (d, *J* = 164.3 Hz), 63.50 (q, *J* = 29.6 Hz), 56.68, 44.75, 43.14 (d, *J* = 20.2 Hz), 28.31 (d, *J* = 24.3 Hz), 25.52 (d, *J* = 24.5 Hz).

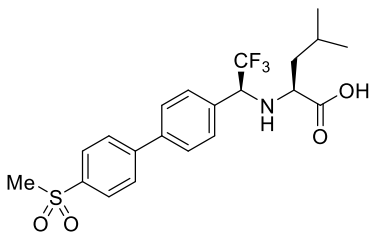

(2S)-4-Methyl-2-[(1S)-2,2,2-trifluoro-1-(4'-methanesulfonyl-biphenyl-4-yl)-ethylamino]-pentanoic acid **8**

According to published procedure,[29] the reaction of ketone **11** (484 mg, 1.5 mmol) with L-Leucine methyl ester hydrochloride (307 mg, 1.7 mmol), potassium carbonate (749 mg, 5.4 mmol), and subsequent reduction with zinc chloride (371 mg, 2.7 mmol) and sodium borohydride (207 mg, 5.5 mmol) afforded a mixture of (S,S)-**8** and (R,S)-**8**, which could be separated by preparative reverse phase HPLC to yield the major isomer (S,S)-**8** as a white solid (93.9 mg, 0.21 mmol, 14%). Spectral data of (S,S)-**8** was in agreement with published data.[31] LCMS (ESI^+); Rt = 7.68 min. m/z = 444.14 $[M+H]^+$. ^1H NMR (300 MHz, $CDCl_3$) δ = 8.06 – 7.96 (m, 2H), 7.81 – 7.69 (m, 2H), 7.68 – 7.58 (m, 2H), 7.52 (d, *J* = 8.1 Hz, 2H), 4.18 (q, *J* = 7.0 Hz, 1H), 3.58 (dd, *J* = 8.7, 5.3 Hz, 1H), 3.10 (s, 3H), 1.93 (dp, *J* = 13.4, 6.5 Hz, 1H), 1.67 – 1.41 (m, 2H), 0.97 (d, *J* = 6.5 Hz, 3H), 0.95 (d, *J* = 6.7 Hz, 3H). ^{13}C NMR (75 MHz, $CDCl_3$) δ = 180.29, 145.89,

140.13, 139.57, 135.22, 129.24, 128.14, 128.12, 127.91, 126.04 (q, *J* = 282.0 Hz), 63.15 (q, *J* = 29.2 Hz), 58.55, 44.69, 42.69, 24.88, 23.00, 21.84.

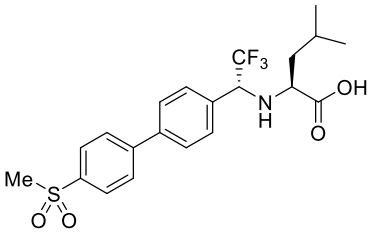

((R)-2,2,2-trifluoro-1-(4'-(methylsulfonyl)-[1,1'-biphenyl]-4-yl)ethyl)-L-leucine **8** (R,S)-**8** was obtained as the minor isomer in above described synthesis. LCMS (ESI^+); Rt = 7.42 min. m/z = 444.14 $[M+H]^+$. ^1H NMR (300 MHz, $CDCl_3$) δ = 8.11 – 7.95 (m, 2H), 7.90 – 7.73 (m, 2H), 7.71 – 7.61 (m, 2H), 7.56 (d, *J* = 8.1 Hz, 2H), 4.31 (q, *J* = 7.1 Hz, 1H), 3.18 – 3.12 (m, 1H), 3.11 (s, 3H), 1.97 – 1.77 (m, 1H), 1.54 (t, *J* = 7.1 Hz, 2H), 0.92 (d, *J* = 6.6 Hz, 3H), 0.76 (d, *J* = 6.5 Hz, 3H). ^{13}C NMR (75 MHz, $CDCl_3$) δ = 178.71, 145.92, 140.52, 139.67, 133.56, 129.98, 128.20, 128.16, 127.90, 124.91 (q, *J* = 280.9 Hz), 63.01 (q, *J* = 29.1 Hz), 56.42, 44.75, 42.87, 24.74, 23.22, 21.67.

Synthesis of Odanacatib derivatives

General procedure A [32]

Precursor (S,S)-**1** (60 mg, 0.13 mmol) was dissolved in 3 mL DMAc and cooled to 0 °C. Amine (0.16 mmol) and HATU (59 mg, 0.16 mmol) were added. The resulting solution was stirred for 15 min and DIPEA (68 mL, 0.39 mmol) was added. The reaction was stirred for 2.5 h. Water was slowly added dropwise and the slurry was stirred 2.5 h at room temperature. The mixture was filtered and the solid material was washed with a 1:1.2 DMF/water solution, water and 2-propanol. The material was removed from the filter by addition of THF. The filtrate was concentrated and purified by FCC (gradient DCM to 2% MeOH in DCM). The product was obtained as a white solid.

General procedure B [5]

Precursor (S,S)-**1** (21.3 mg, 0.046 mmol) was dissolved in 700 mL DMF and cooled to 0 °C. HATU (21.8 mg, 0.057 mmol) and triethylamine (6 μL, 0.043 mmol) were added. To this solution was added to amine (0.067 mmol) and further triethylamine (12 μL, 0.086 mmol) was added to the mixture. After 2 h ice cooling was removed and the mixture was stirred an additional 2 h. The reaction mixture was concentrated *in vacuo*, redissolved in EtOAc and extracted with sat. NH_4Cl solution and brine. The organic layer was dried over Na_2SO_4 and filtered. The filtrate was concentrated *in vacuo* and the residue was purified by FCC (gradient DCM to 2% MeOH in DCM), and if needed, further purified using Reversed phase preparative HPLC/MS and lyophilized to obtain product as a white solid.

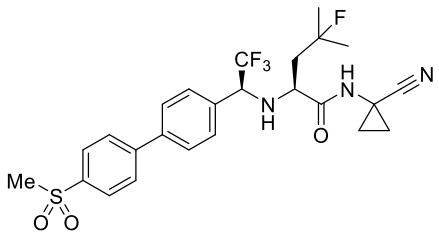

(S)-N-(1-cyanocyclopropyl)-4-fluoro-4-methyl-2-(((S)-2,2,2-trifluoro-1-(4'-(methylsulfonyl)-[1,1'-biphenyl]-4-yl)ethyl)amino)pentanamide **ODN**

According to general procedure A, the reaction between precursor (S,S)-**1** (59.8 mg, 0.13 mmol) and 1-amino-cyclopropanecarbonitrile hydrochloride (18.5 mg, 0.156 mmol) afforded product **ODN** as a white solid (40.7 mg, 0.077 mmol, 60%). TLC Rf = 0.18 (1:1 EtOAc/heptane). LCMS (ESI^+); Rt = 7.43 min. m/z = 526.112 $[M+H]^+$. ^1H NMR (300 MHz, $CDCl_3$) δ = 8.03 (d, *J* = 8.4 Hz, 2H), 7.77 (d, *J* = 8.8 Hz, 2H), 7.65 (d, *J* = 8.1 Hz, 2H), 7.48 (d, *J* = 8.1 Hz, 2H), 7.42 (s, 1H), 4.17 (q, *J* = 7.2 Hz, 1H), 3.59 (dd, *J* = 8.9, 3.3 Hz, 1H), 3.10 (s, 3H), 2.17 – 1.85 (m, 2H), 1.56 – 1.44 (m, 2H), 1.47 (d, *J* = 21.7 Hz, 3H), 1.44 (d, *J* = 22.0 Hz, 3H), 1.11 – 0.85 (m, 2H). ^{13}C NMR (75 MHz, $CDCl_3$) δ = 174.42, 145.69, 140.57, 139.94, 134.53, 129.40, 128.22, 128.20, 126.02 (q, *J* = 279.3 Hz), 119.56, 96.84 (d, *J* = 163.8 Hz), 63.44 (q, *J* = 29.3 Hz), 59.03, 44.75, 43.64 (d, *J* = 19.9 Hz), 28.37 (d, *J* = 24.4 Hz), 25.83 (d, *J* = 24.7 Hz), 20.21, 16.86, 16.48. HRMS (ESI^+): calculated for $C_{25}H_{28}F_4N_3O_3S$ $[M+H]^+$ 526.1788, found: 526.1816.

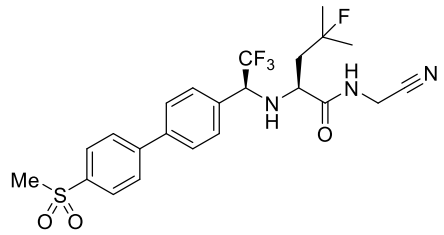

(S)-N-(cyanomethyl)-4-fluoro-4-methyl-2-(((S)-2,2,2-trifluoro-1-(4'-(methylsulfonyl)-[1,1'-biphenyl]-4-yl)ethyl)amino)pentanamide **2**

According to general procedure B, the reaction between precursor (S,S)-**1** (21.3 mg, 0.046 mmol) and aminoacetonitrile (6.2 mg, 0.067 mmol) afforded product **2** as a white solid (15.3 mg, 0.030 mmol, 66%). TLC Rf = 0.15 (1:1 EtOAc/heptane). LCMS Rt = 7.30 min. m/z = 500.144 $[M+H]^+$. ^1H NMR (300 MHz, $CDCl_3$) δ = 8.01 (d, *J* = 8.4 Hz, 2H), 7.76 (d, *J* = 8.4 Hz, 2H), 7.65 (d, *J* = 8.4 Hz, 2H), 7.50 (d, *J* = 8.2 Hz, 2H), 7.45 (t, *J* = 6.7 Hz, 1H), 4.24 (q, *J* = 7.1 Hz, 1H), 4.21 – 3.96 (m, 2H), 3.66 (dd, *J* = 8.8, 3.3 Hz, 1H), 3.10 (s, 3H), 2.21 – 1.89 (m, 2H), 1.47 (d, *J* = 21.7 Hz, 3H), 1.45 (d, *J* = 22.0 Hz, 3H). ^{13}C NMR (75 MHz, $CDCl_3$) δ = 173.80, 145.74, 140.46, 139.70, 134.18, 129.40, 128.21, 128.15, 125.40 (q, *J* = 282.9 Hz), 115.67, 96.84 (d, *J* = 163.7 Hz), 63.12 (q, *J* = 28.7 Hz), 58.45, 44.73, 43.58 (d, *J* = 19.9 Hz), 28.41 (d, *J* = 24.2 Hz), 27.33, 25.72 (d, *J* = 24.7 Hz). HRMS (ESI^+): calculated for $C_{23}H_{26}F_4N_3O_3S$ $[M+H]^+$ 500.1631, found: 500.1638.

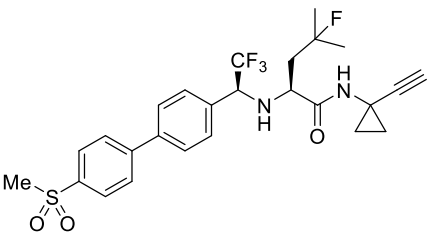

(S)-N-(1-ethynylcyclopropyl)-4-fluoro-4-methyl-2-(((S)-2,2,2-trifluoro-1-(4'-(methylsulfonyl)-[1,1'-biphenyl]-4-yl)ethyl)amino)pentanamide **3**

According to general procedure A, the reaction between precursor (S,S)-**1** (60.7 mg, 0.13 mmol) and 1-ethynylcyclopropan-1-amine hydrochloric acid **16** (18.3 mg, 0.156 mmol) afforded product **3** as a white solid (46.6 mg, 0.089 mmol, 68%). TLC Rf = 0.24 (1:1 EtOAc/heptane). LCMS Rt = 7.66 min. m/z = 525.124 $[M+H]^+$. ^1H NMR (300 MHz, $CDCl_3$) δ = 8.02 (d, *J* = 8.5 Hz, 2H), 7.76 (d, J = 8.4 Hz, 2H), 7.62 (d, *J* = 8.3 Hz, 2H), 7.47 (d, *J* = 8.1 Hz, 2H), 7.32 (s, 1H), 4.14 (q, *J* = 7.2 Hz, 1H), 3.58 (dd, *J* = 9.0, 3.2 Hz, 1H), 3.10 (s, 3H), 2.94 (s, 1H), 2.10 (s, 1H), 2.19 – 1.84 (m, 2H), 1.46 (d, *J* = 21.7 Hz, 6H), 1.43 (d, *J* = 22.0 Hz, 6H), 1.27 – 1.07 (m, 2H), 0.95 – 0.86 (m, 1H), 0.75 – 0.66 (m, 1H). ^{13}C NMR (75 MHz, $CDCl_3$) δ = 173.85, 145.80, 140.20, 139.71, 134.96, 129.34, 128.15, 127.96, 125.50 (q, *J* = 283.1

Hz), 97.00 (d, *J* = 163.3 Hz), 84.69, 66.97, 63.04 (q, *J* = 28.8 Hz), 59.15, 44.71, 43.57 (d, *J* = 19.9 Hz), 28.39 (d, *J* = 24.3 Hz), 25.73 (d, *J* = 24.7 Hz), 22.48, 17.72, 17.20. HRMS (ESI$^+$): calculated for $C_{26}H_{29}F_4N_2O_3S$ $[M+H]^+$ 525.1835, found: 525.1824.

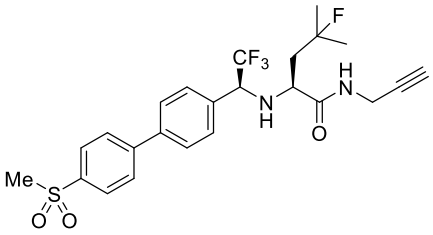

(S)-4-fluoro-4-methyl-N-(prop-2-yn-1-yl)-2-(((S)-2,2,2-trifluoro-1-(4'-(methylsulfonyl)-[1,1'-biphenyl]-4-yl)ethyl)amino)pentanamide **4**

According to general procedure B, the reaction between precursor (S,S)-**1** (20.6 mg, 0.045 mmol) and propargylamine (10 µL, 0.16 mmol) afforded product **4** as a white solid (11.3 mg, 0.023 mmol, 51%). TLC Rf = 0.25 (1:1 EtOAc/heptane). LCMS Rt = 7.50 min. m/z = 499.116 $[M+H]^+$. ^{1}H NMR (300 MHz, $CDCl_3$) δ = 8.02 (d, *J* = 8.5 Hz, 2H), 7.76 (d, *J* = 8.6 Hz, 2H), 7.63 (d, *J* = 8.4 Hz, 2H), 7.51 (d, *J* = 8.1 Hz, 2H), 7.22 (t, *J* = 5.5 Hz, 1H), 4.23 (q, *J* = 7.2 Hz, 1H), 3.94 (qdd, *J* = 17.6, 5.5, 2.6 Hz, 2H), 3.69 (dd, *J* = 9.2, 3.1 Hz, 1H), 3.42 (s, 1H), 3.10 (s, 3H), 2.18 (t, *J* = 2.6 Hz, 1H), 2.14 – 1.89 (m, 2H), 1.48 (d, *J* = 21.7 Hz, 3H), 1.45 (d, *J* = 22.0 Hz, 3H). ^{13}C NMR (75 MHz, $CDCl_3$) δ = 173.80, 145.87, 140.25, 139.68, 134.60, 129.43, 128.17, 128.02, 125.54 (q, *J* = 283.3 Hz), 97.01 (d, *J* = 163.5 Hz), 78.91, 71.89, 62.98 (q, *J* = 28.7 Hz), 58.72, 44.74, 43.73 (d, *J* = 19.8 Hz), 29.19, 28.55 (d, *J* = 24.5 Hz), 25.49 (d, *J* = 24.8 Hz). HRMS (ESI$^+$): calculated for $C_{24}H_{27}F_4N_2O_3S$ $[M+H]^+$ 499.1679, found: 499.1713.

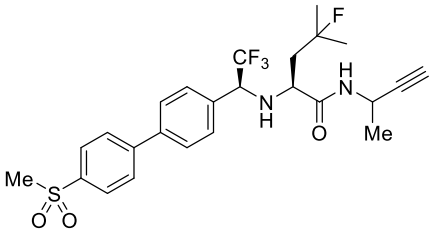

(S)-N-((R/S)-but-3-yn-2-yl)-4-fluoro-4-methyl-2-(((S)-2,2,2-trifluoro-1-(4'-(methylsulfonyl)-[1,1'-biphenyl]-4-yl)ethyl)amino)pentanamide **5**

According to general procedure B, the reaction between precursor (S,S)-**1** (19.9 mg, 0.043 mmol) and 1-methyl-prop-2-ynylamine hydrochloride (16.5 mg, 0.156 mmol) afforded an inseparable 1:1 mixture of diastereoisomers (S,S,R)-**2** and (S,S,S)-**2** as a white solid (10.0 mg, 0.020 mmol, 45%). Reported ppm-values are average values. TLC Rf = 0.31 (1:1 EtOAc/heptane). LCMS Rt = 7.77 min. m/z = 513.130 $[M+H]^+$. ^{1}H NMR (300 MHz, $CDCl_3$) δ = 8.02 (d, *J* = 8.6 Hz, 2H), 7.76 (d, *J* = 8.6 Hz, 2H), 7.63 (d, *J* = 8.3 Hz, 2H), 7.51 (d, *J* = 8.2 Hz, 2H), 7.21 (d, *J* = 8.3 Hz, 1H), 4.74 – 4.58 (m, 1H), 4.20 (q, *J* = 14.5 Hz, 1H), 3.68 (t, *J* = 7.7 Hz, 1H), 3.60 (s, 1H), 3.10 (s, 3H), 2.20 (d, *J* = 9.0 Hz, 1H), 2.16 – 1.86 (m, 2H), 1.47 (dd, *J* = 22.0, 10.0 Hz, 6H), 1.24 (d, *J* = 6.9 Hz, 3H). ^{13}C NMR (75 MHz, $CDCl_3$) δ = 173.04, 145.86, 140.24, 139.69, 134.82, 129.42, 128.09, 125.54 (q, *J* = 283.6 Hz), 97.06 (d, *J* = 163.4 Hz), 83.44, 70.75, 63.03 (q, *J* = 28.6 Hz), 59.03, 44.74, 43.71 (d, *J* = 19.8 Hz), 36.92, 28.62 (d, *J* = 24.3 Hz), 25.37 (d, *J* = 24.7 Hz), 21.95. HRMS (ESI$^+$): calculated for $C_{25}H_{29}F_4N_2O_3S$ $[M+H]^+$ 513.1835, found: 513.1829.

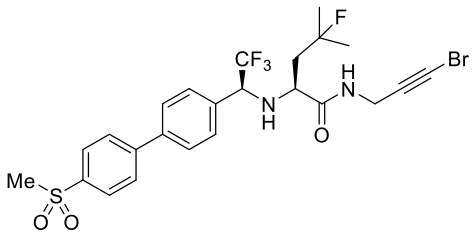

(S)-N-(3-bromoprop-2-yn-1-yl)-4-fluoro-4-methyl-2-(((S)-2,2,2-trifluoro-1-(4'-(methylsulfonyl)-[1,1'-biphenyl]-4-yl)ethyl)amino)pentanamide **6**

According to general procedure A, the reaction between precursor (S,S)-**1** (60.8 mg, 0.13 mmol) and 3-bromoprop-2-yn-1-amine hydrochloric acid **19** (26.6 mg, 0.156 mmol) afforded product **6** as a white solid (13.6 mg, 0.024 mmol, 18%). TLC Rf = 0.33 (1:1 EtOAc/heptane). LCMS Rt = 7.93 min. m/z = 577.036 + 579.038 $[M+H]^+$. ^{1}H NMR (300 MHz, $CDCl_3$) δ = 8.03 (d, *J* = 8.4 Hz, 2H), 7.78 (d, *J* = 8.4 Hz, 2H), 7.65 (d, *J* = 8.2 Hz, 2H), 7.50 (d, *J* = 8.1 Hz, 2H), 7.16 (t, *J* = 5.3 Hz, 1H), 4.21 (q, *J* = 7.2 Hz, 1H), 4.13 – 3.81 (m, 2H), 3.68 (dd, *J* = 9.2, 3.1 Hz, 1H), 3.11 (s, 3H), 2.20 – 1.88 (m, 3H), 1.49 (d, *J* = 21.7 Hz, 6H), 1.45 (d, *J* = 22.0 Hz, 6H). ^{13}C NMR (75 MHz, $CDCl_3$) δ = 173.11, 145.89, 140.18, 139.66, 134.75, 129.38, 128.18, 128.14, 128.00, 125.60 (q, *J* = 283.5 Hz), 97.01 (d, *J* = 163.4 Hz), 75.53, 62.92 (q, *J* = 28.6 Hz), 58.94, 44.73, 43.80 (d, *J* = 19.9 Hz), 43.21, 30.00, 28.57 (d, *J* = 24.4 Hz), 25.51 (d, *J* = 24.7 Hz). HRMS (ESI^+): calculated for $C_{24}H_{26}BrF_4N_2O_3S$ $[M+H]^+$ 577.0784, found: 577.0809 (minor) + 579.0781 (major)

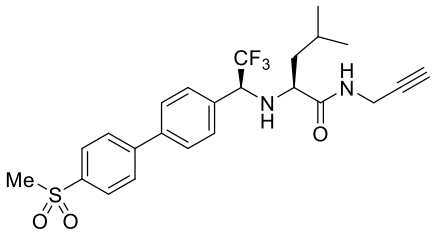

(S)-4-methyl-N-(prop-2-yn-1-yl)-2-(((S)-2,2,2-trifluoro-1-(4'-(methylsulfonyl)-[1,1'-biphenyl]-4-yl)ethyl)amino)pentanamide **7**

According to general procedure B, the reaction between precursor (S,S)-**8** (78.4 mg, 0.177 mmol) and propargylamine (42 μL, 0.66 mmol) afforded product **7** as a white solid (77.7 mg, 0.16 mmol, 91%). TLC Rf = 0.13 (1:2 EtOAc/heptane). LCMS Rt = 8.41 min. m/z = 481.01 $[M+H]^+$. ^{1}H NMR (300 MHz, $CDCl_3$) δ = 8.05 – 7.99 (m, 2H), 7.79 – 7.73 (m, 2H), 7.65 – 7.59 (m, 2H), 7.51 (d, *J* = 8.1 Hz, 2H), 6.87 (t, *J* = 5.4 Hz, 1H), 4.20 (q, *J* = 7.2 Hz, 1H), 4.05 – 3.84 (m, 2H), 3.43 (dd, *J* = 8.9, 4.7 Hz, 1H), 3.11 (s, 3H), 2.19 (t, *J* = 2.6 Hz, 1H), 1.81 (tt, *J* = 12.8, 6.4 Hz, 1H), 1.69 – 1.42 (m, 2H), 0.97 (d, *J* = 6.5 Hz, 3H), 0.96 (d, *J* = 6.6 Hz, 3H). ^{13}C NMR (75 MHz, $CDCl_3$) δ = 174.39, 145.88, 140.31, 139.69, 134.61, 129.38, 128.19, 128.04, 125.49 (q, *J* = 283.1 Hz), 79.07, 71.92, 63.42 (q, *J* = 28.7 Hz), 59.78, 44.76, 43.04, 29.19, 25.04, 23.30, 21.90.

Synthesis of alkyne 16

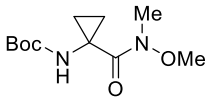

tert-butyl (1-(methoxy(methyl)carbamoyl)cyclopropyl)carbamate **13**

A solution of 1-(Boc-amino)cyclopropanecarboxylic acid (200 mg, 0.99 mmol) in DCM (2.5 mL) under argon was cooled to -15 °C. N,O-Dimethylhydroxylamine hydrochloride (100 mg, 1.02 mmol) was added, followed by 4-methylmorpholine (113 mL, 1.03 mmol). After 5 min, 1-(3-methylaminopropyl-3-ethylcarbodiimide hydrochloride (194.5 mg, 1.01 mmol) was added and the reaction was allowed to reach room temperature and stirred overnight. Water was added and the solution was extracted with DCM (3x). The combined organic phases were washed with brine, dried (Na_2SO_4), and concentrated *in vacuo* to obtain pure Weinreb amide **13** (1.08 gr, 0.99 mmol, quant.) as an offwhite solid. TLC Rf = 0.35 (1:1 EtOAc/heptane). ^{1}H NMR (300 MHz, $CDCl_3$) δ 5.22 (s, 1H), 3.74 (s, 3H), 3.18 (s, 3H), 1.44 (q, *J* = 5.2 Hz, 2H), 1.44 (s, 9H), 1.03 (q, *J* = 4.8 Hz, 2H). ^{13}C NMR (75 MHz, DMSO-d_6) δ = 171.87, 155.31, 78.00, 60.64, 34.00, 28.15, 21.16, 14.69.

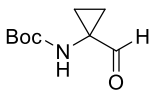

tert-butyl (1-formylcyclopropyl)carbamate **14**

Tert-butyl (1-(methoxy(methyl)carbamoyl)cyclopropyl) carbamate **13** (500 mg, 2.31 mmol) was dissolved in anhydrous Et_2O (50 mL) under argon and cooled to 0 °C. Lithium Aluminum Hydride (3 mL, 1 M in Et_2O, 2.99 mmol) was added dropwise and the reaction mixture was stirred for 2 h at this temperature. The reaction was quenched by addition of 1 N HCl (2.5 mL) and stirred vigorously for a few minutes. The organic layer was extracted with 1 N HCl and brine, dried over Na_2SO_4, filtered and concentrated to obtain the product aldehyde **14** as a colorless oil. Use crude in the next step. TLC Rf = 0.47 (1:1 EtOAc/heptane).

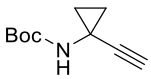

tert-butyl (1-ethynylcyclopropyl)carbamate **15**

Dimethyl (1-diazo-2-oxopropyl)phosphonate (443 mL, 2.77 mmol) was dissolved in MeCN (25 mL) and potassium carbonate (767 mg, 5.55 mmol) was added. The suspension was stirred at room temperature for 10 minutes, then the freshly prepared aldehyde **14** (428 mg, 2.31 mmol) in MeOH (9 mL) was added. Stirring was continued overnight. The solvents were removed *in vacuo* and the residue was dissolved in 1:1 mixture of Et_2O/water. The layers were separated and the organic layer was washed with water and brine, and dried (Na_2SO_4). The yellowish oil was purified by FCC (1:2 EtOAc/heptane) to give product **15** (164.8 mg, 0.90 mmol, 39%) as a pale white solid. TLC Rf = 0.66 (1:1 EtOAc/heptane). ^{1}H NMR (300 MHz, $CDCl_3$) δ = 5.00 (s, 1H), 2.13 (s, 1H), 1.46 (s, 9H), 1.23 – 1.16 (m, 2H), 1.12 – 1.01 (m, 2H). ^{13}C NMR (75 MHz, $CDCl_3$) δ = 155.47, 85.80, 80.34, 66.75, 28.49, 23.72, 18.13.

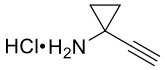

1-ethynylcyclopropan-1-amine hydrochloric acid **16**

To a solution of tert-butyl (3-bromoprop-2-yn-1-yl)carbamate **15** (165 mg, 0.91 mmol) in MeOH (4.5 mL) was added 1.25 M HCl in MeOH (1.82 mL, 2.27 mmol). The reaction mixture was left to stir overnight, volatiles were removed *in vacuo* and the resulting solid was triturated with Et_2O to obtain alkyne **16** (79 mg, 0.67 mmol, 74%) as a white solid. ^{1}H NMR (300 MHz, DMSO-d_6) δ 8.74 (s, 3H), 3.59 (s, 1H), 1.26 (m, 2H), 1.23 – 1.07 (m, 2H). ^{13}C NMR (75 MHz, DMSO-d_6) δ = 81.75, 74.40, 23.86, 13.72.

Synthesis of alkyne 19

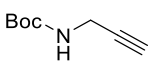

tert-butyl prop-2-yn-1-ylcarbamate **17**

According to published procedure,[33] the reaction between 3-amino-1-propyne (3.2 mL, 50 mmol) and di-tert-butyl dicarbonate (10.9 gr, 50 mmol) afforded product **17** as a yellow solid (7.8 gr, 50 mmol, quant.). TLC Rf = 0.78 (1:1 EtOAc/hept). ^{1}H NMR (300 MHz, $CDCl_3$) δ = 4.92 (s, 1H), 3.86 (dd, *J* = 5.9, 2.5 Hz, 2H), 2.18 (t, *J* = 2.5 Hz, 1H), 1.40 (s, 9H). ^{13}C NMR (75 MHz, $CDCl_3$) δ = 155.36, 80.24, 80.03, 71.23, 30.41, 28.38.

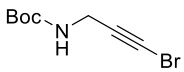

tert-butyl (3-bromoprop-2-yn-1-yl)carbamate **18**

Tert-butyl prop-2-yn-1-ylcarbamate **17** (583.4 mg, 3.75 mmol) was dissolved in 19 mL DMF and silver nitrate (64 mg, 0.38 mmol) was added, followed by the addition of N-bromosuccinimide (735 mg, 4.1 mmol, 1.1 eq). The mixture was covered with aluminum foil and stirred at room temperature for 2 h, and was diluted with EtOAc and extracted with water (2x). The combined organic layers were dried over Na_2SO_4, filtered over celite and concentrated to give a yellow solid. The crude material was purified by FCC (3:1 to 2:1 EtOAc in hept) to give bromoalkyne **18** (618 mg, 2.64 mmol, 70%) as an offwhite solid. TLC Rf = 0.58 (1:2 EtOAc/heptane). ^{1}H NMR (300 MHz, $CDCl_3$) δ = 4.69 (s, 1H), 3.94 (d, *J* = 5.5 Hz, 2H), 1.45 (s, 9H). ^{13}C NMR (75 MHz, $CDCl_3$) δ = 155.31, 80.22, 76.46, 42.75, 31.51, 28.43.

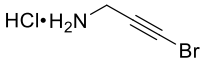

3-bromoprop-2-yn-1-amine hydrochloric acid **19**

To tert-butyl (3-bromoprop-2-yn-1-yl)carbamate **18** (69 mg, 0.29 mmol) was added 4 M HCl in dioxane (2 mL, 8 mmol). The reaction mixture was left to stir 1 h, volatiles were removed *in vacuo* and the resulting solid was triturated with Et_2O to obtain product **19** (51.4 mg, 0.32 mmol, quant.) as a white solid. ^{1}H NMR (300 MHz, DMSO-d_6) δ = 8.58 (s, 3H), 3.75 (s, 2H). ^{13}C NMR (75 MHz, $CDCl_3$) δ = 73.49, 48.94, 29.24.

Figure S22. ^{1}H and ^{13}C NMR spectra for (S,S)-**1**

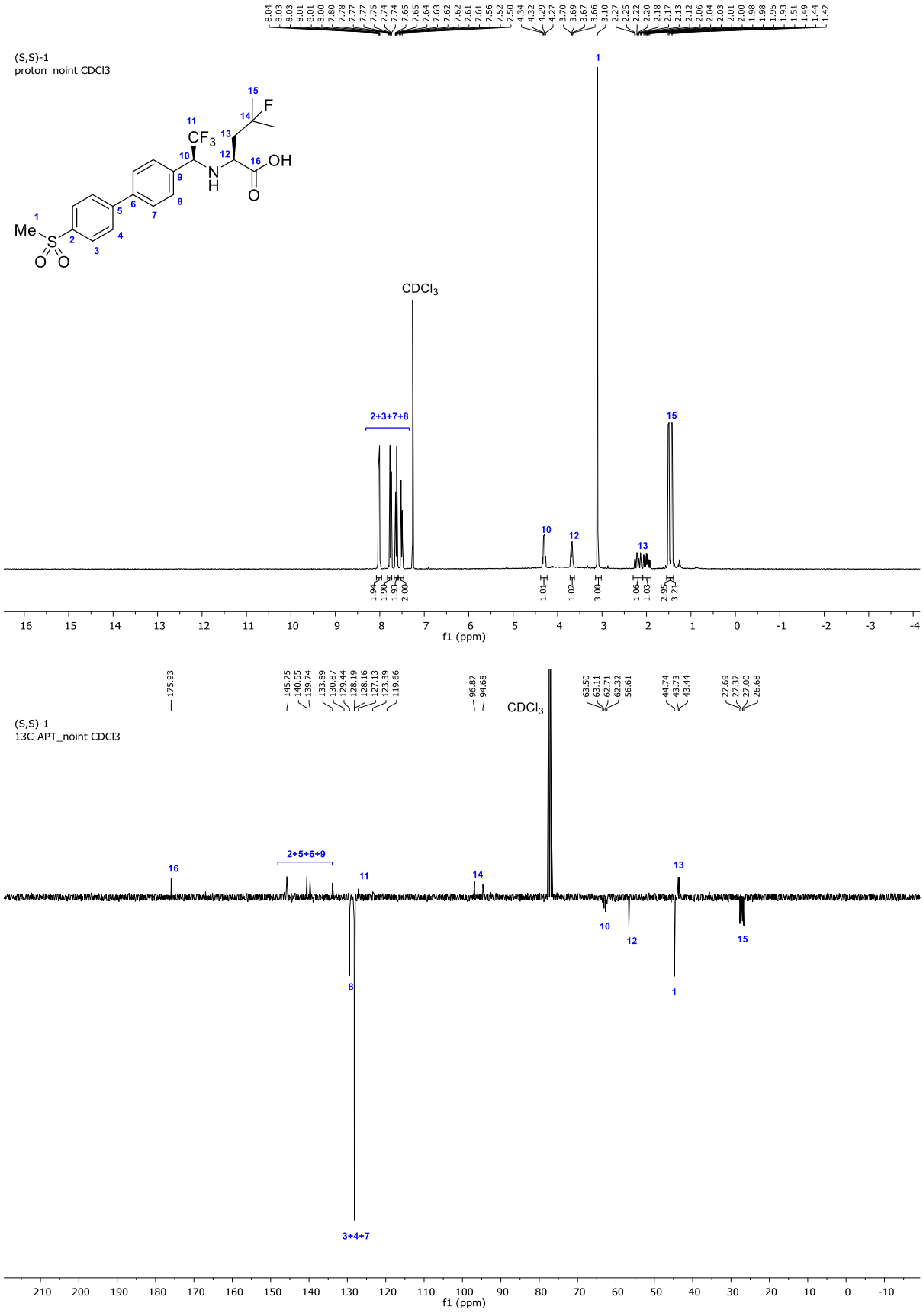

Figure S23. ^{1}H and ^{13}C NMR spectra for (R,S)-**1**

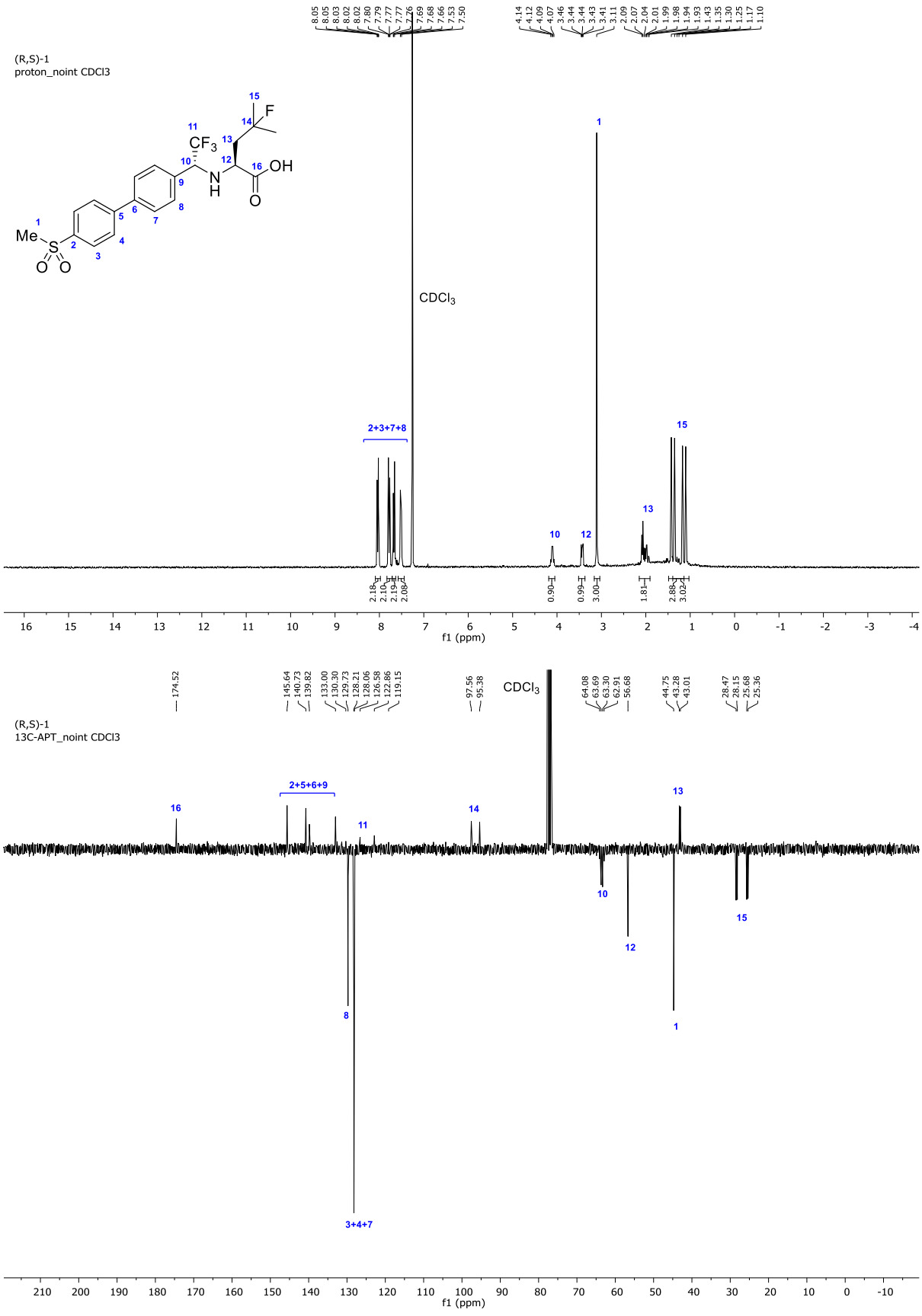

Figure S24. ^{1}H and ^{13}C NMR spectra for ODN

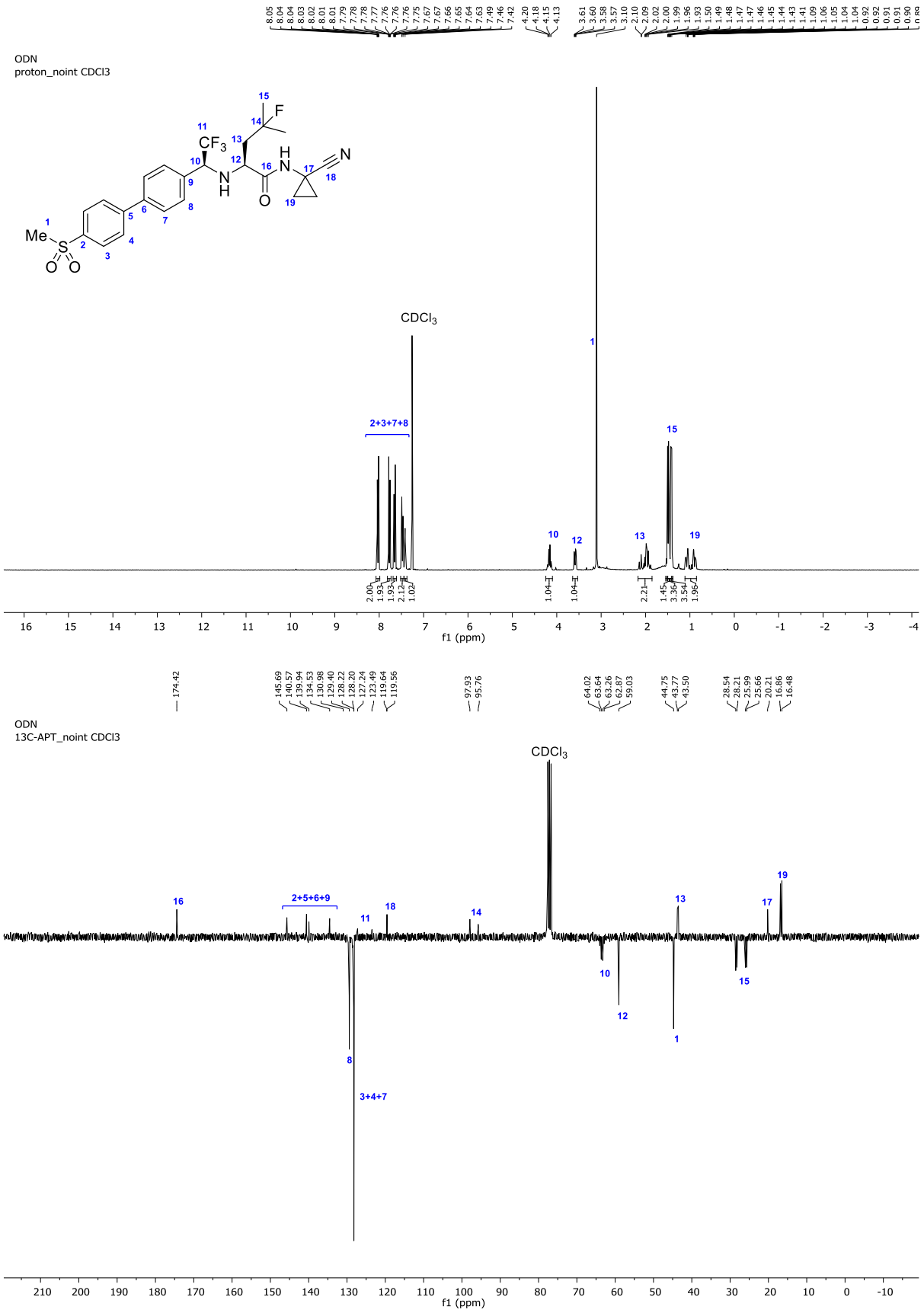

Figure S25. ^{1}H and ^{13}C NMR spectra for Nitrile **2**

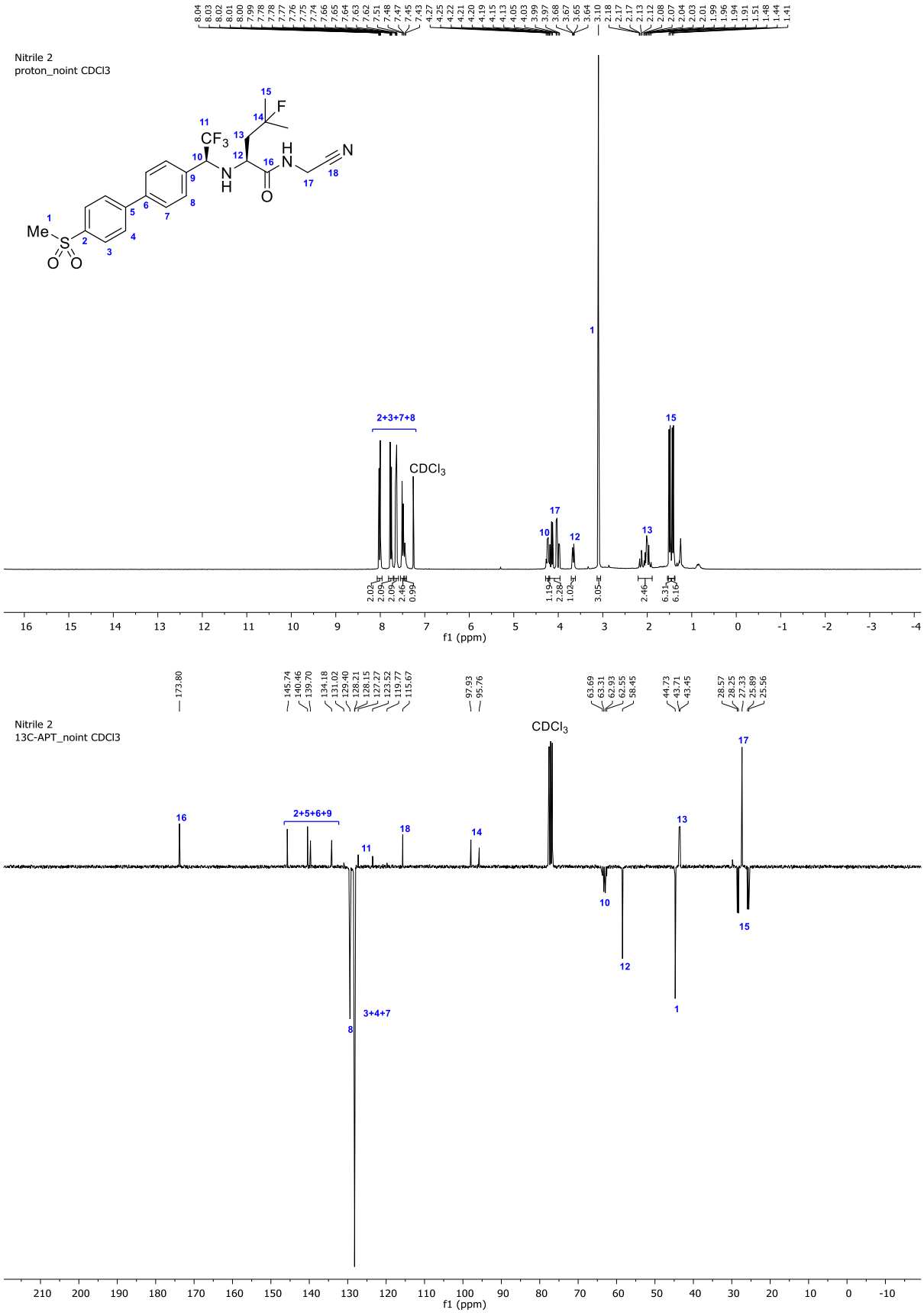

Figure S26. ^{1}H and ^{13}C NMR spectra for Alkyne **3**

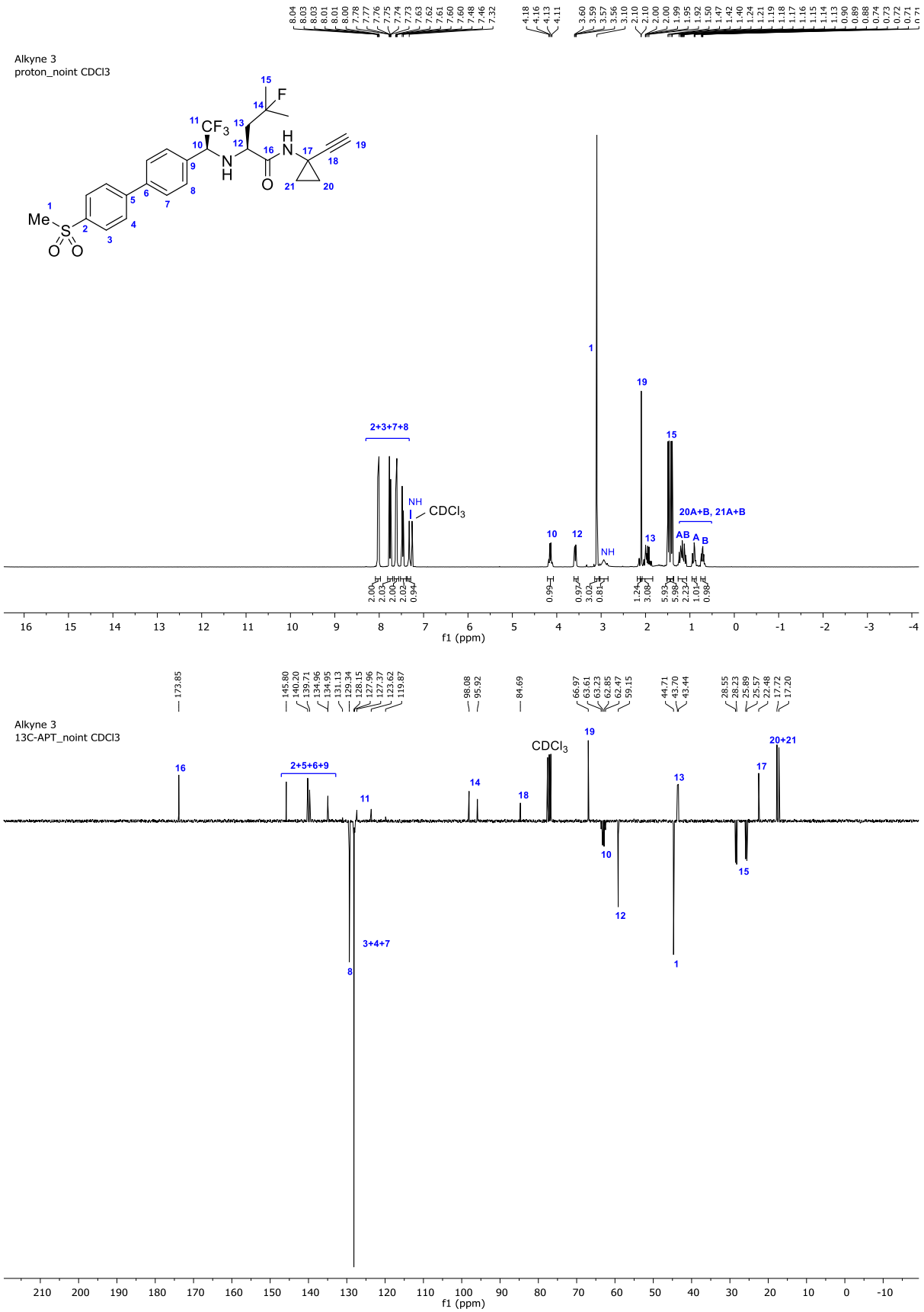

Figure S27. ^{1}H and ^{13}C NMR spectra for Alkyne **4**

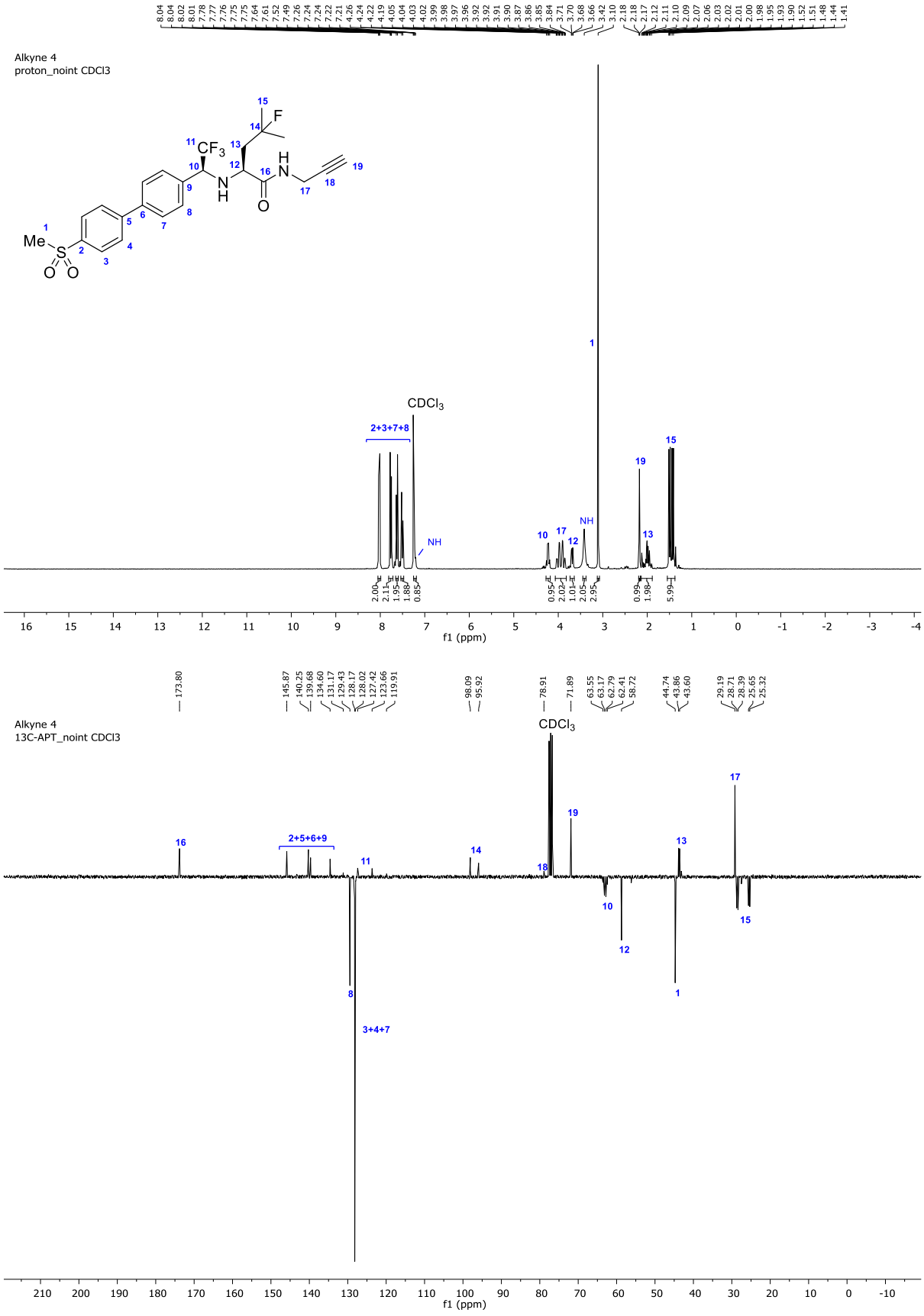

Figure S28. ^{1}H and ^{13}C NMR spectra for Alkyne **5**

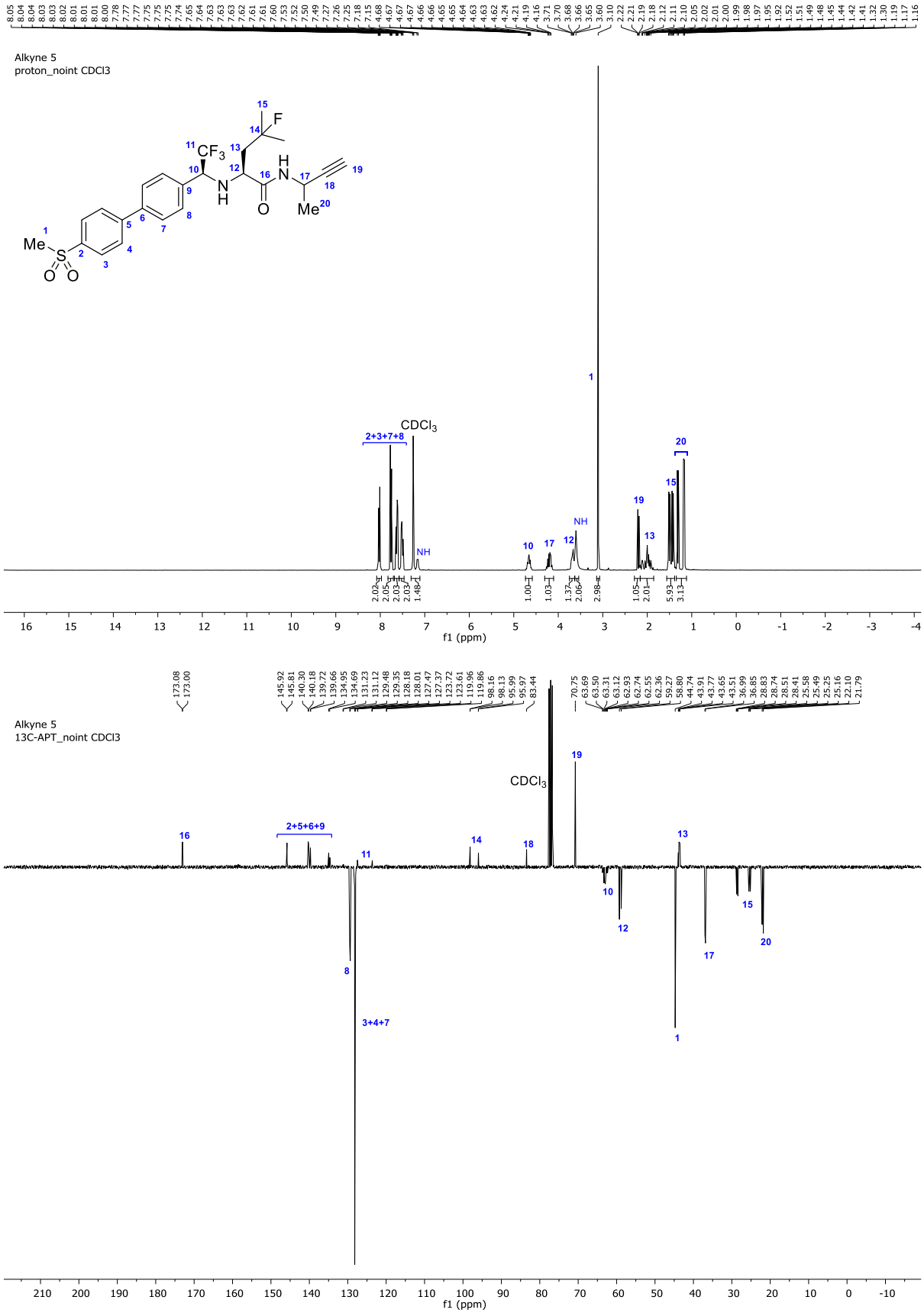

Figure S29. ^{1}H and ^{13}C NMR spectra for Alkyne **6**

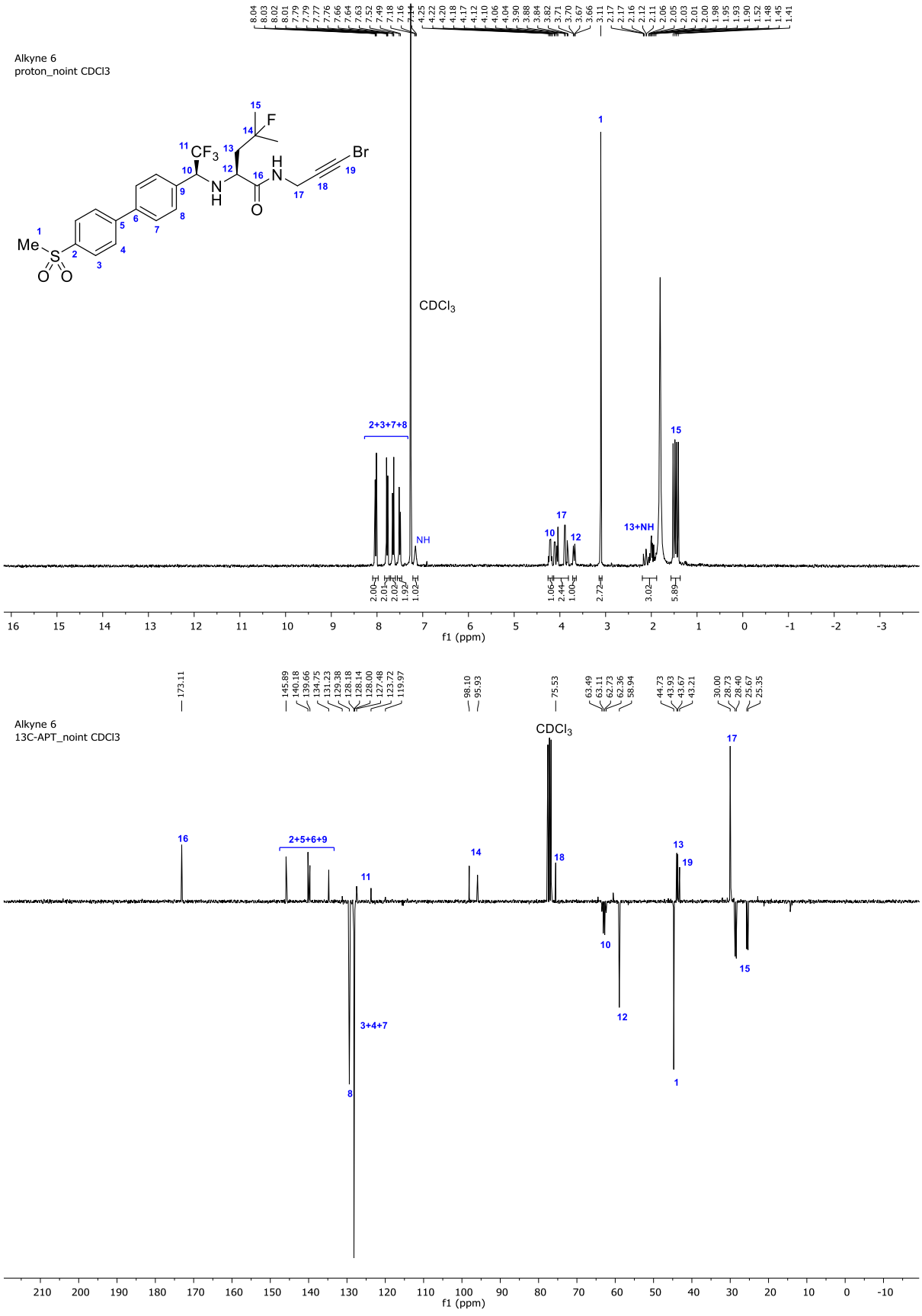

Figure S30. ^{1}H and ^{13}C NMR spectra for Alkyne **7**

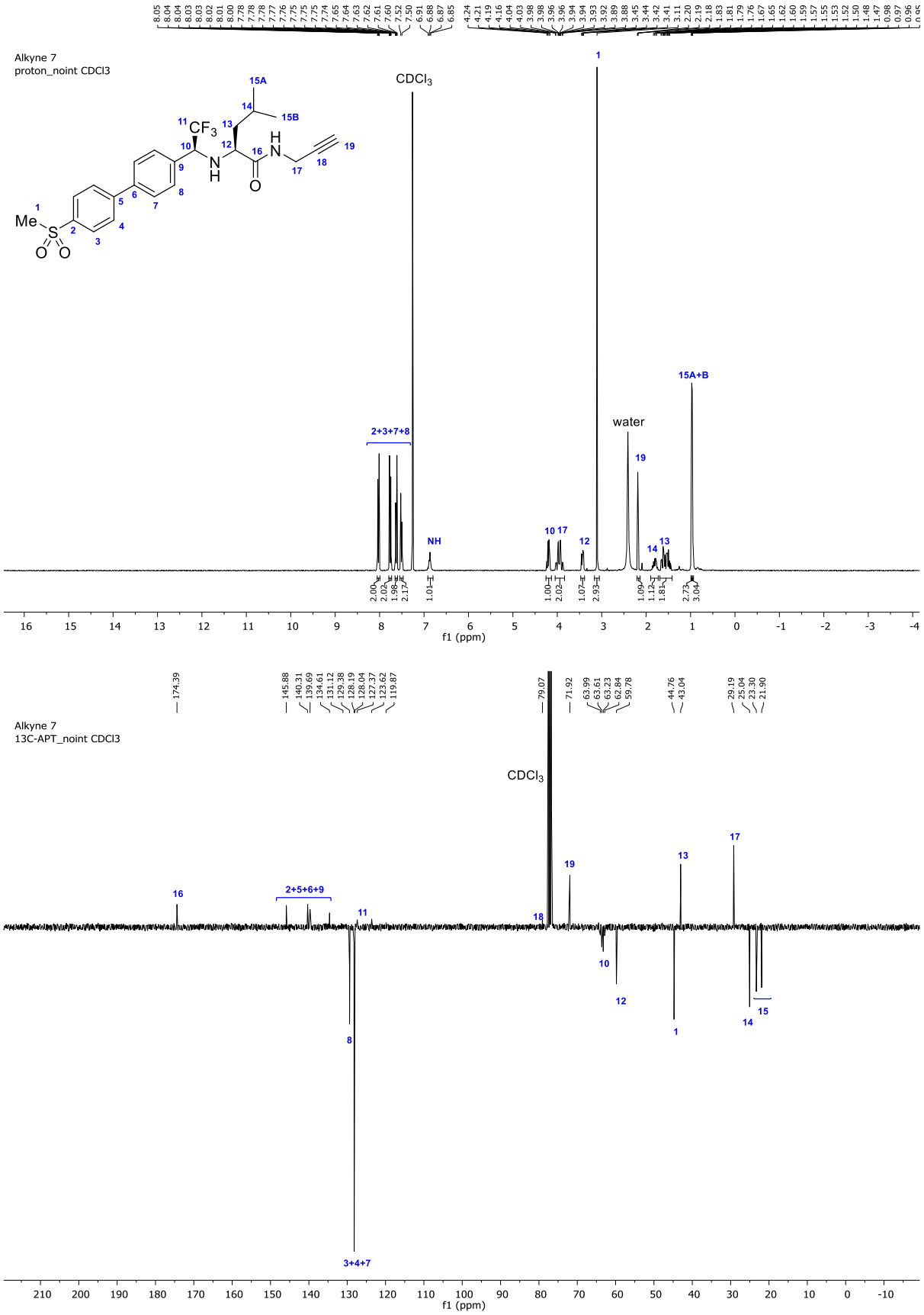

Figure S31. ^{1}H and ^{13}C NMR spectra for (S,S)-**8**

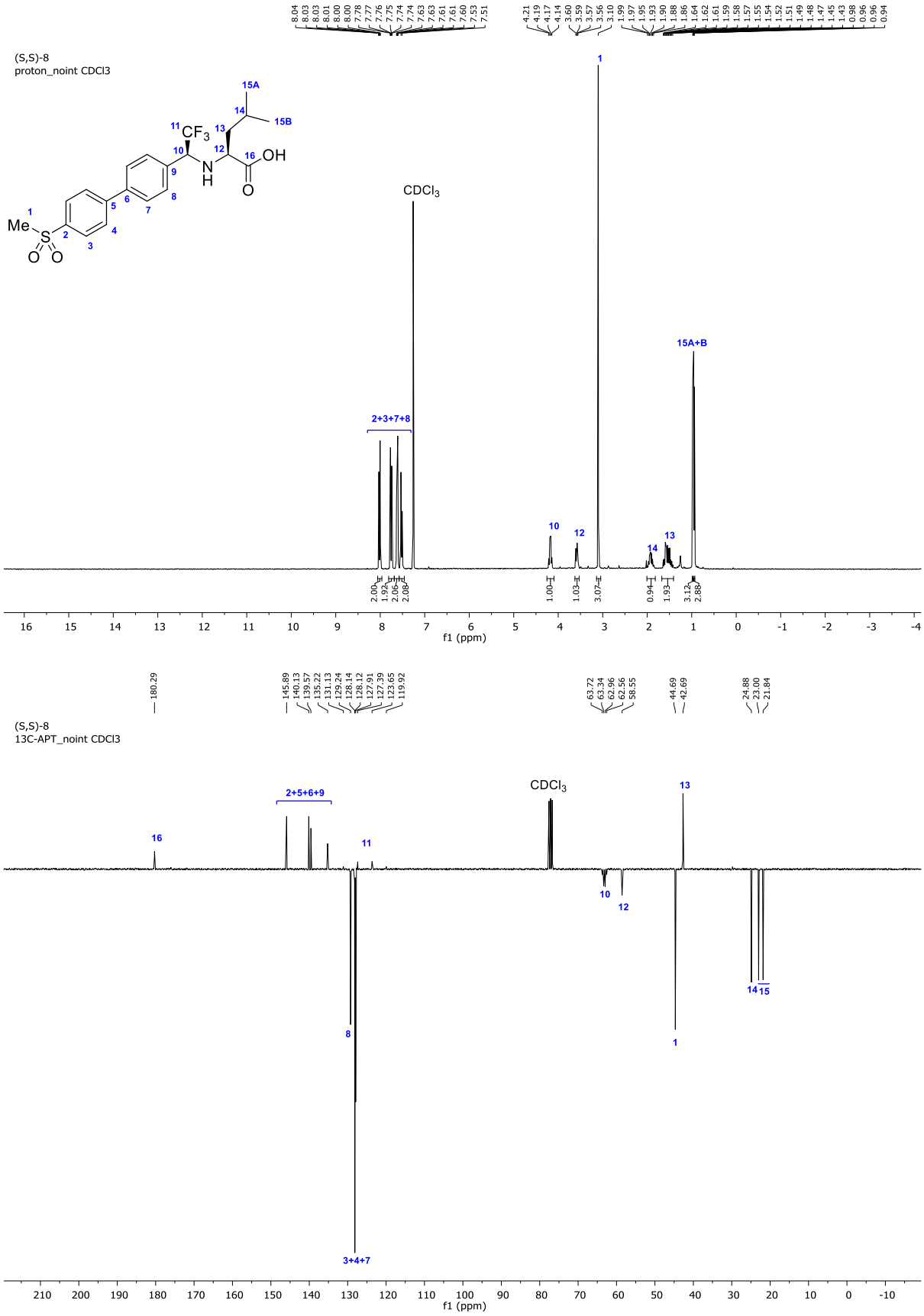

Figure S32. ^{1}H and ^{13}C NMR spectra for Ketone **11**

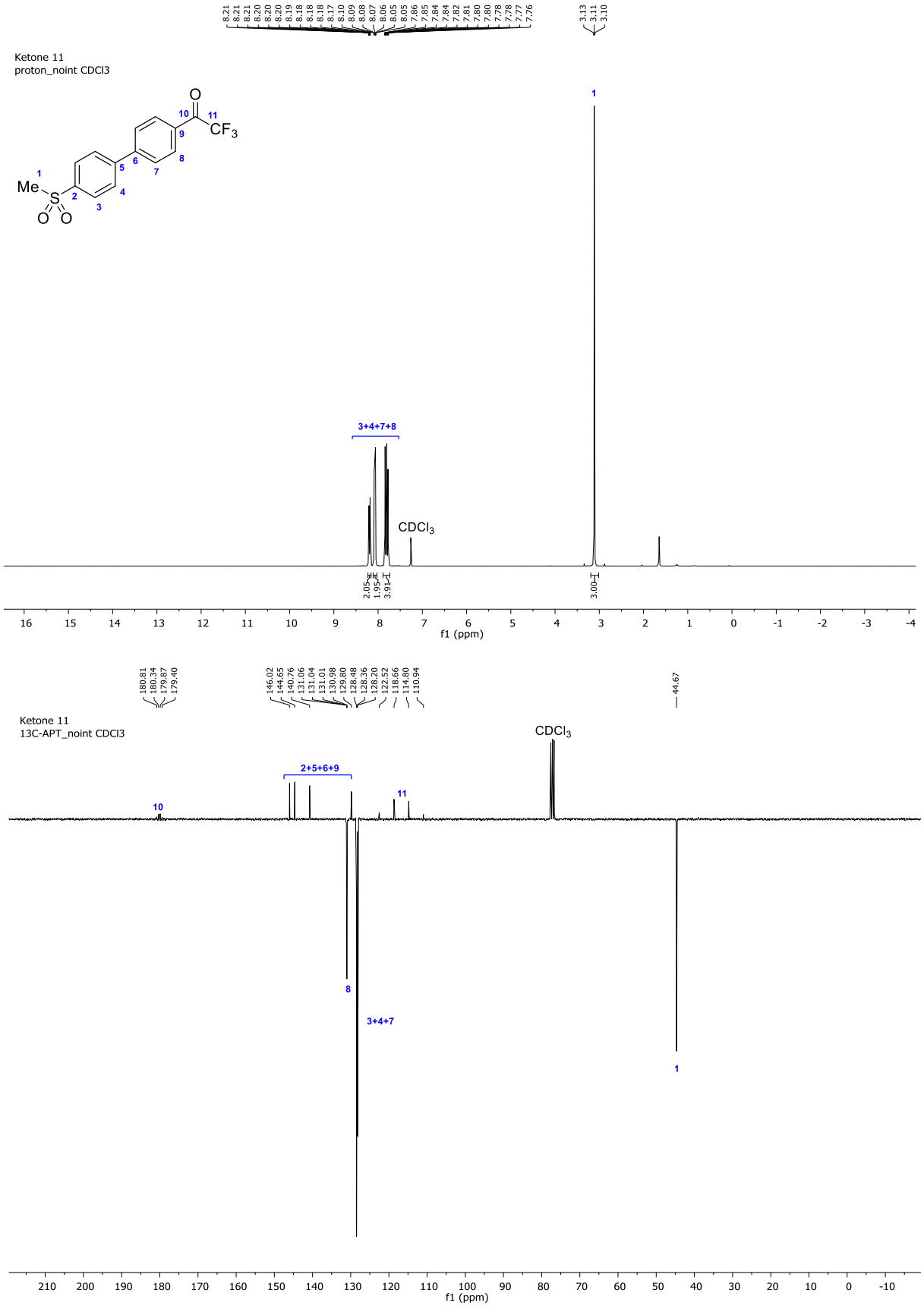

Figure S33. ^{1}H and ^{13}C NMR spectra for Hydrate **12**

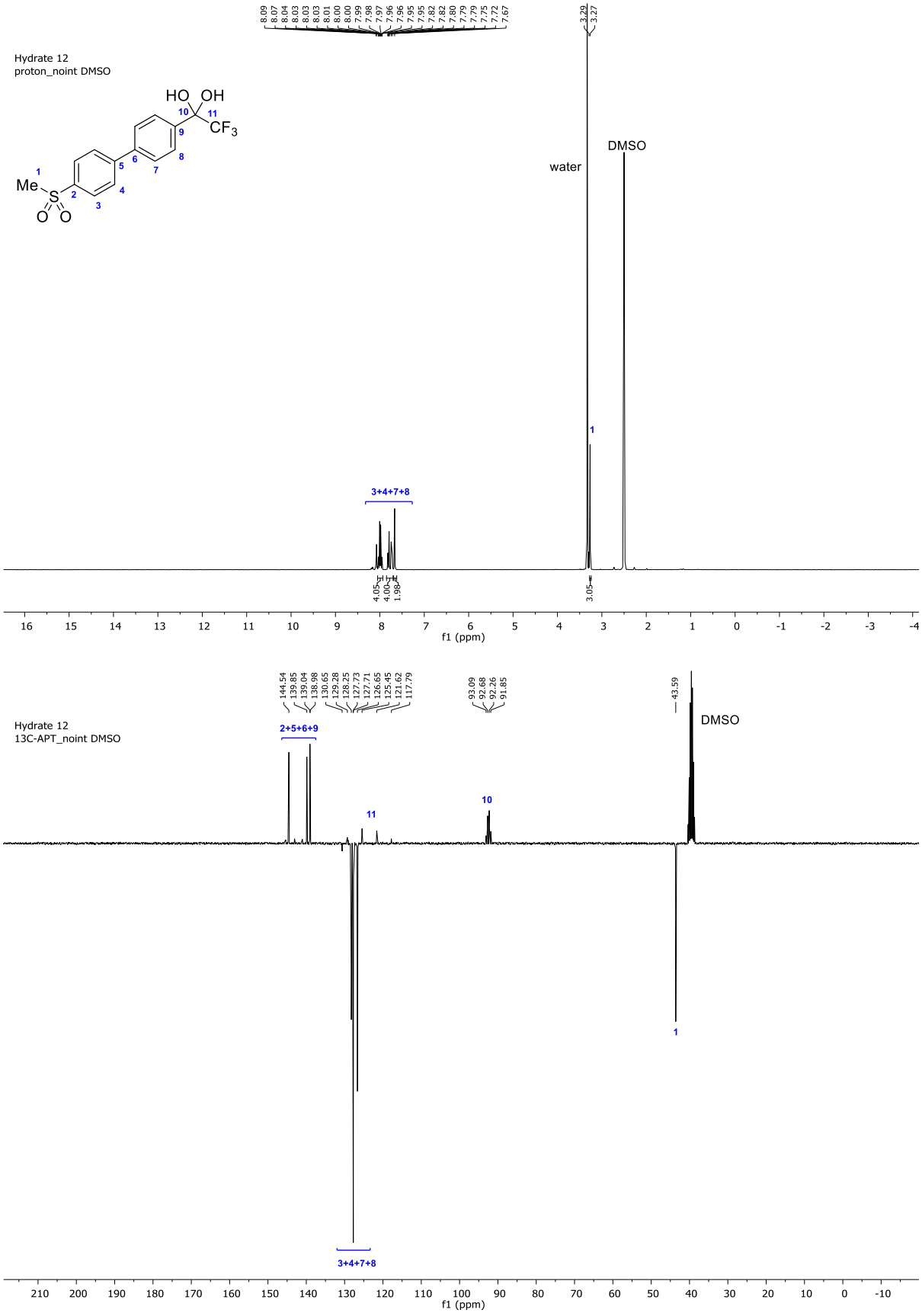

Figure S34. ^{1}H and ^{13}C NMR spectra for Amine **13**

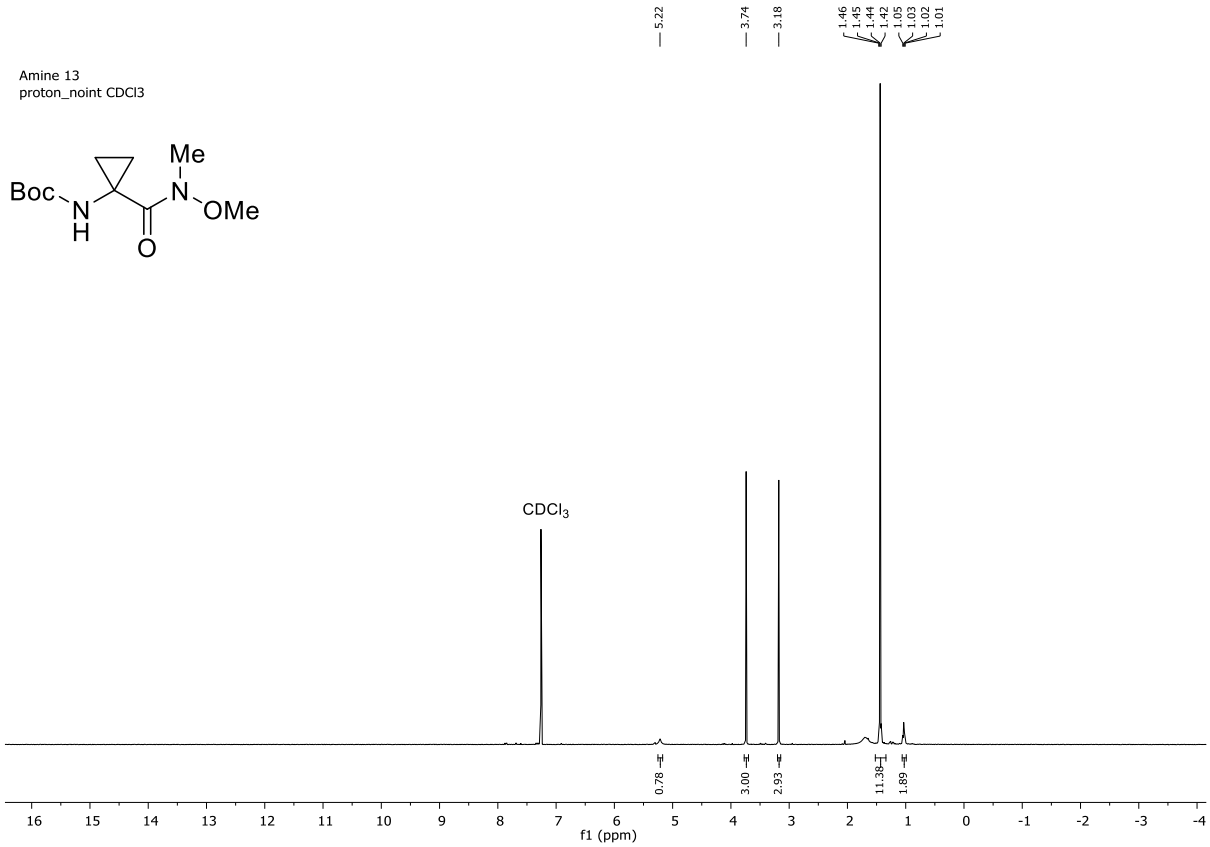

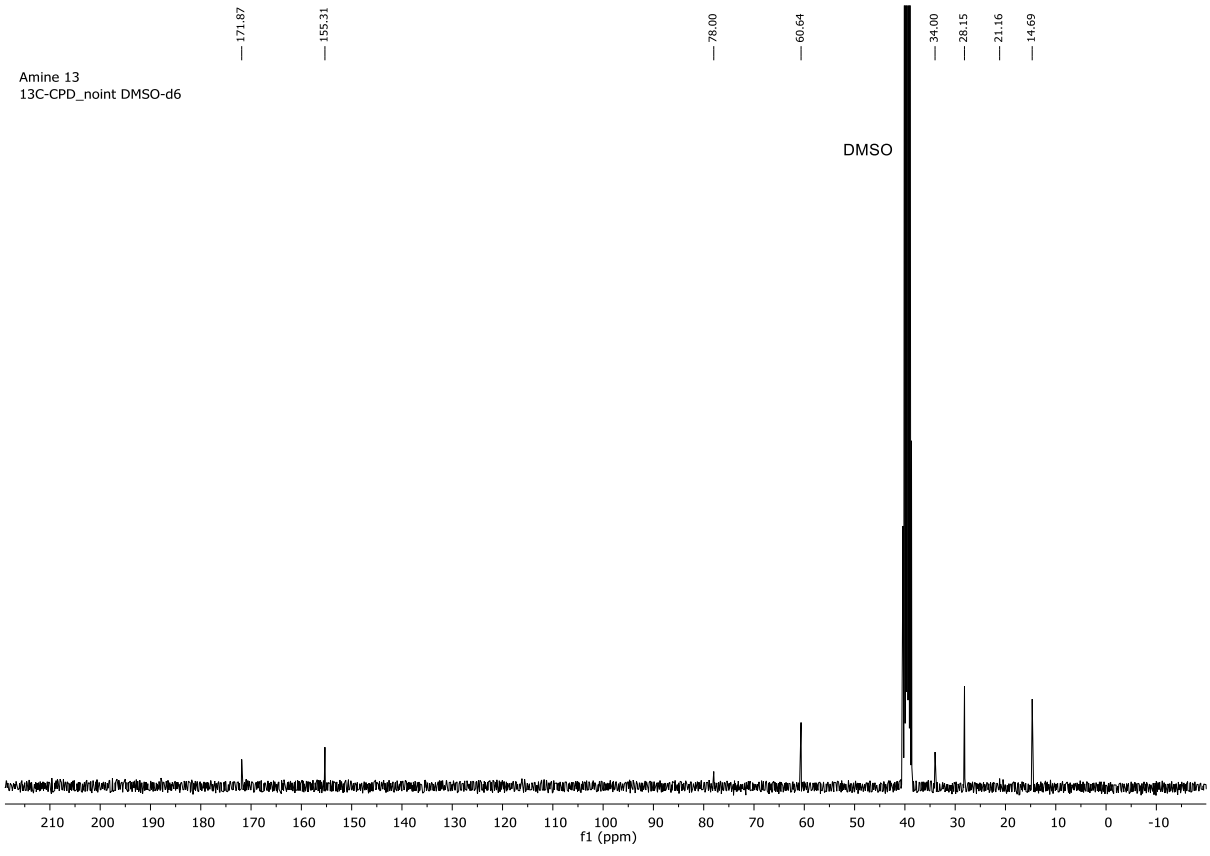

Figure S35. ^{1}H and ^{13}C NMR spectra for Amine **15**

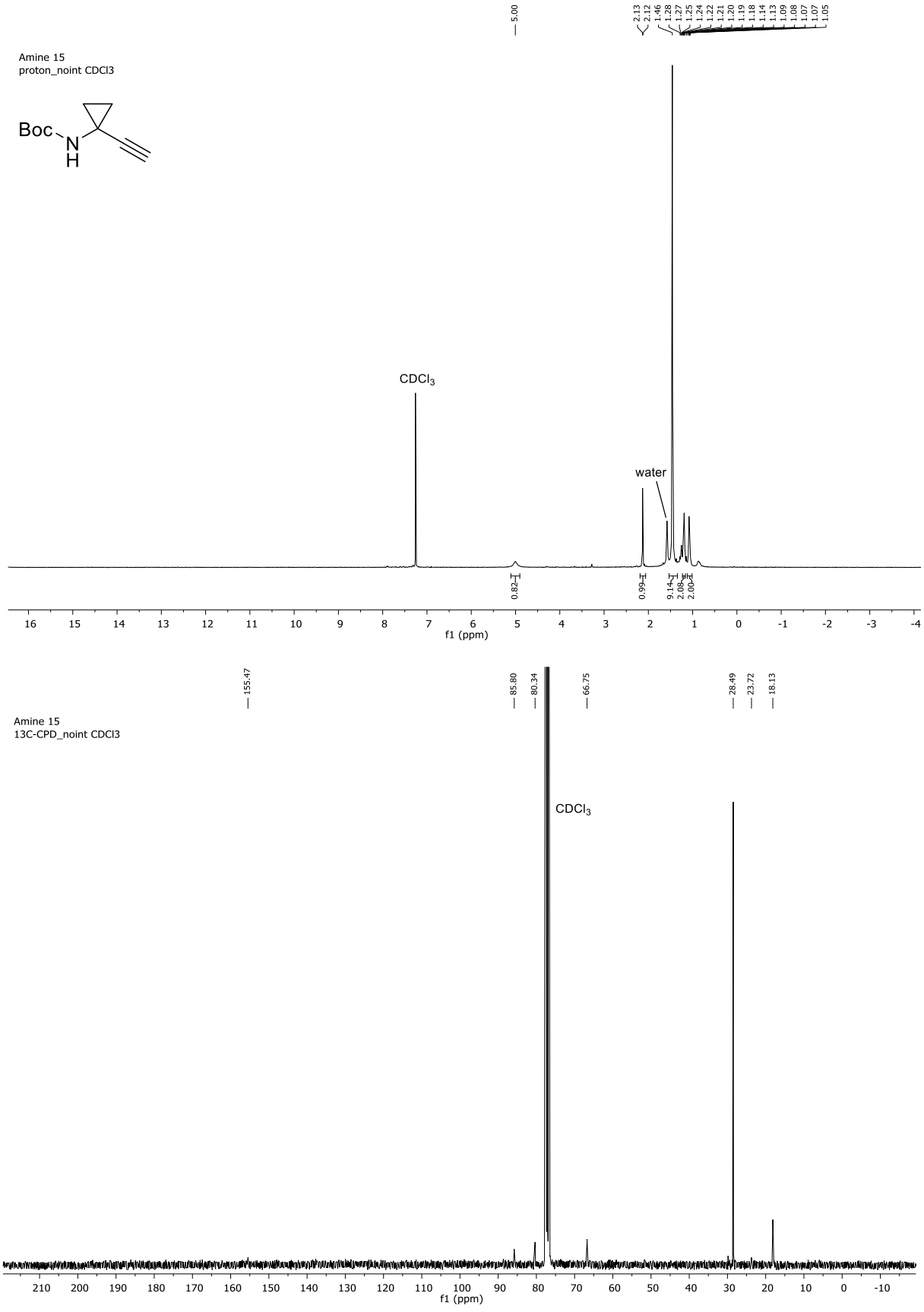

Figure S36. ^{1}H and ^{13}C NMR spectra for Amine **16**

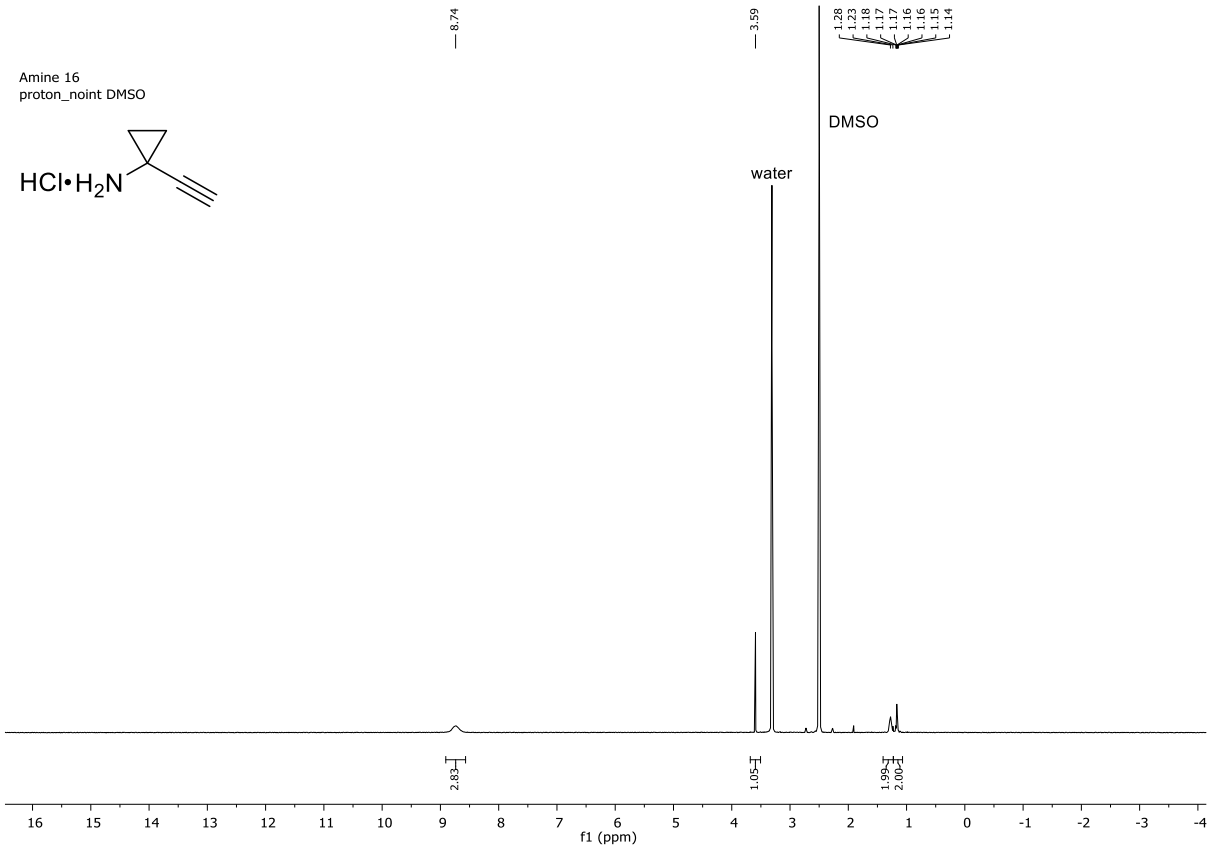

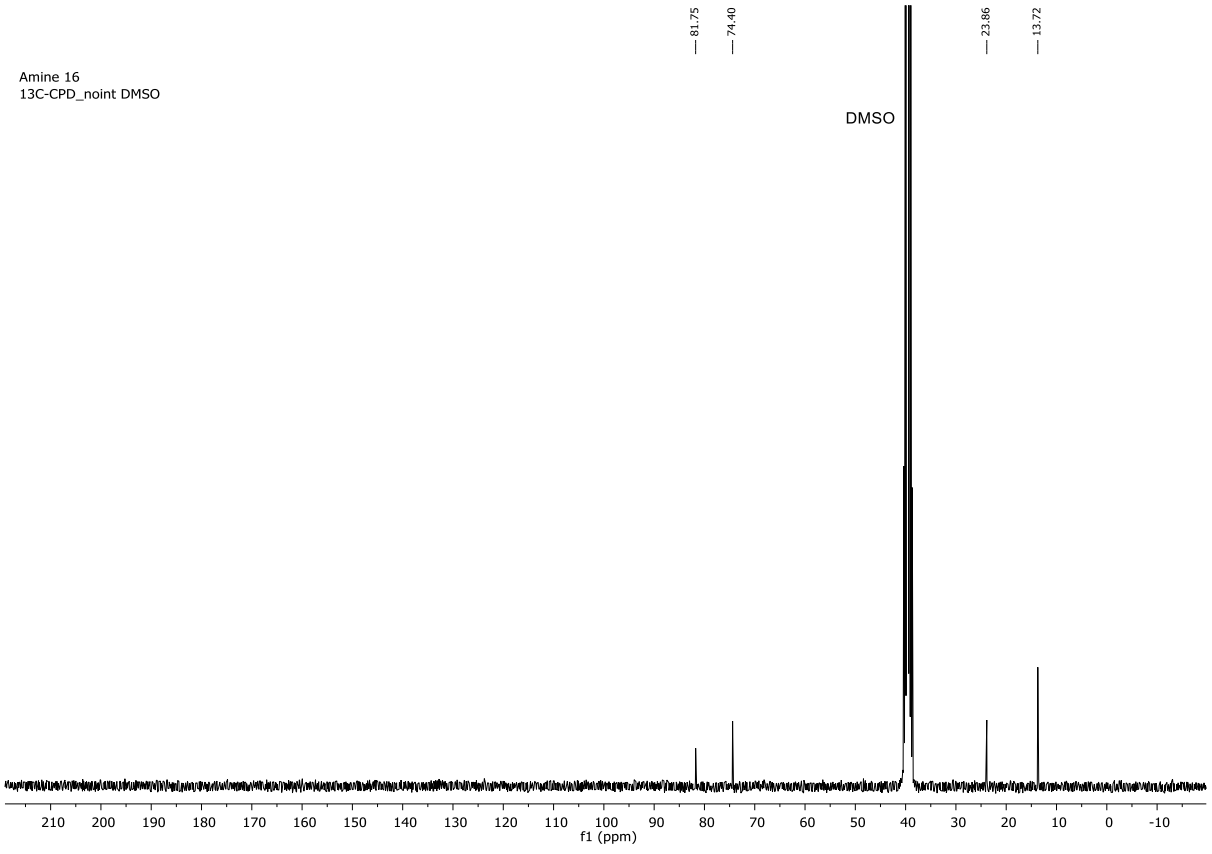

Figure S37. ^{1}H and ^{13}C NMR spectra for Amine **17**

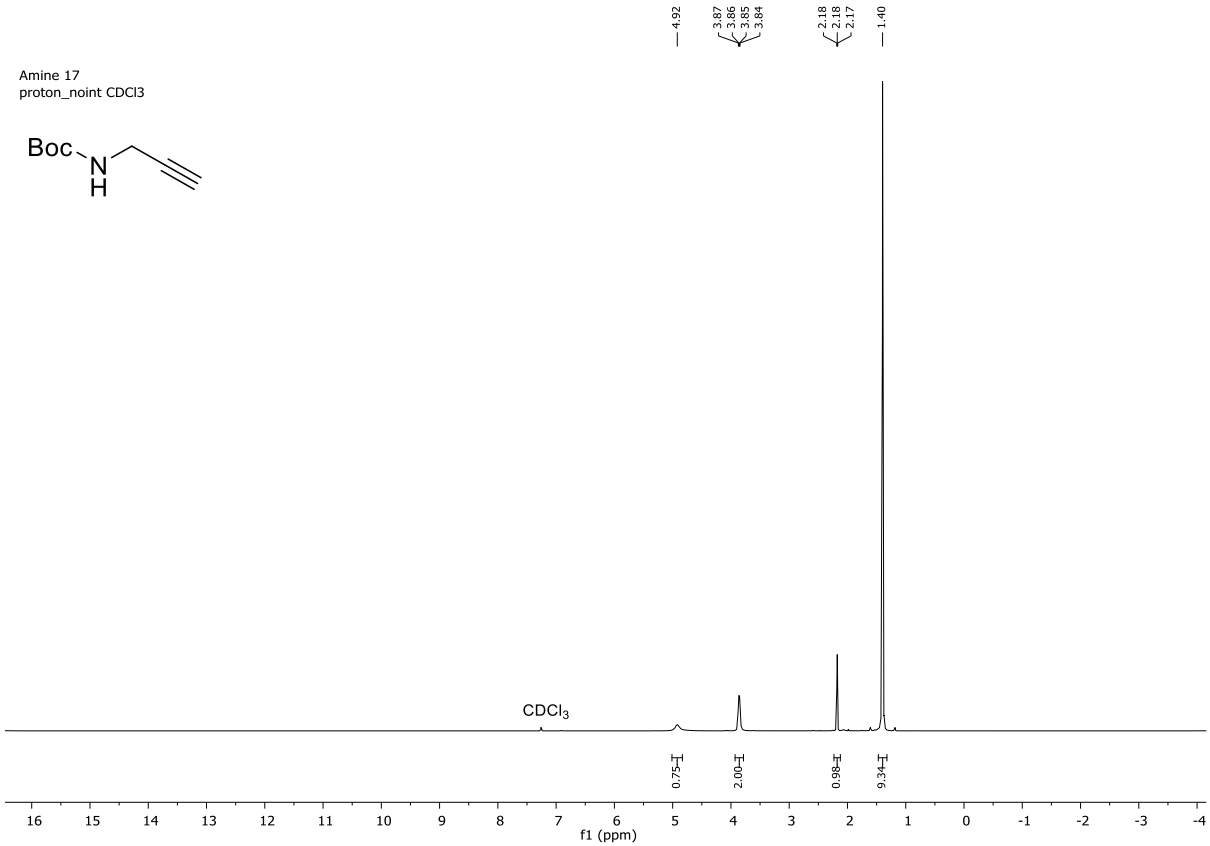

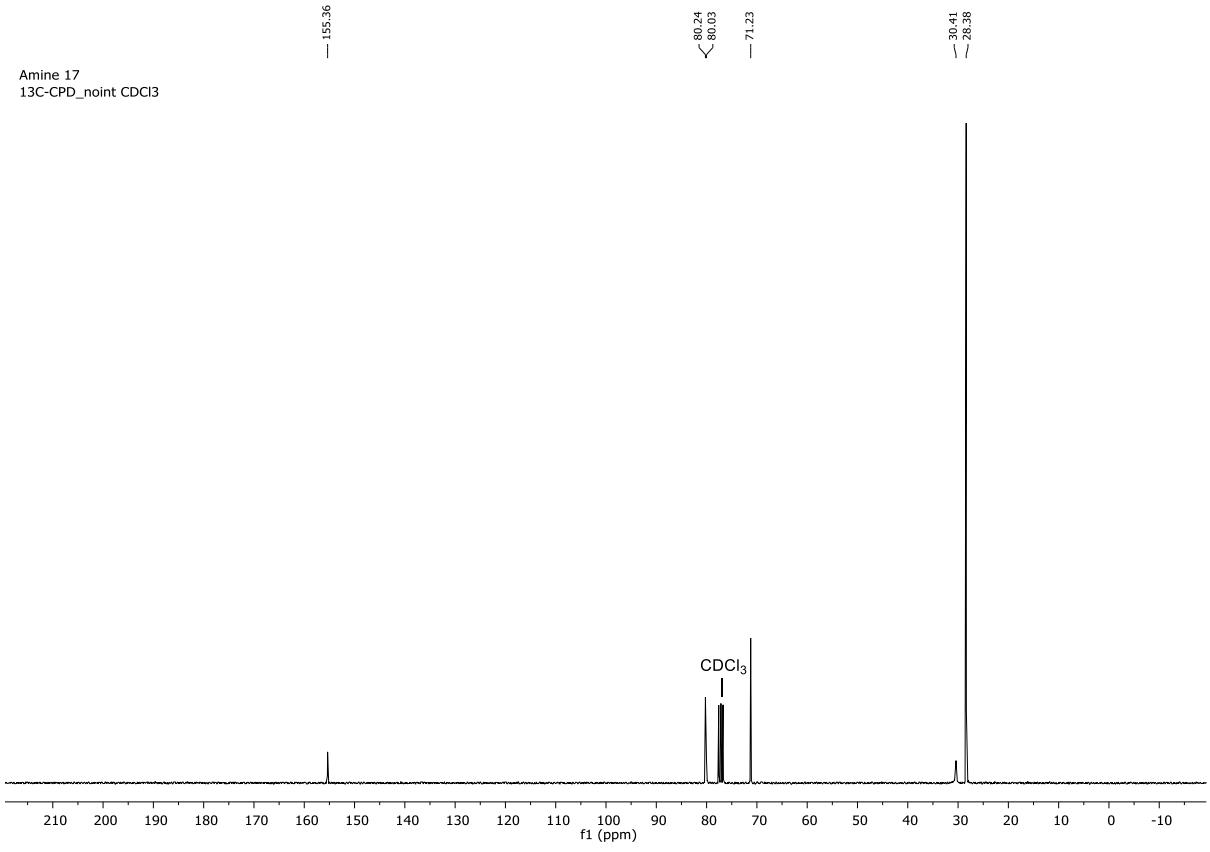

Figure S38. ^{1}H and ^{13}C NMR spectra for Amine **18**

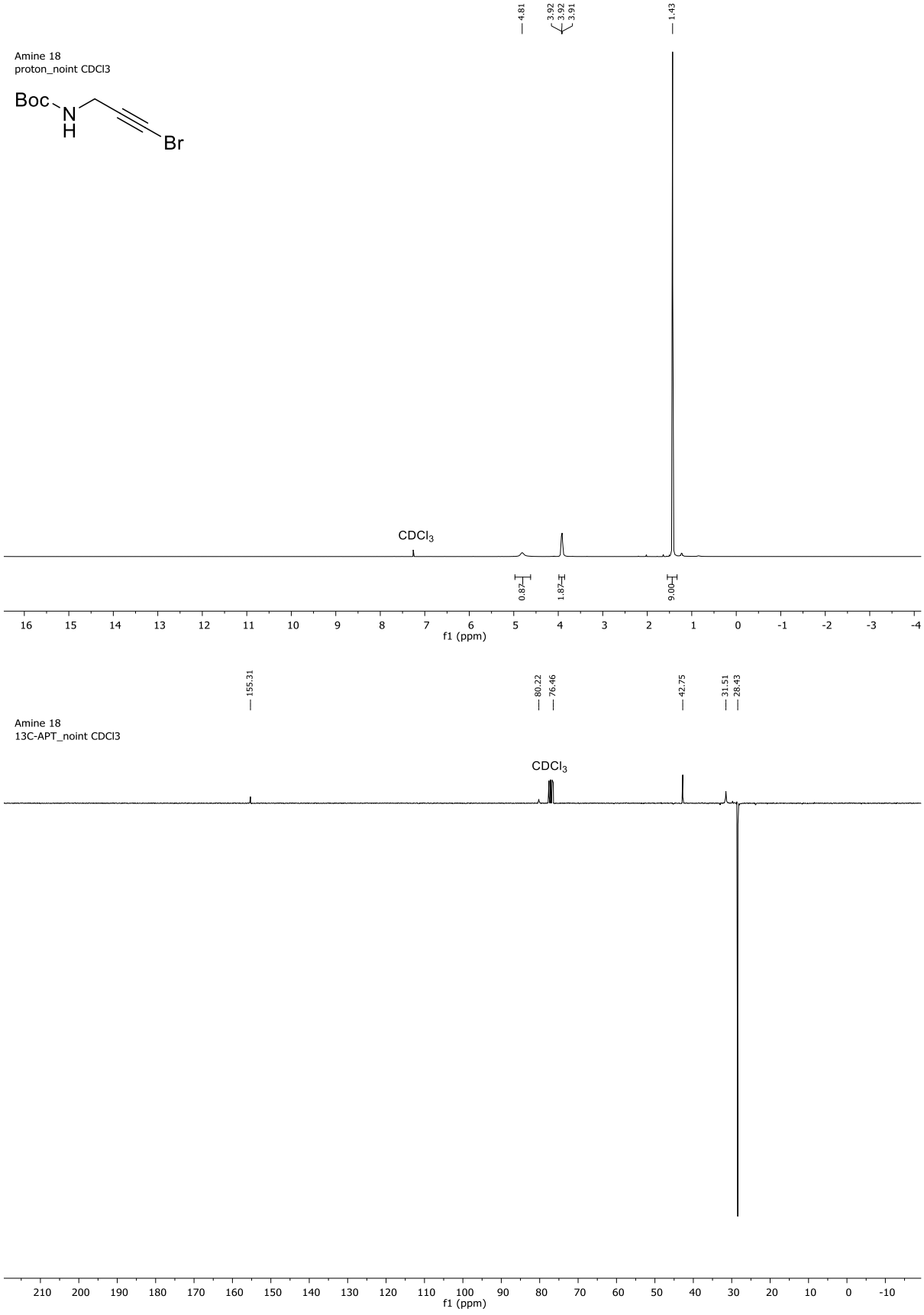

Figure S39. ^{1}H and ^{13}C NMR spectra for Amine **19**

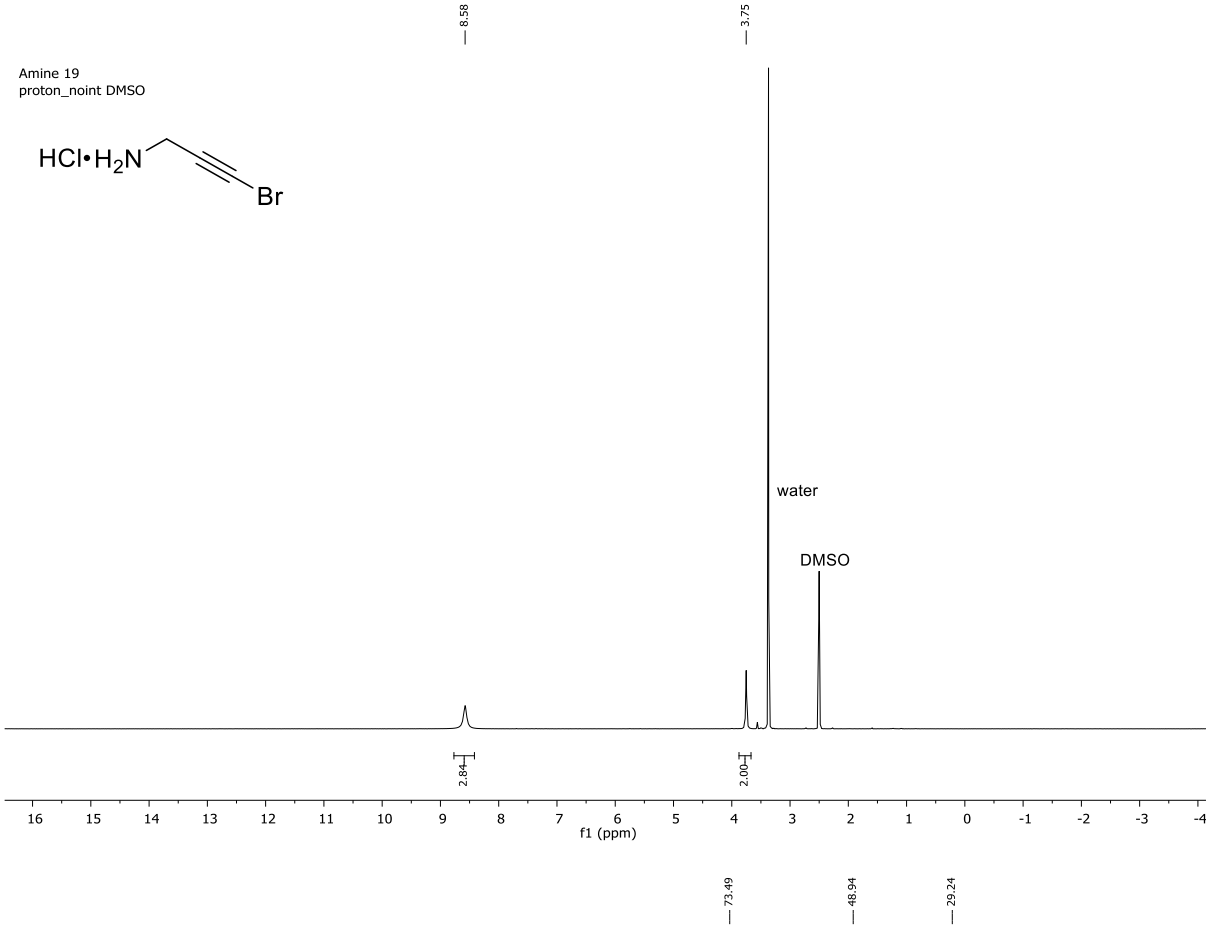

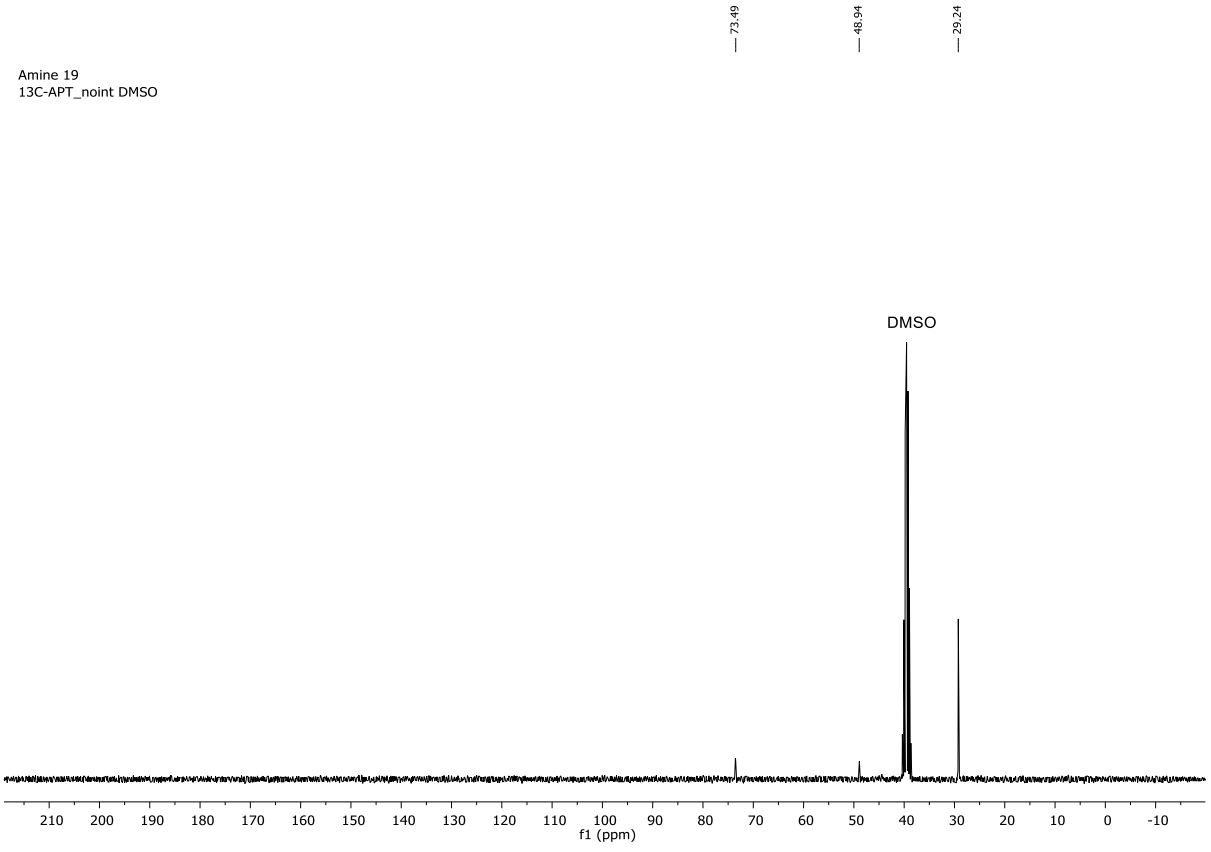

Appendix; Background on kinetic evaluation of (ir)reversible slow-binding inhibitors

Conventional IC_{50} measurements are of limited value for characterizing potency of irreversible inhibitors, because a different value will be found when incubation time is longer or shorter.[34] The covalent inhibitors described in this paper follow a two-step binding, in which initial non-covalent binding to the enzyme under rapid equilibrium conditions is followed by slower covalent bond formation (Table 3).

Slow binding kinetics as a result of two-step covalent inhibition can be observed in the progress curve when the reaction is started by addition of CatK, instead of incubating the inhibitor with CatK prior to addition of the substrate. The progress curve consists of an initial velocity (v_i) as a result of the non-covalent binding and a steady-state velocity (v_s) that approaches zero when all enzyme is covalently inhibited. The faster the plateau is reached, the faster the covalent bond formation is complete. The observed rate constant for inhibition (k_{obs}) is a pseudo first-order rate constant that can be obtained from the product formation by fitting the kinetic data to equation 1 (irreversible) or equation 2 (reversible).

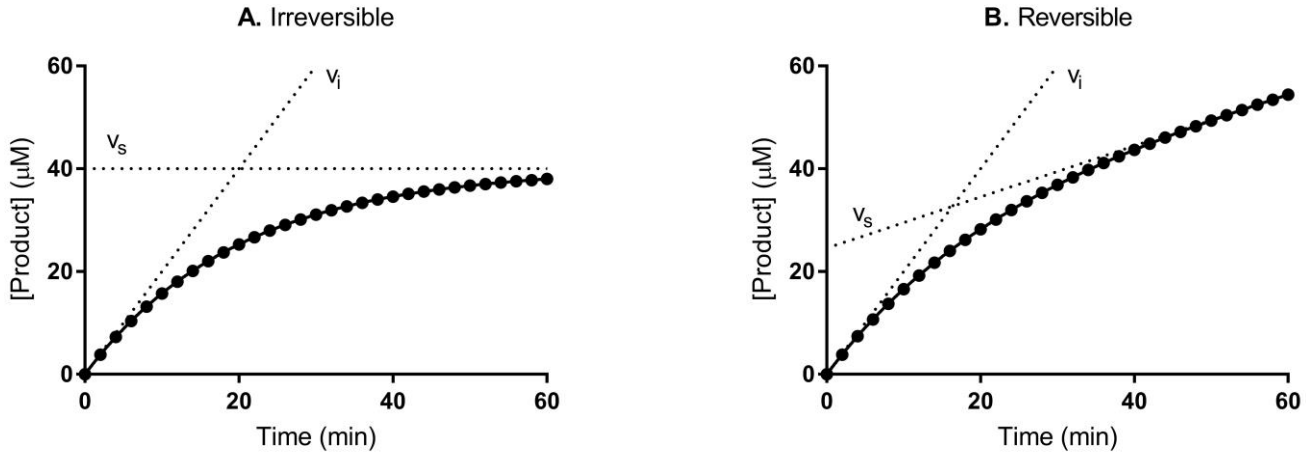

Figure S40. Progress curve for substrate hydrolysis in the presence of an (a) irreversible or (b) reversible slow binding inhibitor. The initial velocity v_i is defined by the slope in the early stage of the curve and the steady state velocity v_s is defined by the slope in the late stage of the curve, as indicated by the dashed lines.

$$[P] = \frac{v_i}{k_{obs}}[1 - e^{-k_{obs}t}] \qquad \text{eq. } \mathbf{1}$$

$$[P] = v_s t + \frac{v_i - v_s}{k_{obs}}[1 - e^{-k_{obs}t}] \qquad \text{eq. } \mathbf{2}$$

[P] = Product formation (pmol). v_i = initial reaction rate (pmol/min). v_s = steady-state reaction rate (pmol/min). k_{obs} = pseudo first-order rate constant (min^{-1}). t = time (min)

For irreversible covalent inhibitors, kinetic parameters k_{inact} (rate of inactivation, maximum k_{obs} at infinite inhibitor concentration) and K_I (concentration inhibitor that yields a half-maximum k_{obs}; ½ k_{inact}) can be obtained from plotting k_{obs} values as a function of [inhibitor], and fitting to equation 3. For SAR analysis of irreversible inhibitors, the k_{inact}/K_I ratio is used to represent the efficiency of inhibition. An increase in non-covalent binding between inhibitor and enzyme is reflected in a decrease K_I, while the rate of covalent bond formation is reflected in an increase of k_{inact}. Only under very specific conditions are K_i and K_I interchangeable (Copeland 2nd ed. p350).[35]

For reversible covalent inhibitors with a two-step binding mode, the kinetic parameters K_i^{app} (apparent inhibition constant, concentration inhibitor that yields a half-maximum k_{obs}), k_5 (rate of covalent bond formation) and k_6 (rate of covalent bond dissociation) can be obtained from plotting k_{obs} values as a function of inhibitor concentration, and fitting to equation 4. Tight binding was not taken into account because the concentration of inhibitor is significantly higher than enzyme concentration (Copeland, 2nd ed. p143).[35] The inhibitor constant for the initial non-covalent binding K_i can be calculated from the apparent inhibitor constant K_i^{app} and rate constants of covalent association/dissociation (k_5 and k_6) using equation 5.

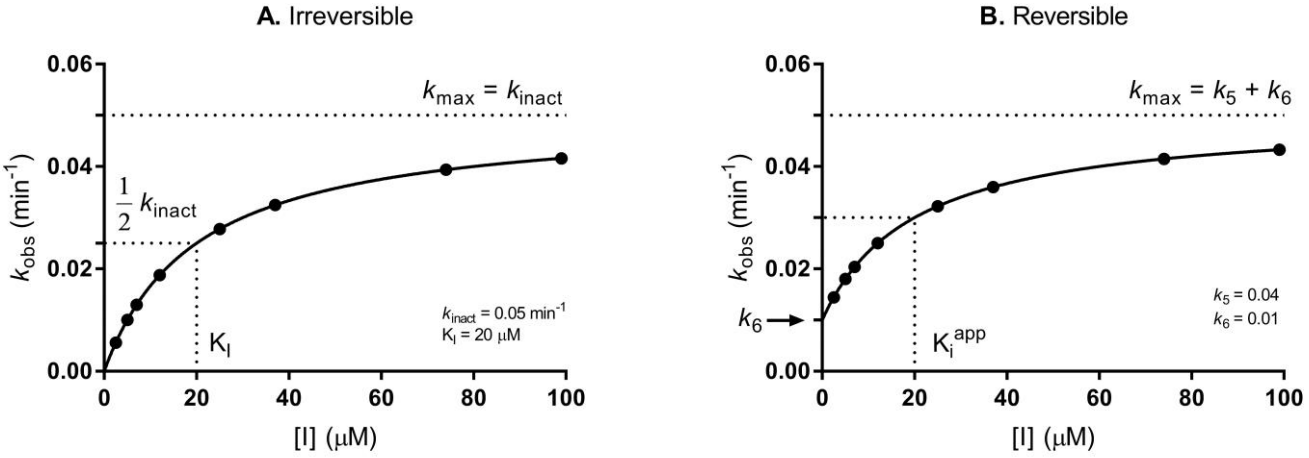

Figure S41. Plot of k_{obs} versus inhibitor concentration for a two-step mechanism of **A**) inactivation (irreversible inhibition) or **B**) reversible inhibition.

$$k_{obs} = \frac{k_{inact}}{1 + \frac{K_I}{[I]}} \qquad \text{eq. } \mathbf{3}$$

$$k_{obs} = k_6 + \frac{k_5}{1 + \frac{K_i^{app}}{[I]}} \qquad \text{eq. } \mathbf{4}$$

$$K_i = \frac{K_i^{app}}{1 + \frac{k_5}{k_6}} = \frac{k_{off}}{k_{on}} \qquad \text{eq. } \mathbf{5}$$

[I] = inhibitor concentration (M). k_{obs} = observed rate constant for inhibition (min^{-1}). k_{inact} = rate constant for irreversible covalent bond association (min^{-1}). k_5 = rate constant for reversible covalent bond association (min^{-1}). k_6 = rate constant for reversible covalent bond dissociation (min^{-1}). K_I = inhibitor concentration at which k_{obs} = ½ k_{inact} (M). K_i^{app} = inhibitor concentration at which k_{obs} = k_6 + ½ k_5 (M). K_i = Dissociation constant for reversible initial inhibitor complex (M).

References

1. Oballa, R. M.; Truchon, J.-F.; Bayly, C. I.; Chauret, N.; Day, S.; Crane, S.; Berthelette, C., A generally applicable method for assessing the electrophilicity and reactivity of diverse nitrile-containing compounds. *Bioorg. Med. Chem. Lett.* **2007,** *17* (4), 998-1002.
2. Fernández, A.; Vendrell, M., Smart fluorescent probes for imaging macrophage activity. *Chem. Soc. Rev.* **2016,** *45* (5), 1182-1196.
3. Verdoes, M.; Oresic Bender, K.; Segal, E.; van der Linden, W. A.; Syed, S.; Withana, N. P.; Sanman, L. E.; Bogyo, M., Improved Quenched Fluorescent Probe for Imaging of Cysteine Cathepsin Activity. *J. Am. Chem. Soc.* **2013,** *135* (39), 14726-14730.
4. Pražnikar, J.; Turk, D., Free kick instead of cross-validation in maximum-likelihood refinement of macromolecular crystal structures. *Acta Crystallogr., Sect. D: Biol. Crystallogr.* **2014,** *70* (Pt 12), 3124-3134.
5. O'Shea, P. D.; Chen, C.-y.; Gauvreau, D.; Gosselin, F.; Hughes, G.; Nadeau, C.; Volante, R. P., A Practical Enantioselective Synthesis of Odanacatib, a Potent Cathepsin K Inhibitor, via Triflate Displacement of an α-Trifluoromethylbenzyl Triflate. *J. Org. Chem.* **2009,** *74* (4), 1605-1610.
6. Mihelič, M.; Doberšek, A.; Gunčar, G.; Turk, D., Inhibitory Fragment from the p41 Form of Invariant Chain Can Regulate Activity of Cysteine Cathepsins in Antigen Presentation. *J. Biol. Chem.* **2008,** *283* (21), 14453-14460.
7. Brömme, D.; Nallaseth, F. S.; Turk, B., Production and activation of recombinant papain-like cysteine proteases. *Methods* **2004,** *32* (2), 199-206.
8. Rozman, J.; Stojan, J.; Kuhelj, R.; Turk, V.; Turk, B., Autocatalytic processing of recombinant human procathepsin B is a bimolecular process11Dedicated to Prof. Pavao Mildner on the occasion of his 80th birthday. *FEBS Lett.* **1999,** *459* (3), 358-362.
9. Borišek, J.; Vizovišek, M.; Sosnowski, P.; Turk, B.; Turk, D.; Mohar, B.; Novič, M., Development of N-(Functionalized benzoyl)-homocycloleucyl-glycinonitriles as Potent Cathepsin K Inhibitors. *J. Med. Chem.* **2015,** *58* (17), 6928-6937.
10. Law, S.; Andrault, P.-M.; Aguda, A. H.; Nguyen, N. T.; Kruglyak, N.; Brayer, G. D.; Brömme, D., Identification of mouse cathepsin K structural elements that regulate the potency of odanacatib. *Biochem. J.* **2017,** *474*, 851-864.
11. McQueney, M. S.; Amegadzie, B. Y.; D'Alessio, K.; Hanning, C. R.; McLaughlin, M. M.; McNulty, D.; Carr, S. A.; Ijames, C.; Kurdyla, J.; Jones, C. S., Autocatalytic Activation of Human Cathepsin K. *J. Biol. Chem.* **1997,** *272* (21), 13955-13960.
12. Lausi, A.; Polentarutti, M.; Onesti, S.; Plaisier, J. R.; Busetto, E.; Bais, G.; Barba, L.; Cassetta, A.; Campi, G.; Lamba, D.; Pifferi, A.; Mande, S. C.; Sarma, D. D.; Sharma, S. M.; Paolucci, G., Status of the crystallography beamlines at Elettra. *Eur. Phys. J. Plus* **2015,** *130* (3).
13. Kabsch, W., Integration, scaling, space-group assignment and post-refinement. *Acta Crystallogr., Sect. D* **2010,** *66* (2), 133-144.
14. Winn, M. D.; Ballard, C. C.; Cowtan, K. D.; Dodson, E. J.; Emsley, P.; Evans, P. R.; Keegan, R. M.; Krissinel, E. B.; Leslie, A. G. W.; McCoy, A.; McNicholas, S. J.; Murshudov, G. N.; Pannu, N. S.; Potterton, E. A.; Powell, H. R.; Read, R. J.; Vagin, A.; Wilson, K. S., Overview of the CCP4 suite and current developments. *Acta Crystallogr., Sect. D: Biol. Crystallogr.* **2011,** *67* (Pt 4), 235-242.
15. Evans, P., Scaling and assessment of data quality. *Acta Crystallogr., Sect. D* **2006,** *62* (1), 72-82.
16. Evans, P. R.; Murshudov, G. N., How good are my data and what is the resolution? *Acta Crystallogr., Sect. D: Biol. Crystallogr.* **2013,** *69* (Pt 7), 1204-1214.
17. Yamashita, D. S.; Marquis, R. W.; Xie, R.; Nidamarthy, S. D.; Oh, H.-J.; Jeong, J. U.; Erhard, K. F.; Ward, K. W.; Roethke, T. J.; Smith, B. R.; Cheng, H. Y.; Geng, X.; Lin, F.; Offen, P. H.; Wang, B.; Nevins, N.; Head, M. S.; Haltiwanger, R. C.; Narducci Sarjeant, A. A.; Liable-Sands, L. M.; Zhao, B.; Smith, W. W.; Janson, C. A.; Gao, E.; Tomaszek, T.; McQueney, M.; James, I. E.; Gress, C. J.; Zembryki, D. L.; Lark, M. W.; Veber, D. F., Structure Activity Relationships of 5-, 6-, and 7-Methyl-Substituted Azepan-3-one Cathepsin K Inhibitors. *J. Med. Chem.* **2006,** *49* (5), 1597-1612.
18. Vagin, A.; Teplyakov, A., MOLREP: an Automated Program for Molecular Replacement. *J. Appl. Crystallogr.* **1997,** *30* (6), 1022-1025.
19. Turk, D., MAIN software for density averaging, model building, structure refinement and validation. *Acta Crystallogr., Sect. D: Biol. Crystallogr.* **2013,** *69* (Pt 8), 1342-1357.
20. Andrejasic, M.; Praznikar, J.; Turk, D., PURY: a database of geometric restraints of hetero compounds for refinement in complexes with macromolecular structures. *Acta Crystallogr., Sect. D* **2008,** *64* (11), 1093-1109.

21. Merritt, E. A.; Bacon, D. J., [26] Raster3D: Photorealistic molecular graphics. In *Methods in Enzymology*, Academic Press: 1997; Vol. 277, pp 505-524.
22. Choe, Y.; Leonetti, F.; Greenbaum, D. C.; Lecaille, F.; Bogyo, M.; Brömme, D.; Ellman, J. A.; Craik, C. S., Substrate Profiling of Cysteine Proteases Using a Combinatorial Peptide Library Identifies Functionally Unique Specificities. *J. Biol. Chem.* **2006,** *281* (18), 12824-12832.
23. Yasuda, Y.; Li, Z.; Greenbaum, D.; Bogyo, M.; Weber, E.; Brömme, D., Cathepsin V, a Novel and Potent Elastolytic Activity Expressed in Activated Macrophages. *J. Biol. Chem.* **2004,** *279* (35), 36761-36770.
24. Kramer, L.; Renko, M.; Završnik, J.; Turk, D.; Seeger, M. A.; Vasiljeva, O.; Grütter, M. G.; Turk, V.; Turk, B., Non-invasive in vivo imaging of tumour-associated cathepsin B by a highly selective inhibitory DARPin. *Theranostics* **2017,** *7* (11), 2806-2821.
25. Menard, R.; Khouri, H. E.; Plouffe, C.; Dupras, R.; Ripoll, D.; Vernet, T.; Tessier, D. C.; Laliberte, F.; Thomas, D. Y.; Storer, A. C., A protein engineering study of the role of aspartate 158 in the catalytic mechanism of papain. *Biochemistry* **1990,** *29* (28), 6706-6713.
26. Hayman, A. R., Tartrate-resistant acid phosphatase (TRAP) and the osteoclast/immune cell dichotomy. *Autoimmunity* **2008,** *41* (3), 218-223.
27. Leung, P.; Pickarski, M.; Zhuo, Y.; Masarachia, P. J.; Duong, L. T., The effects of the cathepsin K inhibitor odanacatib on osteoclastic bone resorption and vesicular trafficking. *Bone* **2011,** *49* (4), 623-635.
28. Dolman, S. J.; Gosselin, F.; O'Shea, P. D.; Davies, I. W., Selective metal-halogen exchange of 4,4′-dibromobiphenyl mediated by lithium tributylmagnesiate. *Tetrahedron* **2006,** *62* (21), 5092-5098.
29. Gauthier, J. Y.; Black, W. C.; Courchesne, I.; Cromlish, W.; Desmarais, S.; Houle, R.; Lamontagne, S.; Li, C. S.; Massé, F.; McKay, D. J.; Ouellet, M.; Robichaud, J.; Truchon, J.-F.; Truong, V.-L.; Wang, Q.; Percival, M. D., The identification of potent, selective, and bioavailable cathepsin S inhibitors. *Bioorg. Med. Chem. Lett.* **2007,** *17* (17), 4929-4933.
30. Gauthier, J. Y.; Chauret, N.; Cromlish, W.; Desmarais, S.; Duong, L. T.; Falgueyret, J.-P.; Kimmel, D. B.; Lamontagne, S.; Léger, S.; LeRiche, T.; Li, C. S.; Massé, F.; McKay, D. J.; Nicoll-Griffith, D. A.; Oballa, R. M.; Palmer, J. T.; Percival, M. D.; Riendeau, D.; Robichaud, J.; Rodan, G. A.; Rodan, S. B.; Seto, C.; Thérien, M.; Truong, V.-L.; Venuti, M. C.; Wesolowski, G.; Young, R. N.; Zamboni, R.; Black, W. C., The discovery of odanacatib (MK-0822), a selective inhibitor of cathepsin K. *Bioorg. Med. Chem. Lett.* **2008,** *18* (3), 923-928.
31. Roy, A.; Gosselin, F.; O'Shea, P. D.; Chen, C.-y., Diastereoselective Arylithium Addition to an α-Trifluoromethyl Imine. Practical Synthesis of a Potent Cathepsin K Inhibitor. *J. Org. Chem.* **2006,** *71* (11), 4320-4323.
32. O'Shea, P.; Gosselin, F. (Merck Frosst Canada LTD.), Amidation Process for the preparation of Cathepsin K inhibitors. WO2008/119176A1, 2008.
33. Ishida, T.; Kobayashi, R.; Yamada, T., Novel method of tetramic acid synthesis: silver-catalyzed carbon dioxide incorporation into propargylic amine and intramolecular rearrangement. *Org. Lett.* **2014,** *16* (9), 2430-3.
34. Singh, J.; Petter, R. C.; Baillie, T. A.; Whitty, A., The resurgence of covalent drugs. *Nat. Rev. Drug Discovery* **2011,** *10* (4), 307-317.
35. Copeland, R. A., *Evaluation of Enzyme Inhibitors in Drug Discovery: A Guide for Medicinal Chemists and Pharmacologists, Second Edition*. John Wiley & Sons, Inc.: 2013.